INVESTIGATION OF THE DETECTIVITY OF RADIATION-PRODUCED DEFECT LEVELS IN n- AND p-TYPE SILICON AND GERMANIUM

Final Report
NASA Grant NGR-47-005-093

Submitted to:
National Aeronautics and Space Administration
Washington, D.C. 20546

Submitted by:
Robert J. Mattauch

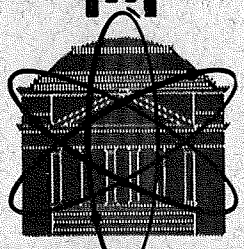

Research Laboratories for the Engineering Sciences

University of Virginia

Charlottesville

Report No. EE-4031-103-69U

July 1969

INVESTIGATION OF THE DETECTIVITY OF RADIATION-PRODUCED DEFECT LEVELS IN n- AND p-TYPE SILICON AND GERMANIUM

Final Report
NASA Grant NGR-47-005-093

Submitted to:
National Aeronautics and Space Administration
Washington, D.C. 20546

Submitted by:
Robert J. Mattauch

Division of Electrical Engineering
RESEARCH LABORATORIES FOR THE ENGINEERING SCIENCES
SCHOOL OF ENGINEERING AND APPLIED SCIENCE
UNIVERSITY OF VIRGINIA
CHARLOTTESVILLE, VIRGINIA

Report No. EE-4031-103-69U
July 1969

Copy No. 5

TABLE OF CONTENTS

LIST OF FIGURES

I. GENERAL SUMMARY

A. Introduction

This report not only briefly summarizes the work performed during the entire duration of grant NGR-47-005-093 but also presents as an appendix a thesis, presented by A. M. Barnwell in partial fulfillment of the requirements for the Master of Science in Electrical Engineering degree, which deals with this work and most important presents infrared photoconductivity results for semiconductor materials tested.

B. System

The first system used to determine infrared photoconductivity of high energy electron irradiated silicon consisted of a liquid nitrogen dewar which was fabricated at the Langley Research Center and a black-body source which was fabricated at the University of Virginia. This system had three main drawbacks which seriously limited both the speed with which data could be taken and the accuracy of that data. These drawbacks were:

(1) A device mounting scheme which used a conductive epoxy which in turn could not stand thermal shock.

(2) Screw type vacuum feed through insulators which periodically developed leaks and which also shorted out due to moisture present because of their placement close to the liquid nitrogen filling port.

(3) A cumbersome black-body source which created difficulties during device change operations.

A cut-away view of the original dewar is shown in Fig. 3.3 on page 43 of Appendix A.

Because of the relative difficulty experienced in using the original system a new one was designed which incorporated a different black-body source, a spectral source, and a new commercially fabricated liquid helium research dewar. A block diagram of this system is given in Fig. 3.8 on page 57 of Appendix A.

C. Nature of Obtained Data

So far as the device is concerned the new system enabled one to:

(a) Surround the device with a vacuum on the order of 10^{-5} Torr.

(b) Cool the device to nearly 77°K.

(c) Determine the temperature of the upper device holder to within 1° absolute.

(d) Apply a bias potential to the device in excess of 1000 volts.

(e) Determine the device resistance by means of a Keithly electrometer.

The dewar containing the device was fitted with two radiation shields and a germanium window and could be placed in either of two positions. One of these positions allowed the black-body source to be used while the other permitted use of the spectral source.

With the black-body source used one could obtain curves of device output voltage, Vd, as a function of chopping frequency. A direct result of this data were device black-body responsivity, R_{bb}, versus chopping frequency

curves with bias voltage as a parameter. Device noise voltage, Vdn, was directly obtainable with this system since under measurement conditions the circuit noise was immeasurably small.

The spectral source being used, one could obtain both device output voltage, V_{ds}, and reference bolometer output voltages, V_{bol}. This enabled one to determine the device relative spectral responsivity, $L(\lambda)$.

This subject is covered in much greater detail in pp. 34-60 of Appendix A.

D. Processing of Obtained Data

The total energy flux onto the device, J, from the black-body was calculated by means of the Stéffan-Boltzmann law knowing:

(a) Black-body temperature,

(b) Emissivity of oxide covering black body,

(c) Black body aperture and distance from device,

(d) Infrared transmission of the germanium dewar window as a function of wavelength,

(e) RMS of the chopping radiation.

As a consequence of this the device black-body responsivity

$$R_{bb} = \frac{Vd}{J}$$

was determined as mentioned above.

The relative spectral responsivity

$$L(\lambda) = \frac{V_{ds}(\lambda)}{V_{bol}(\lambda)}$$

was easily determined by means of the spectral source.

The device absolute black body spectral responsivity, $R(\lambda)$, was determined by means of computer from the relation

$$R(\lambda) = \frac{R_{bb} L(\lambda) J}{\int L(\lambda) J(\lambda) d\lambda}$$

Finally, the device spectral detectivity, D^*_λ, was determined from the relation

$$D^*_\lambda = \frac{(A\Delta f)^{1/2} R(\lambda)}{Vdn}$$

where A = the device adopeded area (cm^2)

Δf = the bandwidth of the voltage measuring instrument (Hz)

The following chapter will present one typical set of curves for each of the above mentioned quantities for one device and will then present the best data obtained for both n- and p-type silicon and germanium as available.

II. RESULTS

A. Introduction

This chapter presents data obtained with the new system mentioned in the previous chapter but does not, however, reflect the trends found most recently since it reports on work carried out during the period beginning February 1, 1968 and ending June 30, 1969. As can be seen from the following information a high degree of infrared photoconductivity has been observed for high energy electron irradiated silicon. The same is not true of germanium.

B. n-Type Silicon

The data obtained from device number SI3N.4, the pre-irradiation resistivity of which was .4Ω cm will serve as an example. Figure 2.1 contains curves of device black-body responsivity as a function of chopping frequency with bias potential as a parameter. Figure 2.2 bears curves of device noise as a function of frequency with bias potential as a parameter. In all cases the measured voltage was the actual device noise since the circuit noise was always immeasurably small and hence negligible.

Fig. 2.3 exhibits the variation of the relative spectral responsivity, $L(\lambda)$, of the device with wavelength. It should be remarked at this point that $L(\lambda)$ was basically the same for all such n-type devices tested. Fig. 2.4 shows the device absolute spectral responsivity while Fig. 2.5 exhibits a curve of device spectral detectivity, D^*_λ, as a function of wavelength.

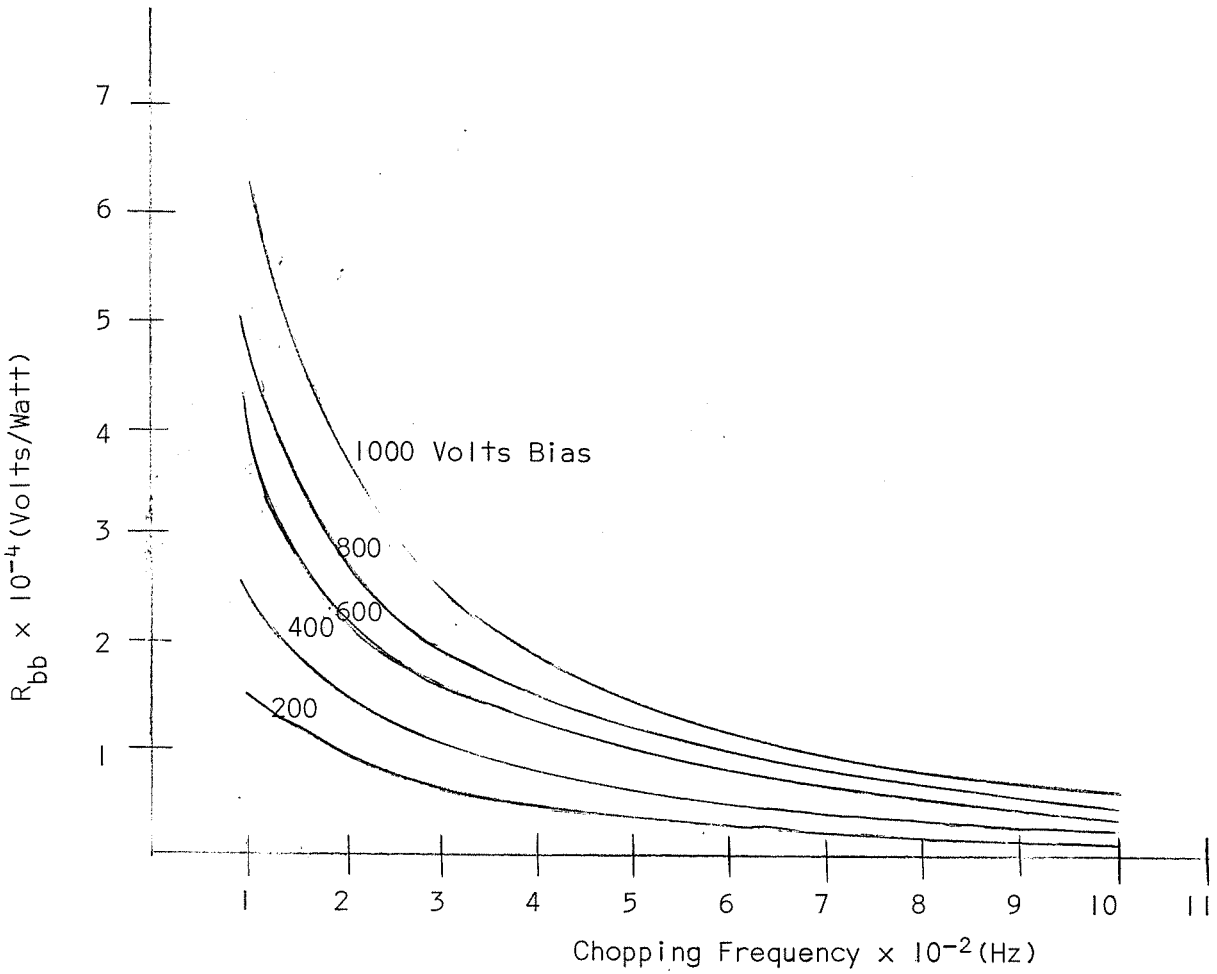

Figure 2.1 Black-body Responsivity as a Function of Chopping Frequency with Bias Potential as a Parameter for n-type Device S13N.4

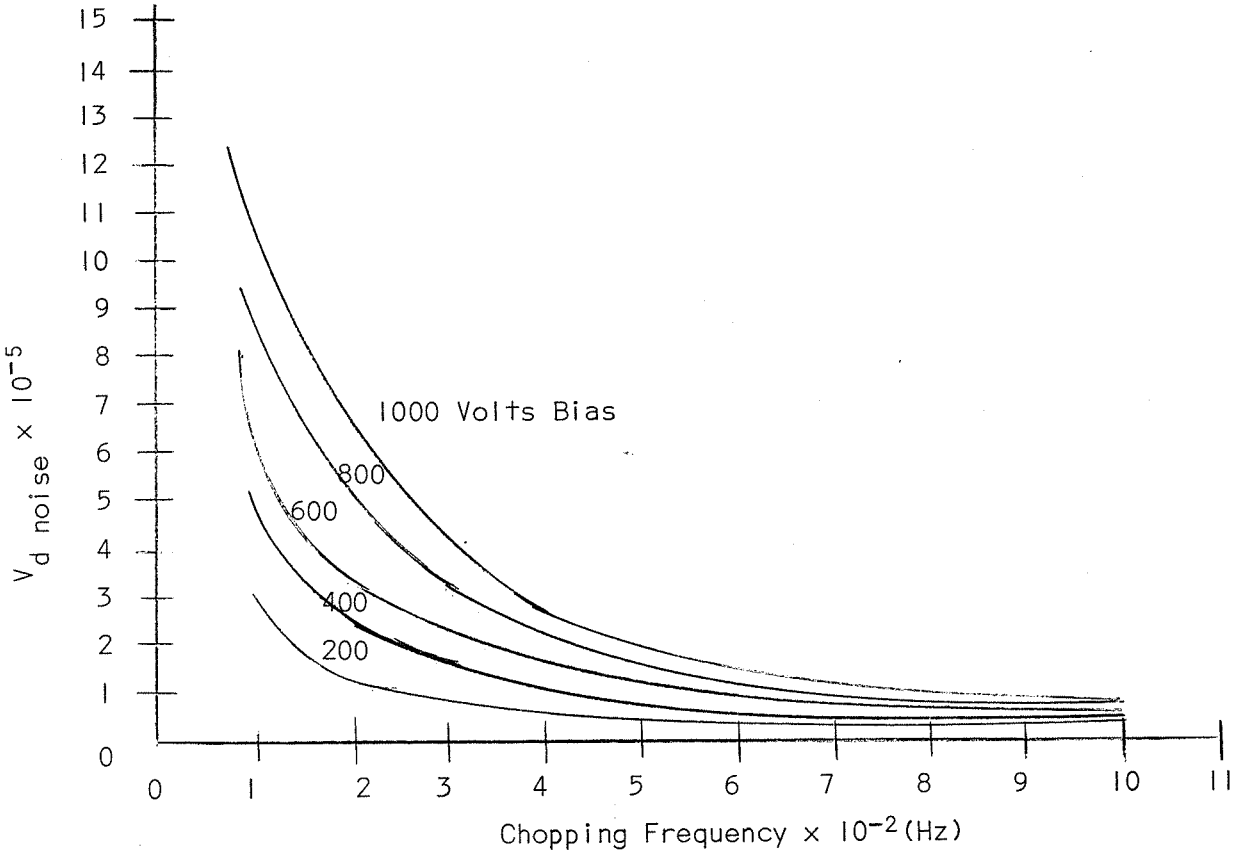

Figure 2.2 Device Noise as a Function of Measuring Frequency with Bias Potential as a Parameter for n-type Device S13N.4

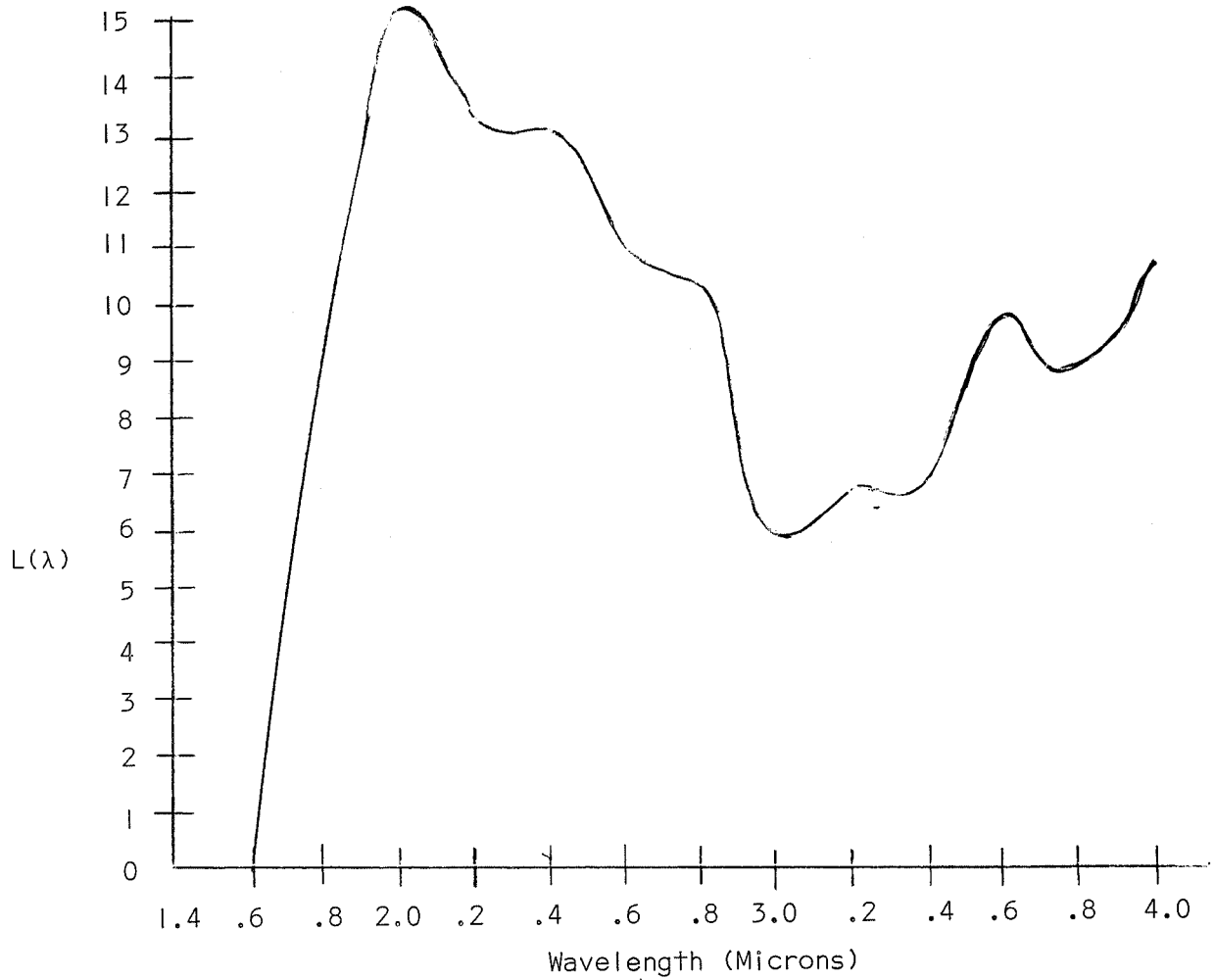

Figure 2.3 Relative Spectral Responsivity for n-type Device S13N.4

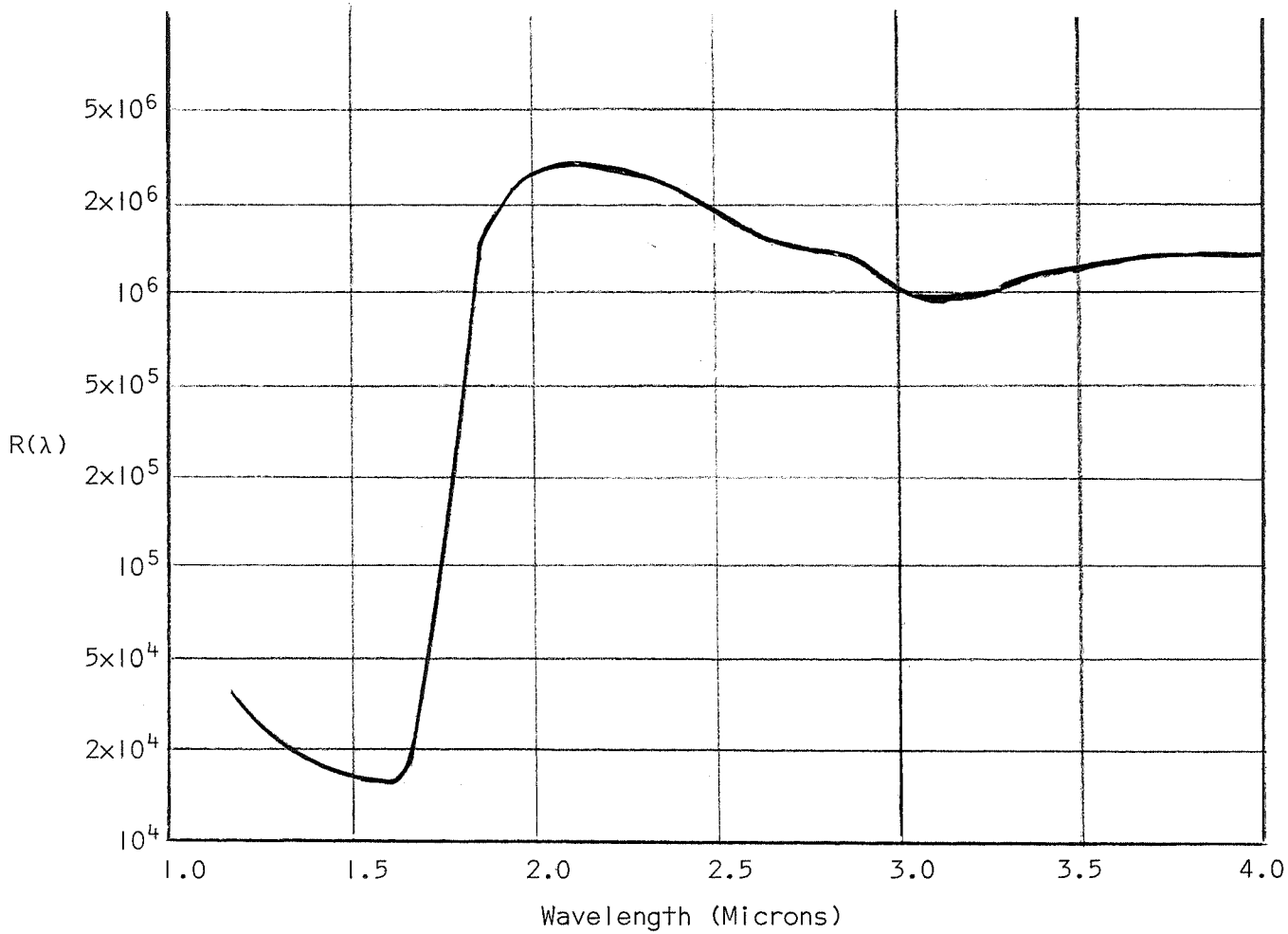

Figure 2.4 Absolute Spectral Responsivity for n-type Device SI3N.4

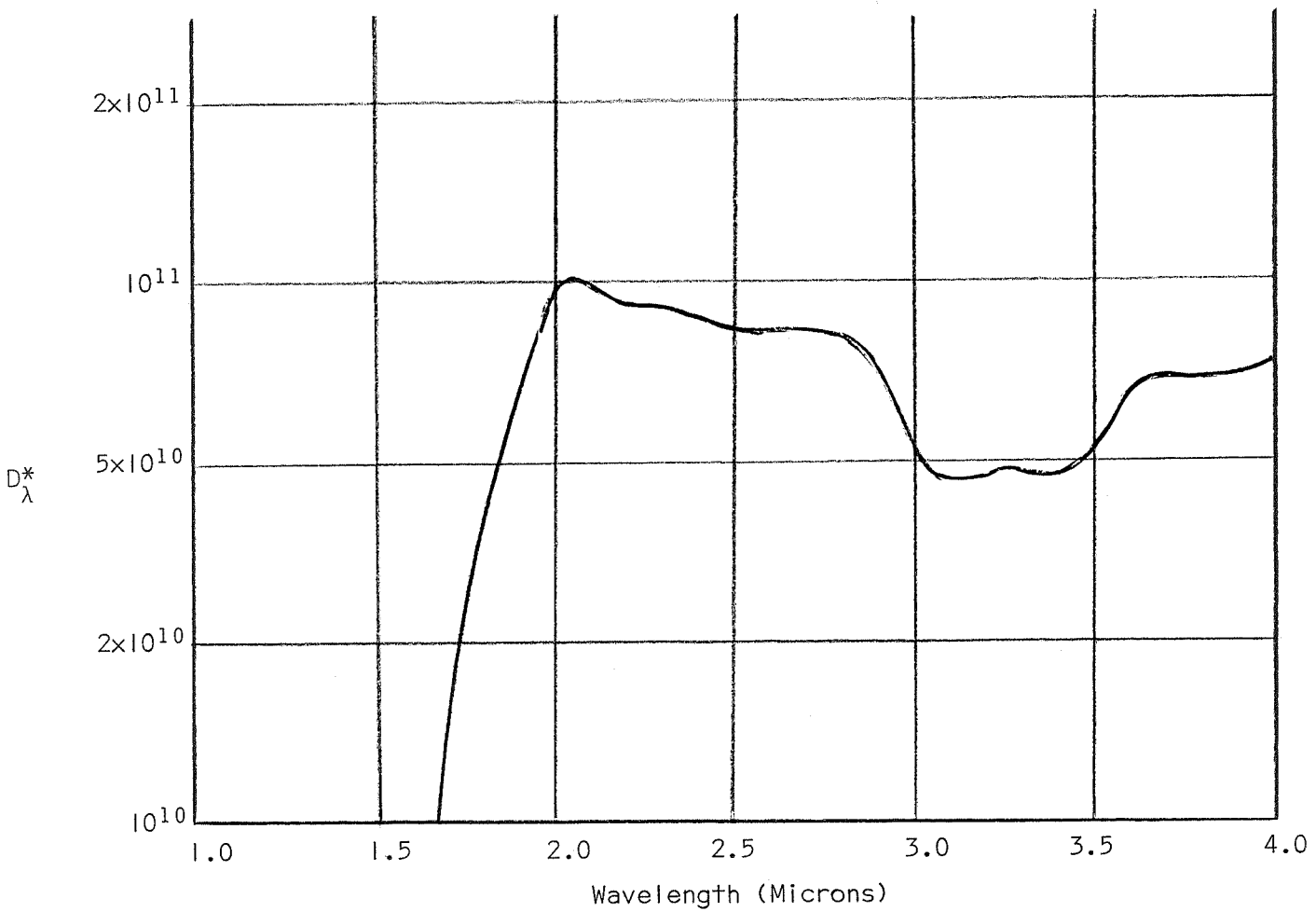

Figure 2.5 Spectral Detectivity for n-type Device SI3N.4

C. p-Type Silicon

Figs. 2.6, 2.7, 2.8, 2.9, and 2.10 bear curves of black-body responsivity, device noise, relative spectral responsivity, absolute spectral responsivity, and spectral detectivity respectively for p-type device number 436P.1 whose pre-irradiation resistivity was .1Ω cm.

D. Germanium

Fig. 2.11 bears a curve of black body responsivity versus chopping frequency for an n-type germanium device. Fig. 2.12 exhibits the variation in device noise with chopping frequency for the same device. No output could be detected from irradiated p-type germanium. It can be seen by comparing these curves with the corresponding ones for silicon that the electron irradiated germanium offers little as an infrared detector.

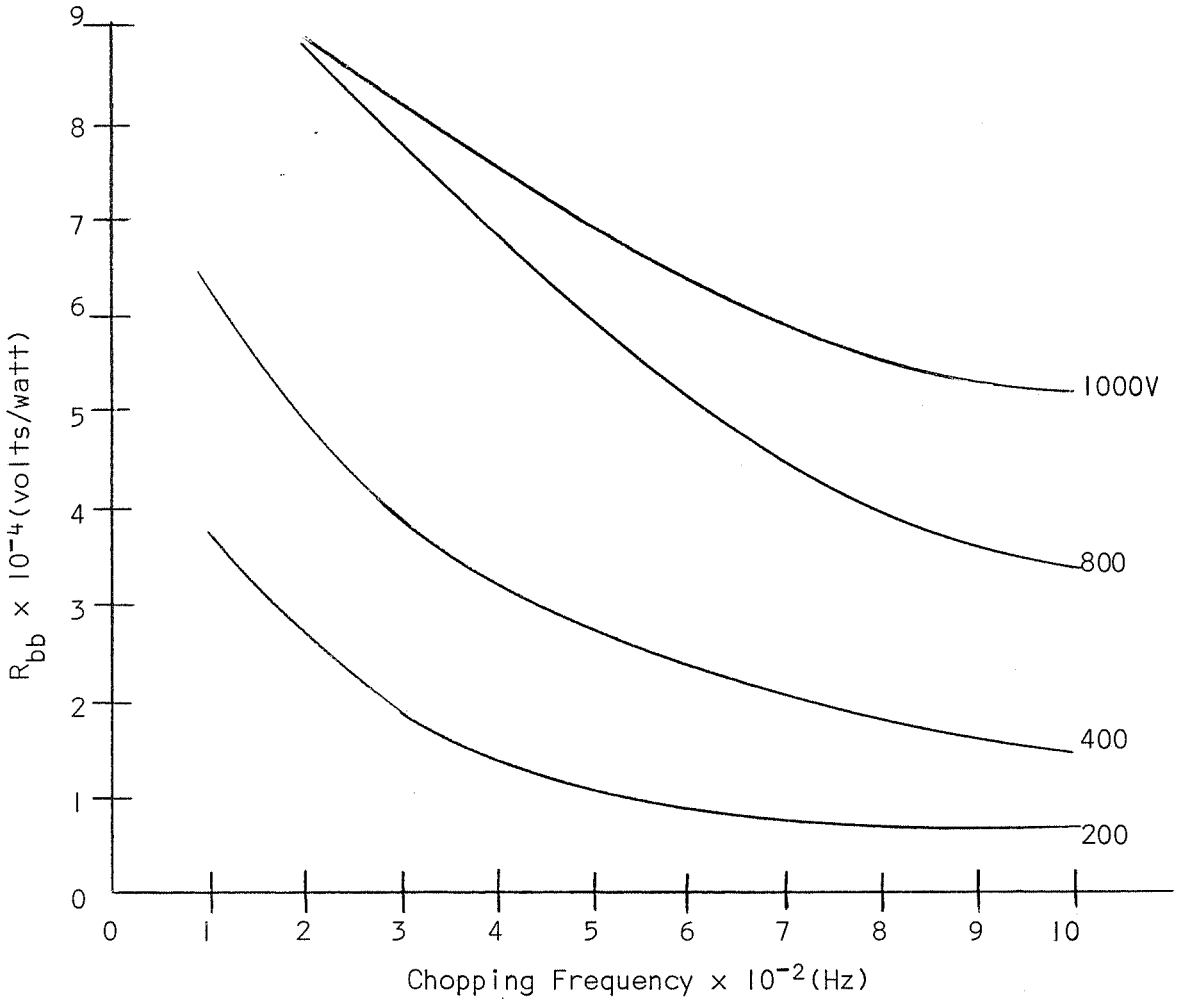

Figure 2.6 Black-body Responsivity as a Function of Chopping Frequency with Bias Potential as a Parameter for p-type Device 436P.1

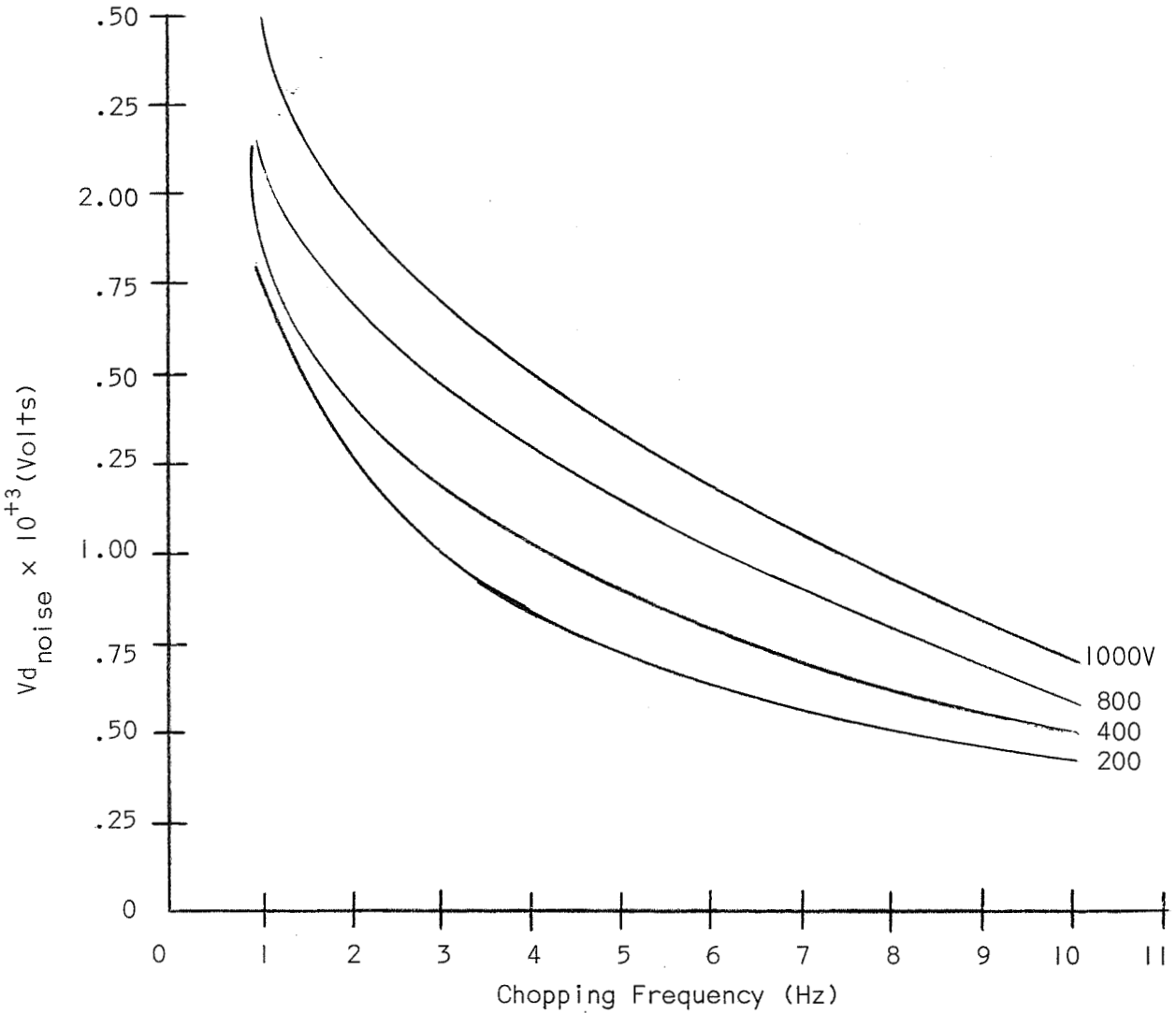

Figure 2.7 Device Noise as a Function of Measuring Frequency with Bias Potential as a Parameter for p-type Device 436P.1

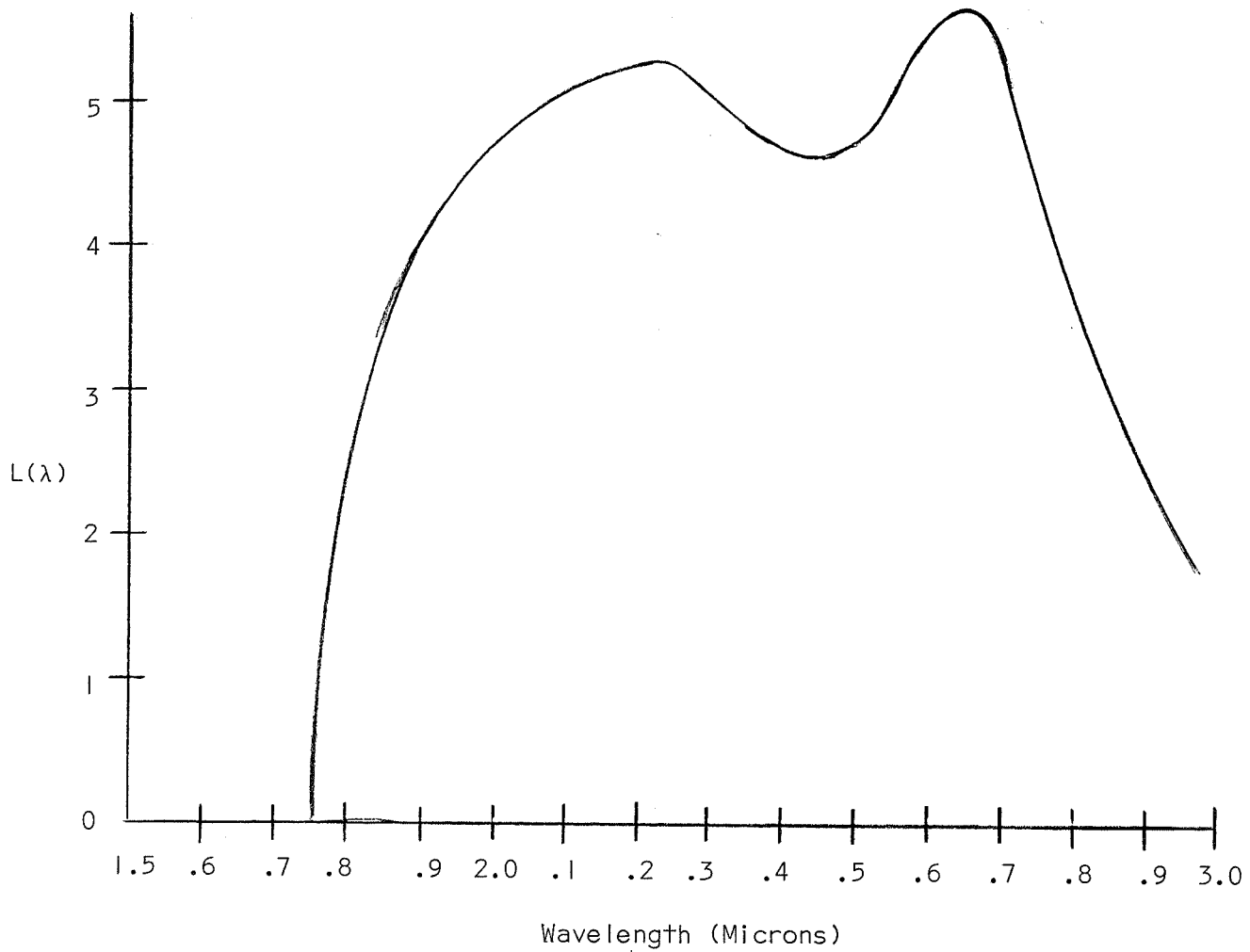

Figure 2.8 Relative Spectral Responsivity for p-type Device 436P.1

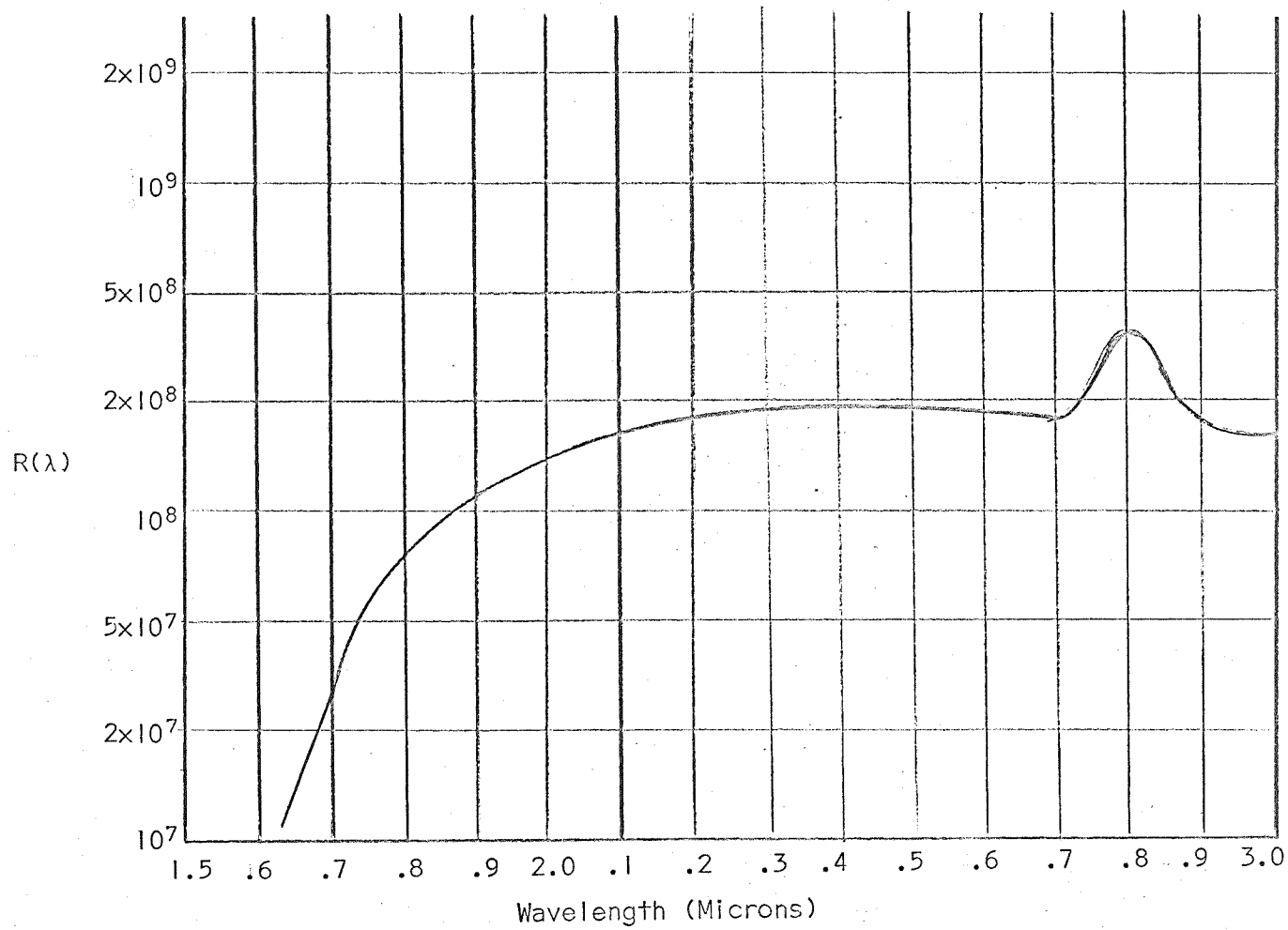

Figure 2.9 Absolute Spectral Responsivity for p-type Device 436P.1

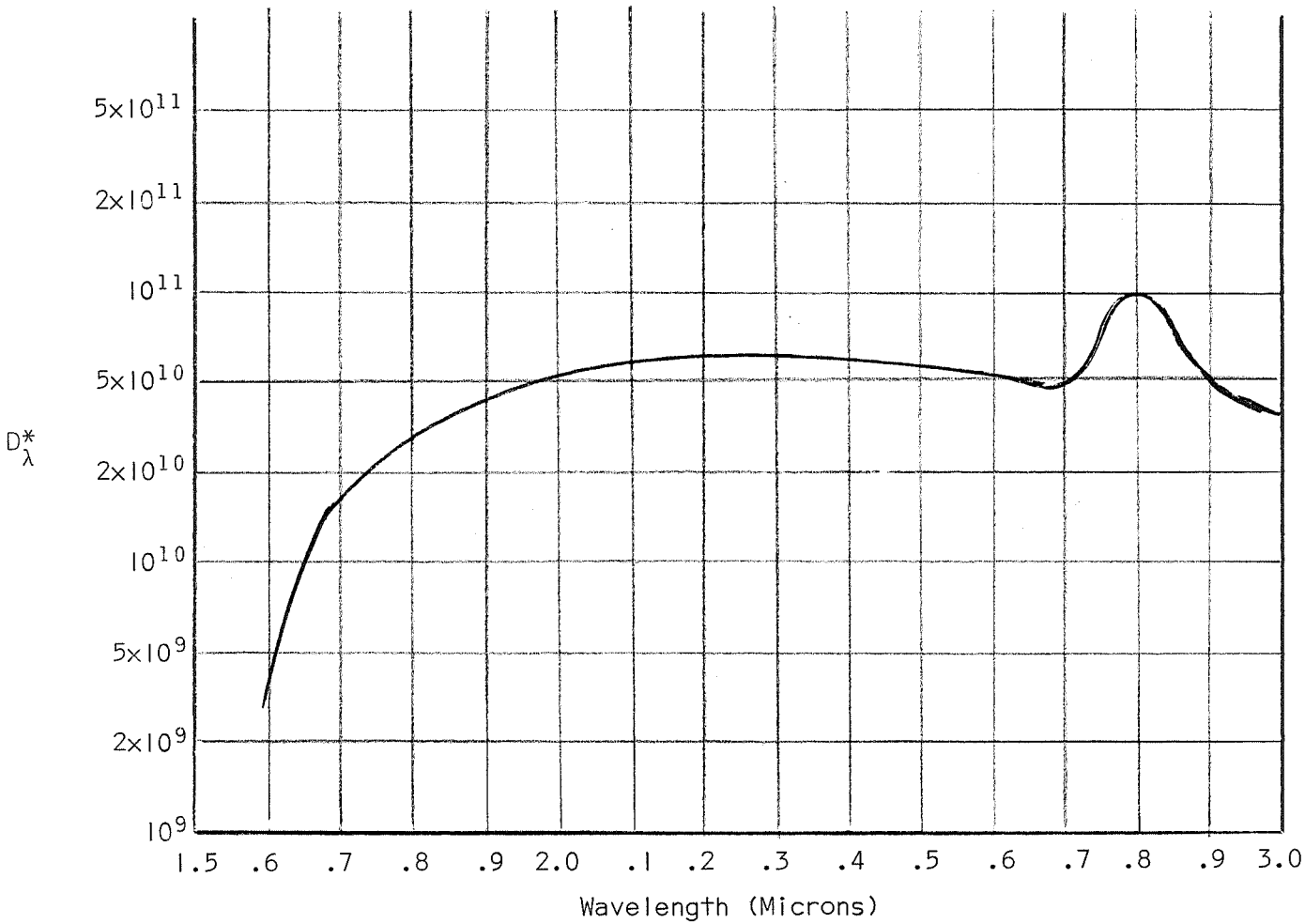

Figure 2.10 Spectral Detectivity for p-type Device 436P.1

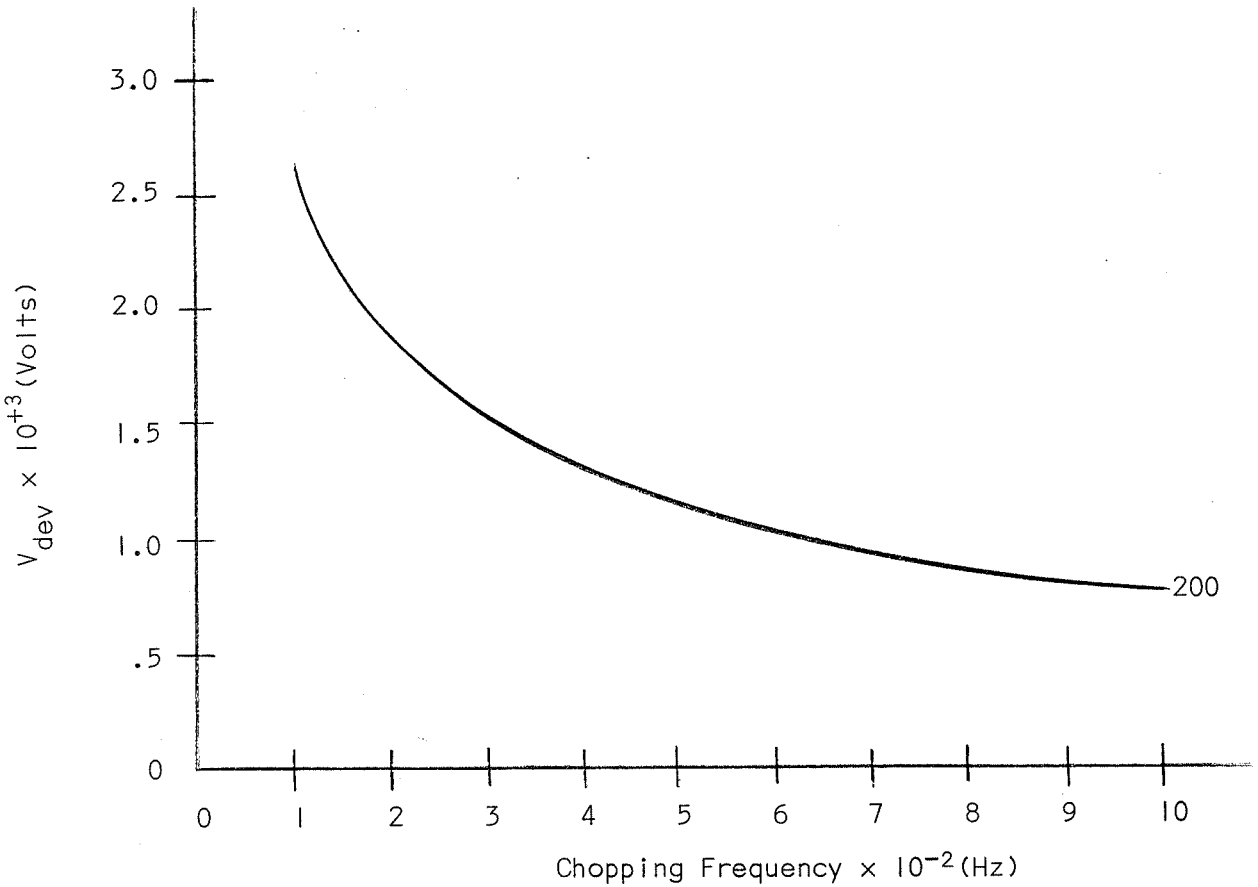

Figure 2.11 Black-body Responsivity as a Function of Chopping Frequency for a Typical n-type Germanium Device.

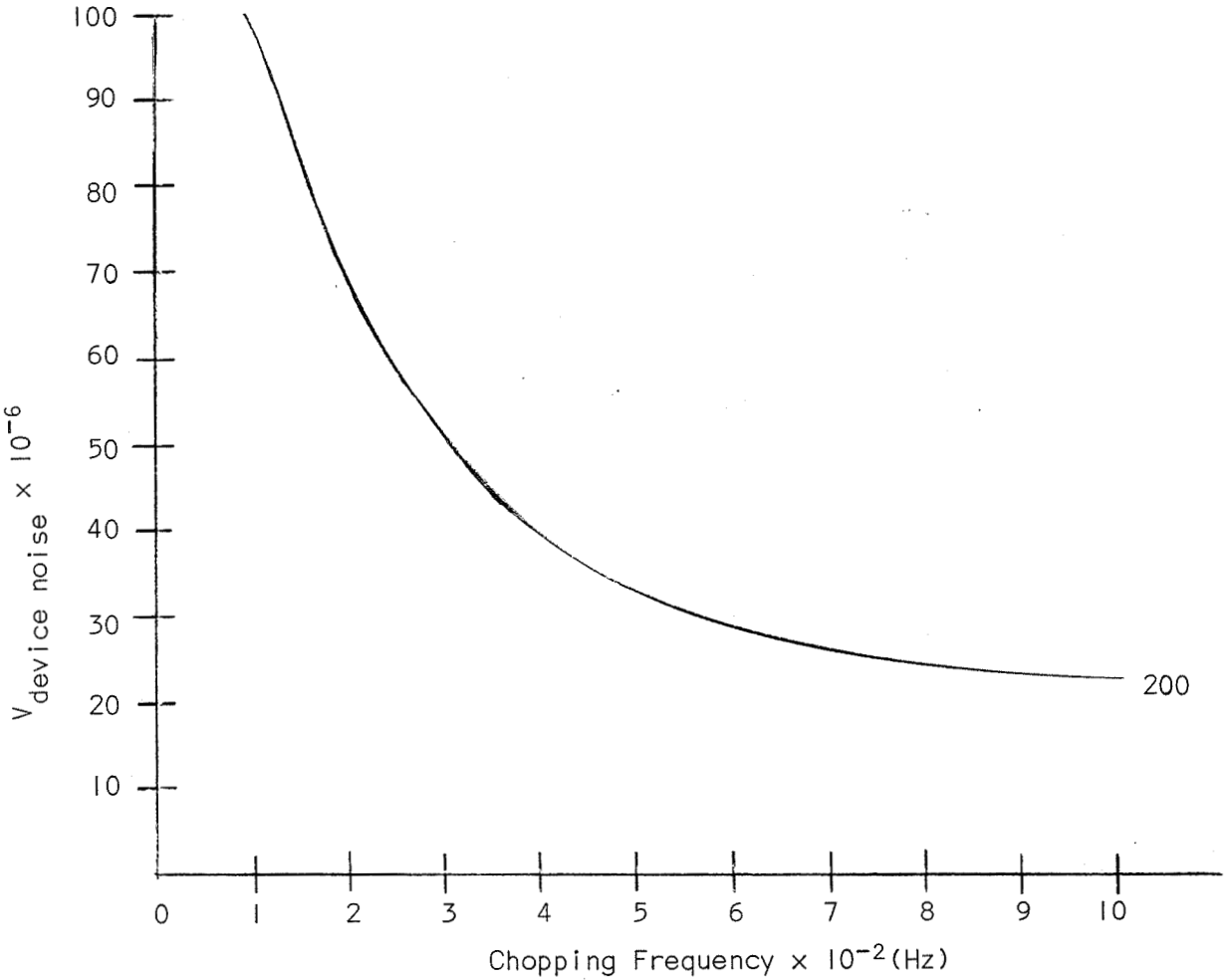

Figure 2.12 Device Noise as a Function of Measuring Frequency for a Typical n-type Germanium Device

III. CONCLUSIONS

As can be seen from the spectral results for the n-type silicon, the onset of increased photoconductivity occurs for a wavelength the energy of which is approximately .42eV. This is the distance from the silicon E-center (phosphorous-vacancy complex) to the conduction band and hence is attributed to an increase in conduction band electron population due to transitions from the E-center to the conduction band. The spectral results for p-type silicon show the highest spectral response for infrared photons the energy of which is greater than approximately .27eV. This value of energy is the same as the spacing between the valence band and a radiation induced donor type center believed due to an oxygen atom associated with an interstitial atom.

It can be concluded that since the black-body responsivity of silicon is rather high in comparison with that for germanium the former has much more potential as an infrared detector. With electron mobilities in the same order of magnitude for both materials one would conclude that if the 77°K resistivities of devices from both materials is nearly the same then the infrared photon cross section of the silicon centers is greater than that for those of germanium.

Future work will deal with optimization of the spectral detectivity for both p- and n-type electron irradiated silicon. Details of the optimization steps to be followed can be found in the proposal submitted for the renewal of the grant which supports this project.

PUBLICATIONS

1. R. J. Mattauch, "Comparison of Exact and Measured Open Circuit Photoconductor Voltages," Review of Scientific Instruments, Vol. 40, pp. 574-577, April 1969.

APPENDIX A

DETERMINATION OF THE PRESENCE AND DEGREE OF PHOTOCONDUCTIVITY DUE TO RADIATION INDUCED DEFECT LEVELS IN SILICON

A Thesis

Presented to

the Faculty of the School of Engineering and Applied Science

University of Virginia

In Partial Fulfillment

of the Requirements for the Degree

Master of Electrical Engineering

Allen M. Barnwell, Jr.

June 1969

APPROVAL SHEET

This thesis is submitted in partial fulfillment

of the requirements for the degree of

Master of Electrical Engineering

_____

Author

Approved:

_____

Faculty Adviser

_____

Dean, School of Engineering and
Applied Science

June 1969

ABSTRACT

The fact that irradiated silicon exhibits extrinsic photoconductivity is shown. Reasons to suspect this fact are presented, as is a discussion of the defect levels causing this photoconductivity. Experimental methods for determining the degree of photoconductivity are discussed, and the development of a system which enables the researcher to make this determination is described.

Results showing the performance of the detector characterized by accepted figures of merit are given. The response of the photoconductor to monochromatic radiation in the range from 1μ to 20μ is shown, as is the response to changes in other parameters. An investigation of the determination of the dominant mechanism causing photoconductivity in irradiated silicon is made.

ACKNOWLEDGMENTS

The author wishes to express his gratitude to Dr. R. J. Mattauch for his assistance, guidance, and encouragement on this research. Special thanks are given to J. H. Highfill and T. J. Viola for technical advice and assistance.

The author also expresses his gratitude to the University of Virginia and the 3-M Company for their financial support during the period of this research.

TABLE OF CONTENTS

TABLE OF CONTENTS (continued)

LIST OF TABLES

LIST OF FIGURES

LIST OF FIGURES (continued)

LIST OF SYMBOLS

A_0	Device area
c	Speed of electromagnetic propagation
D	"Detectivity" (not to be mistaken for D^*)
D^*_λ	Spectral detectivity
e	Charge of carrier
$E_1(\lambda)$	Device output from a spectral source
$E_2(\lambda)$	Bolometer output from a spectral source
E_a	Energy of acceptor level
E_c	Energy level of bottom of conduction band
E_{cir}	Circuit noise
E_d	Energy of donor level
E_f	Fermi level
E_g	Gap energy
E_i	Intrinsic Fermi level $[1/2\ (E_c+E_v) + 1/2\ kT(\frac{N_v}{N_c})]$
E_T	Total noise voltage
E_v	Energy level at the top of the valence band
f	Chopping frequency
Δf	Noise bandwidth of measuring instrument
g	System gain
G	Generation rate of free carriers
h	Planck's constant
H	Irradiance

LIST OF SYMBOLS (continued)

$\overline{i_{N^2}}$	Mean square noise current
I_0	Radiation incident on chopper
J_1	First order Bessel function
J_{rms}	r.m.s. value of fundamental component of radiant energy flux
k	Boltzmann's constant
$L(\lambda)$	Ratio of $E_1(\lambda)$ to $E_2(\lambda)$
n	Density of free carriers
n_i	Density of electrons in intrinsic material
n_0	Thermal equilibrium density of electrons
N_a	Net density of acceptors
N_c	Effective density of states in the conduction band
N_d	Net density of donors
N_v	Effective density of state in valence band
N(f)	Root power spectrum of device noise
N(t)	Number of photons per unit time striking the detector
NEI	Noise equivalent input
NEP	Noise equivalent power
p_0	Thermal equilibrium density of holes
P	r.m.s. incident radiant power on device
P_{rms}	r.m.s. black body power
$P(\lambda)_{rms}$	Spectral power of P_{rms}

r	Half the chopping tooth width where the tooth-notch ratio is unity
R_a	Radius of collimator aperture
R_{bb}	Black body responsivity
R_{cal}	Calibration resistor resistance
R_d	Device resistance
R_L	Load resistor resistance
$R(\lambda)$	Spectral responsivity
v_{cal}	Calibration signal voltage
v_0	Bias voltage
v_N	Noise voltage in bandwidth Δf
$\Delta v_{RL}, v_s$	Device signal output voltage
β	Spin degeneracy factor
λ	Wavelength of incident radiation
μ	Free carrier mobility
ν	Electromagnetic frequency
σ	Conductivity
τ_n	Free carrier lifetime

CHAPTER I

INTRODUCTION AND SUMMARY

This thesis reflects work accomplished in the past 15 months on a research grant supported by the National Aeronautics and Space Administration. The main purpose of this grant is to determine the possibility of using irradiated silicon as a photoconductive infrared detector. Devices currently being used for this purpose, the most notable being the lead sulfide cell, are extremely delicate and somewhat unstable. Devices of comparable performance made of irradiated silicon would offer advantages in physical strength, economy of production, and low level radiation resistance.

This thesis consists of three chapters and an Appendix in addition to the present chapter. The second chapter is devoted to presentation of theory outlining reasons to suspect that irradiated silicon does exhibit photoconductivity. Included are sections on the theory of extrinsic photoconduction in semiconductors and on figures of merit with which one assesses the relative value of photodetectors. Another section discusses the fact that irradiation introduces acceptor levels in n-type silicon and donor levels in p-type silicon. A synopsis of research done to determine the location of these energy levels within the forbidden gap and to identify the mechanisms involved in producing these levels will be presented for the two dominant cases, the Si-A

and Si-E centers. These centers will be identified as vacancy-impurity complexes; the impurity atom being oxygen in the case of the Si-A center and the dopant atom for the Si-E center. The final section of this chapter will relate the two previously mentioned subjects to explain why photoconductivity in irradiated silicon was suspected.

The third chapter presents the instrumentation used to experimentally determine that irradiated silicon does in fact exhibit photoconductivity. Procedures through which the various figures of merit were determined are explained. Sections are devoted to a description of the development of the original system which was used to obtain black body data and to a description of the subsequent development of an improved and consolidated system presently being used which incorporates both spectral and black body capabilities.

Chapter four presents results obtained in this investigation to date. Definite trends have been established concerning the effects of chopping frequency of incident radiation, of bias voltage across the device, and of annealing on the black body responsivity, R_{bb}, of devices of n-type irradiated silicon of various initial resistivities (1.0, 0.4, 0.1, and 0.03 ohm-cm.). Similar, but less definite, observations have been made on p-type material with initial resistivities of 10, 1.0, and 0.1 ohm-cm. With the final development of the consolidated system, data concerning the response to

incident radiation of wavelength from 1μ to 20μ has become available. The perfection of a computer program which calculates various spectral figures of merit has enabled the researcher to find spectral detectivity, D^*_λ, as a function of modulation frequency of incident radiation and bias voltage across the device as well as wavelength of incident radiation. From the peak response one can identify the dominant mechanism causing photoconductivity in this material.

The Appendix deals with the procurement, preparation, irradiation, and mounting of samples. Included is a description of the accelerator used for irradiation, and the procedures used to determine the total number of particles bombarding the samples.

Based on the results obtained to date, irradiated silicon promises definite possibilities as a useable photoconductor. The peak response for n-type devices appears at a wavelength close to that of lead sulfide. Although spectral detectivities for these devices have been found to generally be at least an order of magnitude less than those of lead sulfide, further work in noise reduction in and in optimization of irradiated silicon photoconductors should produce a competitive infrared detector.

CHAPTER II

THEORY

2.1. PHOTOCONDUCTIVITY

2.1a. Definition and History

A photoconductor is defined as a material whose electrical conductivity is increased by the absorption of radiation incident upon the material. The discoverer of this effect is acknowledged to be Willoughby Smith [1], who in 1873 noticed a decrease in the resistance of selenium when illuminated. Although this effect was investigated during the following years, cells sensitive enough to be useful for most practical applications were not developed until the Second World War. The most notable of these cells were the lead salt cells which even today find extensive use. Until development of these cells most photoconductors consisted of one of three materials: selenium, cuprous oxide, or thallous sulfide. Included in this category was Case's famous "thalofide" cell of thallous sulfide. The development and rapid growth of solid-state technology has caused photoconductivity to assume a very important role in research and in practical applications. Prior to the lead salt cells the most widely used radiation detectors were thermally sensitive thermoelectric detectors, or bolometers. The lead salt and solid state cells with their greater sensitivity and faster response times have virtually replaced these thermal

detectors for most useful applications. Presently the majority of photoconductors are based almost exclusively on the three lead salts (lead sulfide, lead selenide, and lead telluride), compound semiconductors (such as cadmium sulfide and cadmium selenide), and impurity bulk semiconductors (such as doped germanium). Uses for these devices include radiation detectors, control devices, applications in computer technology, television cameras, electrophotography, x-ray intensifiers, and picture reproduction and display.

As previously stated photoconductivity is a property of a material which causes its electrical conductivity to be increased by the absorption of radiation; the absorption freeing bound charge carriers which contribute to the conductivity. This photoeffect is therefore an important aid in the determination of such material parameters as carrier lifetime, carrier mobility, trapping levels, and imperfection level locations. There are other important photoeffects, but the photoconductor has been the most extensively employed for the reasons of the simplicity of the mechanism and of the fast speed of response. Two of the more important of these other photoeffects are the photovoltaic effect, in which the action of photons produce a voltage which can be detected directly without need of external elements, and the photoelectromagnetic effect which occurs in a semiconductor immersed in a magnetic field.

As the title of this thesis implies, the material being investigated for possible photoconductive properties is irradiated

silicon. The fact that irradiation produces acceptor or donor levels, depending upon substrate type, in the forbidden gap will be demonstrated in the next section of this chapter. Thus the investigation will involve an extrinsic semiconductor, and consequently from this point theoretical development will be toward that of photoconduction in extrinsic semiconductors.

2.1b. Elementary Mathematical Treatment

An intrinsic semiconductor in thermal equilibrium contains carriers whose concentrations are determined by such parameters as temperature, effective masses of electrons and holes, and gap energy of the material. The absorption of photons from incident radiation excites bound electrons in the valence band across the forbidden energy gap to become free electrons in the conduction band, thereby creating free electrons and free holes. The absorbed photons must therefore have energies great enough to excite electrons across the gap; the minimum energy to meet this requirement is given by the relation

$$E_g = h\nu = \frac{hc}{\lambda} \tag{2.1}$$

where E_g = gap energy

h = Planck's constant

c = speed of light

ν = frequency of incident radiation

λ = wavelength of incident radiation.

In an extrinsic semiconductor photon absorption will cause transitions between impurity levels lying within the forbidden gap and the conduction or valence band. For this type of material either free holes and bound electrons, or bound holes and free electrons are produced. For example, in an extrinsic semiconductor with donor levels electrons are freed through absorption of photons of minimum energy E_0, the energy difference between the donor level and the bottom of the conduction band. The corresponding minimum frequency, ν_0, and maximum wavelength, λ_0, of incident radiation are thus given by the relation

$$E_0 = h\nu_0 = \frac{hc}{\lambda_0}. \tag{2.2}$$

In an extrinsic semiconductor with acceptor levels, free holes are formed when photons of energy greater than the energy difference between the acceptor level and the valence band are absorbed. Electrons are thus excited from the valence band to the acceptor level creating free holes in the valence band.

An elementary mathematical analysis can be performed to determine mechanisms affecting photoconductivity in a given extrinsic semiconductor. Consider such material in which one type of carrier is considered to dominate the conductivity. Then

$$\sigma \simeq ne\mu_n \tag{2.3}$$

where n = density of free carriers

e = charge of free carriers

μ_n = mobility of free carriers.

Upon illumination the conductivity will change, this change being caused by either a change in free carrier density or the carrier mobility or both.

Then (2.3) becomes

$$\sigma + \Delta\sigma = (n + \Delta n)\, e\, (\mu + \Delta\mu) \tag{2.4}$$

where $\Delta\sigma$, Δn, $\Delta\mu$ refer to the change from the original values in (2.3). Then

$$\sigma + \Delta\sigma = ne\mu + \Delta ne\mu + \Delta\mu en + \Delta n\Delta\mu e \tag{2.5}$$

leading to

$$\Delta\sigma \simeq \Delta ne\mu + \Delta\mu en. \tag{2.6}$$

Thus a change in conductivity can result from a change in the density of free carriers or a change in their mobility.

Illumination causes carriers in excess of those produced by normal thermal generation, hence Δn refers to those excess carriers produced by illumination of the material. The rate at which these excess carriers are produced will be related to the intensity of incident radiation through the quantum efficiency of the process.

The change in the density of free carriers, Δn, is directly related to the intensity of excitation, G, through the free-carrier lifetime, τ_n [1].

$$n = G\tau_n \tag{2.7}$$

where $G = cm^{-3}sec^{-1}$

$$\Delta n = \Delta G\tau_n + \Delta\tau_n G \tag{2.8}$$

giving

$$\Delta\sigma = (\Delta G\tau_n + \Delta\tau_n G)e\mu + \Delta\mu en \tag{2.9}$$

or

$$\Delta\sigma = \Delta G\tau_n\mu e + \Delta\tau_n Ge\mu + \Delta\mu en. \qquad (2.10)$$

Each of the terms in the above equation thus represents at least one mechanism for photoconductivity. The most important of these terms is the first, $\Delta G\tau_n e\mu$, in which the conductivity is changed because of a change in the intensity of photoexcitation. The generation rate of free carriers increases, but the carrier lifetime remains the same. This term will be the dominant one in practically all cases. The second term, $e\mu G\Delta\tau_n$, includes those effects in which the lifetime is a function of photoexcitation. For example, if the probability of recombination becomes greater with photoexcitation, $\Delta\tau_n$ could become negative, decreasing the sensitivity of the photoconductor. The third term, $\Delta\mu en$, includes those effects in which the mobility is affected by photoexcitation. An example of this effect would be the excitation of carriers from one state with a given mobility to another state with a higher mobility.

In order to evaluate the performance of the photoconductor some scheme of measurement of the output must be found. To detect the change in conductivity, a change in voltage across or current through the photoconductor must be detected. This detection could be accomplished by means of a detector circuit consisting of a battery, or d.c. voltage source, in series with the photoconductor and a load resistor.

Time varying radiation absorbed by the photoconductor will cause a changing resistance, R_d, giving rise to a time varying

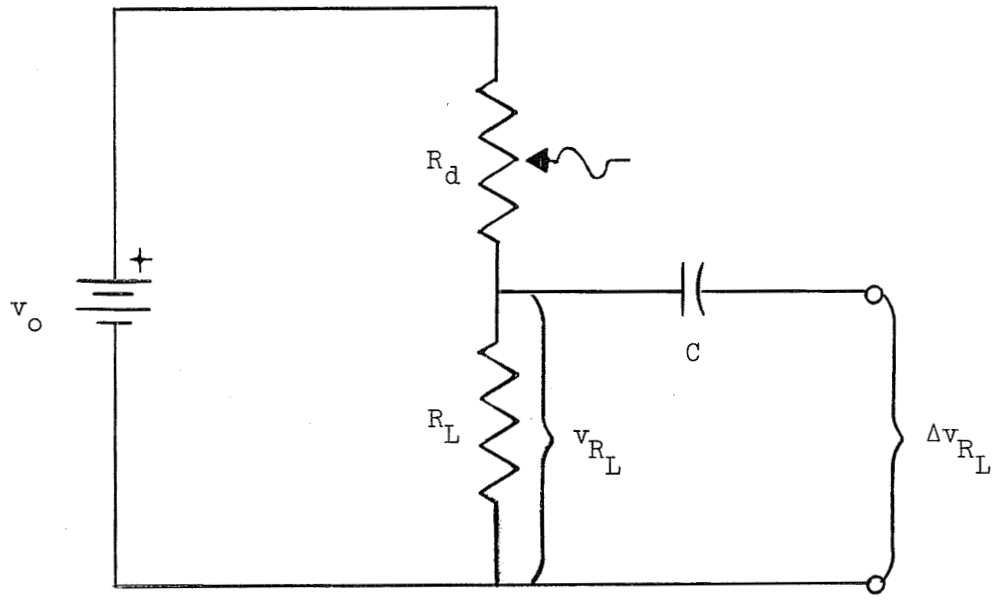

Figure 2.1 An Elemental Detection Circuit

voltage across R_L. This voltage provides a measure of the effectiveness of the photoconductor to convert radiant energy to electrical energy.

Initially

$$v_{R_L} = v_0 \frac{R_L}{R_d + R_L}. \tag{2.11}$$

Upon illumination R_d decreases by ΔR_d causing v_{R_L} to change by Δv_{R_L}, giving

$$\Delta v_{R_L} \simeq - \frac{v_0 R_L \Delta R_d}{(R_d + R_L)^2}. \tag{2.12}$$

Equation 2.12 shows that the time-varying voltage Δv_{R_L} will be directly proportional to the change in device resistance.

For maximum signal output per unit of radiant flux, R_L should be chosen equal to R_d so that 2.12 becomes

$$\Delta v_{R_L} = - \frac{v_0 \Delta R_d}{4R_d}. \tag{2.13}$$

This consideration provides a means of measuring the change of conductivity of the photoconductor upon illumination.

2.1c. Noise in Semiconductors

Another important parameter that should be discussed before considering figures of merit is noise. In semiconductors, noise plotted as a function of frequency follows roughly the shape of the curve shown in Fig. 2.2.

At high frequencies the dominant noise is thermal noise arising

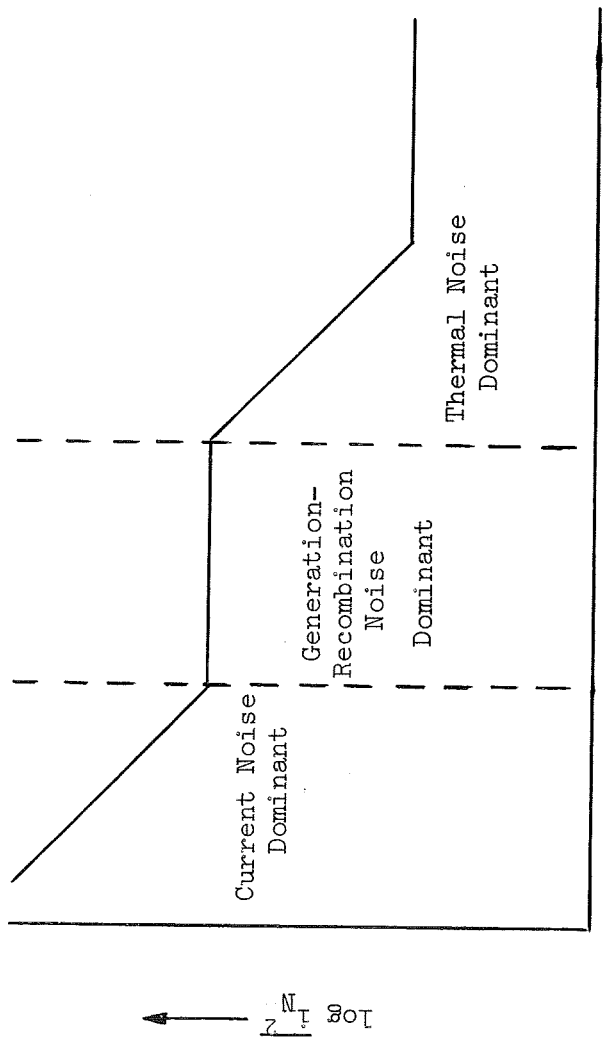

Figure 2.2 Spectrum of Noise Current in Semiconductors

from the random motion of charge carriers. In the intermediate frequency range generation-recombination noise becomes dominant. This noise is caused by fluctuations in the instantaneous values of the free carrier densities due to the random character of the generation, recombination, and trapping processes. The dominant noise at low frequencies is current noise. The power spectrum of current noise resembles the form of "flicker" noise in tubes, the relation determined experimentally being [2]

$$\overline{i_N^2} = \frac{K_1 I^{\alpha} \Delta f}{f^{\beta}} \tag{2.14}$$

where $\overline{i_N^2}$ = the power spectrum of current noise

$\alpha \approx 2$

$\beta \approx 1$

K_1 = a constant

Δ_f = noise bandwidth.

Several sources of this noise have been suggested, but the most widely accepted theories associate this noise with electrical contacts and with surface effects.

The importance of achieving a low level of noise in photoconductors cannot be overemphasized. This fact will become even more apparent upon presentation of the figures of merit which show the ultimate limiting factor of the photoconductor performance to be noise.

2.1d. Figures of Merit

In evaluating a photodetector the researcher assesses its relative value by means of generally accepted figures of merit. By presentation of these figures of merit one should be able to judge the capabilities of the device. Kruse et al [2] states that the most important of these figures of merit can be grouped into four categories:

(1) those figures of merit which show the minimum intensity of radiant power falling on a detector which will give rise to a signal voltage equal to the noise voltage across the detector (The signal voltage being that time-varying voltage, Δv_{R_L}, appearing across R_L in the circuit of Fig. 2.1);

(2) those figures of merit which provide a measure of the signal voltage obtained per unit of radiant power falling on the detector;

(3) those figures of merit that relate signal output to wavelength of the radiation;

(4) those figures of merit which provide a measure of the detector's response to the modulation frequency of the incident radiation.

In presenting figures of merit, certain parameters should also be specified due to the fact that in most cases the output signal is highly dependent upon operating conditions. These specifications

should include, as a minimum, the type and spectral distribution of the radiation source, the device operating temperature, the device resistance, and the device area exposed to radiation. Other operating conditions could be included for more complete assessment of the device's performance.

A common figure of merit used to relate the radiative power necessary to produce a signal-to-noise ratio of unity is the noise equivalent power, NEP. It is defined as the r.m.s. value of modulated radiation falling on a detector necessary to cause the r.m.s. signal voltage to be equal to the r.m.s. noise voltage. The noise equivalent power is given by the relation [2]

$$\text{NEP} = H\, A_0 \left(\frac{v_n}{v_s}\right) \frac{1}{(\Delta f)^{1/2}} \quad \frac{\text{watts}}{(\text{cps})^{1/2}} \tag{2.15}$$

where H = r.m.s. value of the irradiance (the radiation power incident per unit of surface area, $\frac{\text{watts}}{m^2}$)

A_0 = area of device

v_n/v_s = the ratio of the r.m.s. noise voltage in the bandwidth Δf to the r.m.s. signal voltage.

A less widely used figure of merit is the detectivity, D, not to be mistaken for D^*. This figure of merit expresses the signal-to-noise voltage ratio obtained per watt of radiant power, the reciprocal of the NEP. The general practice presently in use is to refer to D^*, which will be discussed shortly, as "detectivity" since D is no longer a widely used figure of merit. Any future

reference to detectivity will therefore refer to D^*.

In order to discuss D^*, a presentation of the noise equivalent input, NEI, must be made. NEI is the radiant power per unit of detector area required to produce a signal-to-noise ratio of unity. Hence [2]

$$NEI = \frac{NEP}{A_0} = \frac{1}{A_0 D} \quad \frac{\text{watts}}{\text{cm}^2(\text{cps})^{1/2}}. \tag{2.16}$$

D^* (pronounced dee-star) is an area independent figure of merit found by the relation [2]

$$D^* = \frac{1}{(NEI)\ A_0^{1/2}} = \frac{A_0^{1/2}}{NEP} = DA_0^{1/2} \quad \frac{\text{cm. cps}^{1/2}}{\text{watt}}. \tag{2.17}$$

This figure of merit provides an area independent measure of the r.m.s. signal-to-noise ratio per unit of radiant power.

The preceding figures of merit could be best classified as falling into the first of the four mentioned categories. If the magnitude of the output signal per unit radiant power is considered, a figure of merit falling into the second category is found. The figure of merit, responsivity, R, is defined as the r.m.s. signal voltage, v_s, per unit r.m.s. radiant power, P, incident upon the detector [2].

$$R = \frac{v_s}{P} \quad \frac{\text{volts}}{\text{watt}}. \tag{2.18}$$

For the figures of merit already listed, the response was considered due to a source with known spectral distribution such as a black body operated at a known temperature. These figures of

of merit can also be expressed in terms of their response to monochromatic radiation, becoming NEP_λ, NEI_λ, D_λ, D^*_λ, and R_λ. The third category is most adequately portrayed by one of the aforementioned figures of merit given as a function of wavelength.

Relative response given as the relative signal voltage per unit monochromatic radiant power as a function of the wavelength also falls into this category. The fourth category can best be described by taking the responsivity as a function of the frequency of modulated incident radiation, R(f).

Before proceeding to the next chapter there are details that require further explanation. The figures of merit presented characterize not only photoconductors but the entire range of photodetectors. Other figures of merit exist exclusively for photoconductors, but the figures of merit chosen were so selected because of their generality and widely accepted use. From the discussions thus far it is seen that there are many variables which can affect any figures of merit determined. To gain a complete analysis of the photoconductor under investigation the effects of these variables on device signal output should be investigated and optimum operating conditions determined.

2.1e. Comparative Analysis of Some Presently Used Photoconductors

Having discussed the means by which the relative value of a photoconductor is assessed a comparison of the characteristics of and of the performance of some of the more widely used types is

given. These photoconductors are generally prepared in one of two forms, thin film or sliced single crystal. The thin films have thicknesses usually on the order of 1μ, while the sliced crystals generally have thicknesses exceeding 1mm. The thin films exhibit less desirable characteristics in that the polycrystalline deposited state results in nonuniformity and has a tendency to be more current noise limited than the sliced crystals. Reproducibility of similar devices is poorer in the thin films in addition to the obvious physical strength deficiency [2]. Intrinsic photoconduction generally exhibits better qualities than the extrinsic case. Controlling of doping is not a severe limitation in intrinsic detectors, and the responsivity and optical absorption coefficient are generally higher in this type. The resistance of the photoconductor is another important comparison as this parameter determines amplifier needs. Devices are grouped into three categories when considering this parameter: low resistance detectors, $R_d < 100\Omega$; medium resistance detectors, $10^2\Omega$-$10^6\Omega$; and high resistance detectors, $>10^6\Omega$. In addition to amplifier requirements, the resistance also determines noise levels to some degree. High resistance may cause RC time constants, due to the low capacitance present in the detection circuit, considerably greater than the material lifetime resulting in reduced frequency response. The temperature of operation is another important comparison. Most of the photoconductors in wide use show a much improved performance at reduced

temperatures. Generally they are maintained at one of four temperatures: room temperature, 295°K; dry ice temperature, 195°K; liquid nitrogen temperature, 77°K; or liquid helium temperature, 4°K.

Having discussed a number of generalizations, particular types of photoconductors will be examined:

A. Lead sulfide (PbS) is used extensively for applications involving detection of radiation of wavelength below 3μ. It is prepared in two ways, either by chemical deposition or by sublimination in a vacuum. Cells made of this material are considered to be the best photocells available. These cells are thin film, intrinsic (0.37ev band gap) detectors usually operated below room temperature, but also extremely useful at room temperature. D^*_λ is usually in the 10^{11} $(\frac{\text{cm. Hz.}^{1/2}}{\text{watt}})$ range at optimum operation conditions. Its resistance remains in the 10^6 ohm range for temperatures as low as 77°K [2, 3, 4].

B. Lead selenide (PbSe) is another lead salt thin film operated at room temperature or below. It is prepared similarly to PbS and is used mainly as an uncooled detector of radiation in the 3μ to 4μ range or as a 77°K detector of 4μ - 6μ wavelength radiation. Typical detectivities range from 10^8 for uncooled detectors to 10^{10} at 77°K. Typical resistances range from 10^4 to 10^7 ohms in the same temperature interval [2, 3, 4].

C. Lead telluride (PbTe) is an intrinsic (0.30ev band gap) thin film photoconductor usefully sensitive at 77°K or below only.

It is usually prepared by vacuum sublimination and has a much higher resistance than PbS or PbSe. Its peak response occurs for radiation of wavelength 4.0μ [2, 3, 4].

D. Germanium (Ge) is not used as an intrinsic photoconductor because of its wide band gap (0.67ev). Considerable use has been found as an extrinsic photoconductor with dopants including gold, gold-antimony, zinc, zinc-antimony, copper, and cadmium. These extrinsic, sliced crystal photoconductors are usually operated at cryogenic temperatures and exhibit detectivities in the 10^{10} range at peak responses occuring at radiation wavelengths of 5μ - 20μ. Resistances lie in the $10^{6}\Omega$ region [2, 3, 4].

E. Indium Antimonide (InSb) is a compound semiconductor formed by melting stoichiometric amounts of indium and antimony. It is a single crystal operated at room temperature or below exhibiting detectivities on the order of 10^{7} at 295°K to 10^{10} at 77°K. Its resistance is low (~100Ω) above 195°K, but reaches ~10^{5} at 77°K [2, 4].

F. Indium Arsenide (InAs) is another intermetallic compound semiconductor, but is more difficult to manufacture than InSb. It is generally operated at 295°K, exhibiting a detectivity on the order of 10^{8} at a wavelength of 3.6μ [2].

G. Tellurium (Te) is a single crystal photoconductor exhibiting a peak D^{*}_{λ} in the order of 10^{10} at 3.5μ. Resistance is on the order of 10^{3} at its operating temperature of 77°K.

It is prepared from crystals grown by the Czochralski method [2].

H. Thallous sulfide (Tl_2S) is a thin film intrinsic photoconductor used mainly as a detector in infrared communications systems and is useful only at wavelengths less than 1.3μ. It is prepared by vacuum deposition, and exhibits a peak D^*_λ value in the 10^{12} range at 0.9μ at room temperature [2].

I. Silicon (Si) doped with group III or V impurities exhibits extrinsic photoconductivity at wavelengths ranging from 2μ to 38μ. Only recently have useful cells been produced. These cells exhibit detectivities on the order of 10^{10} while operating at temperatures of 23°K to 40°K [4, 5].

2.2. RADIATION DEFECTS IN SILICON

R. A. Soreff [5] has shown that extrinsic infrared photoconductivity is exhibited in chemically doped silicon, and that the peak response lies in the infrared range (2μ to 38μ). This particular investigation also involves the use of extrinsic silicon but is unusual in the fact that the silicon was "doped" by irradiation. Work done by E. Sonder and L. C. Templeton [6 - 8] of the Solid State Division of the Oak Ridge National Laboratory and G. Watkins and J. W. Corbett [9 - 11] of the General Electric Research Laboratory proved that electron or γ-ray irradiation of silicon produces net acceptor levels within the forbidden gap in n-type silicon and net donor levels in p-type silicon.

The author feels that a brief synopsis of the work of the aforementioned men will be beneficial to a more complete understanding of this investigation. Details involved with the location of these levels and with the models of the mechanisms causing them will be discussed, while discussion of the techniques used to arrive at these findings will be neglected due to the feeling that such a discussion is beyond the scope of this thesis.

In 1960, Sonder and Templeton [6] noted that the predominant effect of irradiating oxygen-containing n-type silicon was the production of a single discrete net acceptor level 0.17ev below the conduction band. This report substantiated the findings of a number of researchers in this field. Additional acceptor levels lying deeper in the gap were noted being introduced at a rate 50 times less than that of the E_c-0.17ev level. Cobalt 60 gamma-ray bombardment, which created Compton electrons of energies of 1 Mev or less within the silicon lattice, was used for the irradiation. These electrons were uniformly distributed, thereby causing a uniform distribution of damage sites within the lattice. The researchers noted that a rate of introduction of trapping sites would have been approximately an order of magnitude higher with the use of accelerator electrons (the rate being $\sim 10^{-3}$ trap/cm^3/photon/cm^2 or in terms of the Compton electrons $\sim 10^{-2}$ trap/cm^3/photon/cm^2).

In 1961, Corbett and Watkins [9] proposed a model of the

mechanism causing the level at E_c-0.17ev based upon spin resonance measurements. Subsequent work involving the identification of an absorption band at 12μ in the irradiated material confirmed the proposed model [10]. These researchers also found that the introduction rate of the Si-A center, the mechanism causing the E_c-0.17ev level, was lower in vacuum floating zone silicon than in pulled crucible silicon (the floating zone silicon has an oxygen concentration some 100 times lower than that of pulled crucible). The detailed model proposed by these researchers is shown in Fig. 2.3 and consisted of a vacancy associated with an oxygen atom. The oxygen atom bonds with two of the four bonds broken by the vacancy, while the remaining two broken bonds forms a molecular bond which could trap an additional electron. This trapping state was the level at E_c-0.17ev. The verification of this model thus implied that the silicon lattice vacancy introduced by the irradiation was mobile at room temperature.

Sonder and Templeton [6] reported findings on levels in n-type float-zone silicon in 1963. The Si-A center was again found being introduced at a rate comparable to that in oxygen-containing (pulled crucible) silicon as long as the donor concentration of the float zone silicon was less than 10^{16} donors/cm^3. An additional acceptor level was found at 0.47ev below the conduction band in phosphorous-doped silicon and E_c-0.43ev in antomony-doped silicon. This deeper level was found to anneal between

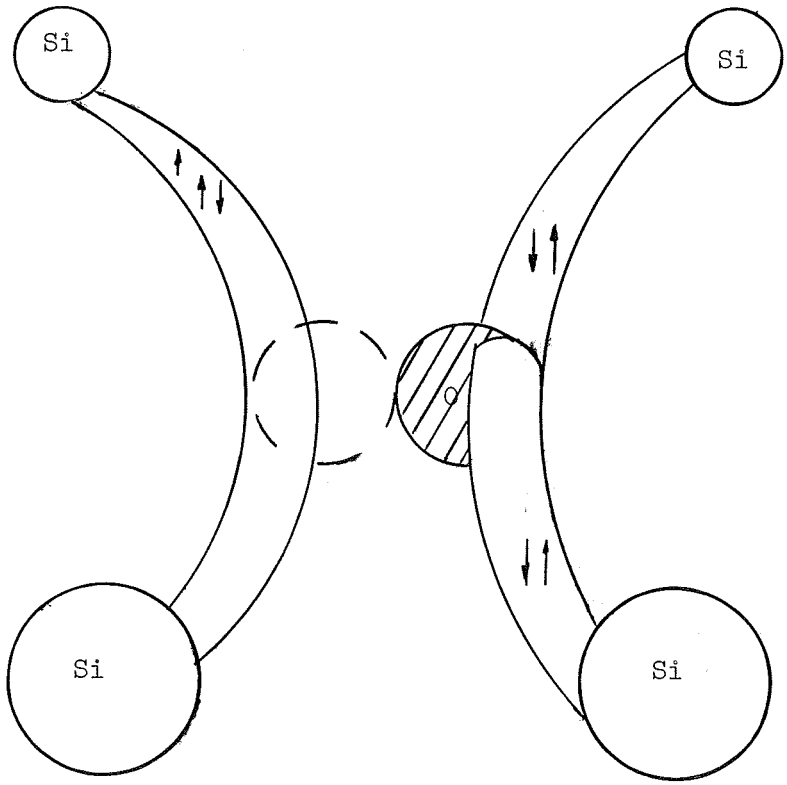

Figure 2.3 A Model of the Si-A Center

100°C and 150°C but even higher temperatures would not remove all the acceptors in this level.

Corbett and Watkins concluded that this level at E_c-0.47ev was the dominant level in float zone n-type silicon [11]. Again a model was proposed for the mechanism, the Si-E center, causing the acceptor level. The model for this center consisted of a mobile vacancy created by irradiation trapped by an impurity phosphorous (the dopant) atom. The model proposed that two of the three silicon atoms adjacent to the vacancy pulled together to form a pair bond with the unpaired electron left primarily to the third silicon atom.

Sonder and Templeton also reported findings on the location of levels in p-type materials [8]. They found that irradiation introduced donor levels in the lower half of the forbidden gap. For pulled crucible p-type silicon a level 0.35ev above the valence band was located; in float zone material a dominant level at E_v + 0.21ev and a weak level at E_v + 0.28ev were found. Similar mechanisms as those in n-type material were thought to cause these levels but no formal proof was offered.

The two centers, the Si-A and Si-E, were by no means the only ones found in irradiated silicon. Spin resonance techniques pointed out that irradiation caused many complex effects in the silicon lattice. The two mentioned, however, were the dominant ones for the given types of silicon. The Si-A was dominant in

pulled crucible, the Si-E center not being present. The Si-E center appeared dominant in float-zone material although the Si-A center was present in this type of irradiated silicon.

2.3. PHOTOCONDUCTIVITY IN IRRADIATED SILICON

Thus far this chapter has been concerned with two subjects, photoconductivity and defect levels in irradiated silicon. The only relation shown or implied between the two has been the fact that extrinsic photoconduction depends upon impurity levels within the forbidden gap. It is the purpose of this section to further relate the two subjects, to show why extrinsic photoconductivity in irradiated silicon is thought to be superior to intrinsic photoconductivity in a material whose gap energy is the same as the energy difference between the valence band and acceptor level in the extrinsic case, and finally to pose an experimental question.

In phosphorous doped float-zone irradiated silicon the energy levels appear as in Fig. 2.4. One would thus expect to observe extrinsic photoconductivity in irradiated silicon.

The question should arise as to why extrinsic photoconduction would be of greater degree than intrinsic photoconduction in a material whose band gap is equal to that of the energy difference involved in the transitions in the extrinsic case. One would suspect from previous discussion that the intrinsic case would be preferred. However previous research has shown that the resistivity

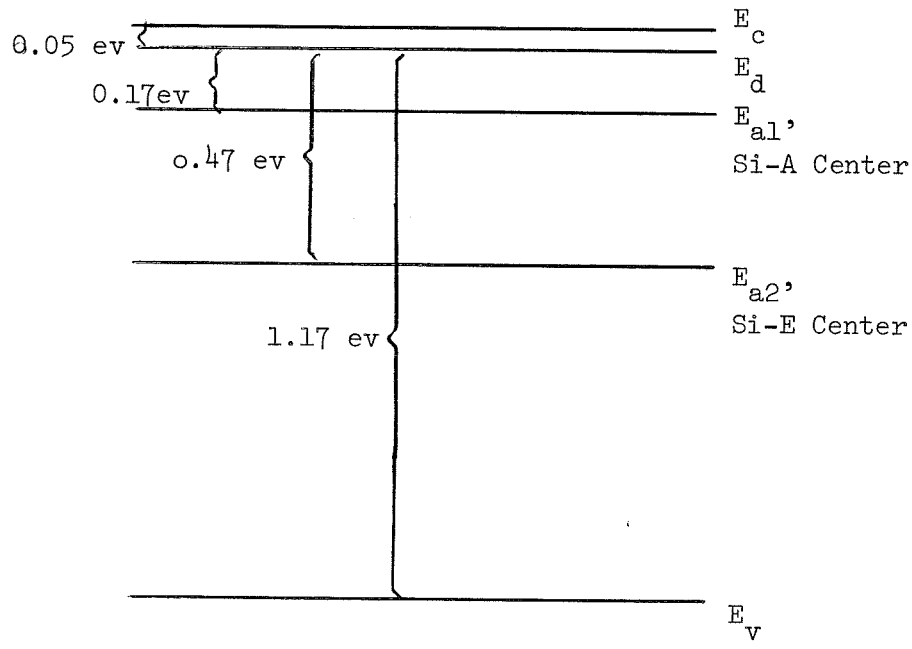

Figure 2.4 Energy Level Diagram of Irradiated Silicon

of irradiated silicon, unlike non-irradiated silicon, actually increased significantly at cryogenic temperatures [12]. Fig. 2.5 shows the temperature-resistivity characteristics of a 100 ohm-cm. sample before and after irradiation. This fact leads one to suspect that a change in conductivity in the higher resistivity material would be more significant than a change in the much lower resistivity one.

Consider the difference in the thermal equilibrium density of electrons at 77°K for the two cases mentioned:

1. An intrinsic material with 0.47ev as the band gap (the Si-E center is assumed dominant).
2. An extrinsic material with E_g = 1.15ev, N_d at E_d = E_c - 0.05ev, and N_a at E_c - 0.47ev.

In the intrinsic case, Maxwell Boltzmann statistics can be applied giving

$$n_0 = N_c \exp. \{-(E_c - E_f)/kT\} \tag{2.19}$$

$$p_0 = N_v \exp. \{(E_v - E_f)/kT\}. \tag{2.20}$$

Now

$$n_0 p_0 = n_i^2 = N_c N_v e^{-E_g/kT}$$

or

$$n_0 = \sqrt{N_c N_v}\, e^{-E_g/2kT} \tag{2.21}$$

where

$$N_c = 2 (2\pi m_e kT/h^2)^{3/2} \tag{2.22}$$

$$N_v = 2 (2\pi m_h kT/h^2)^{3/2}. \tag{2.23}$$

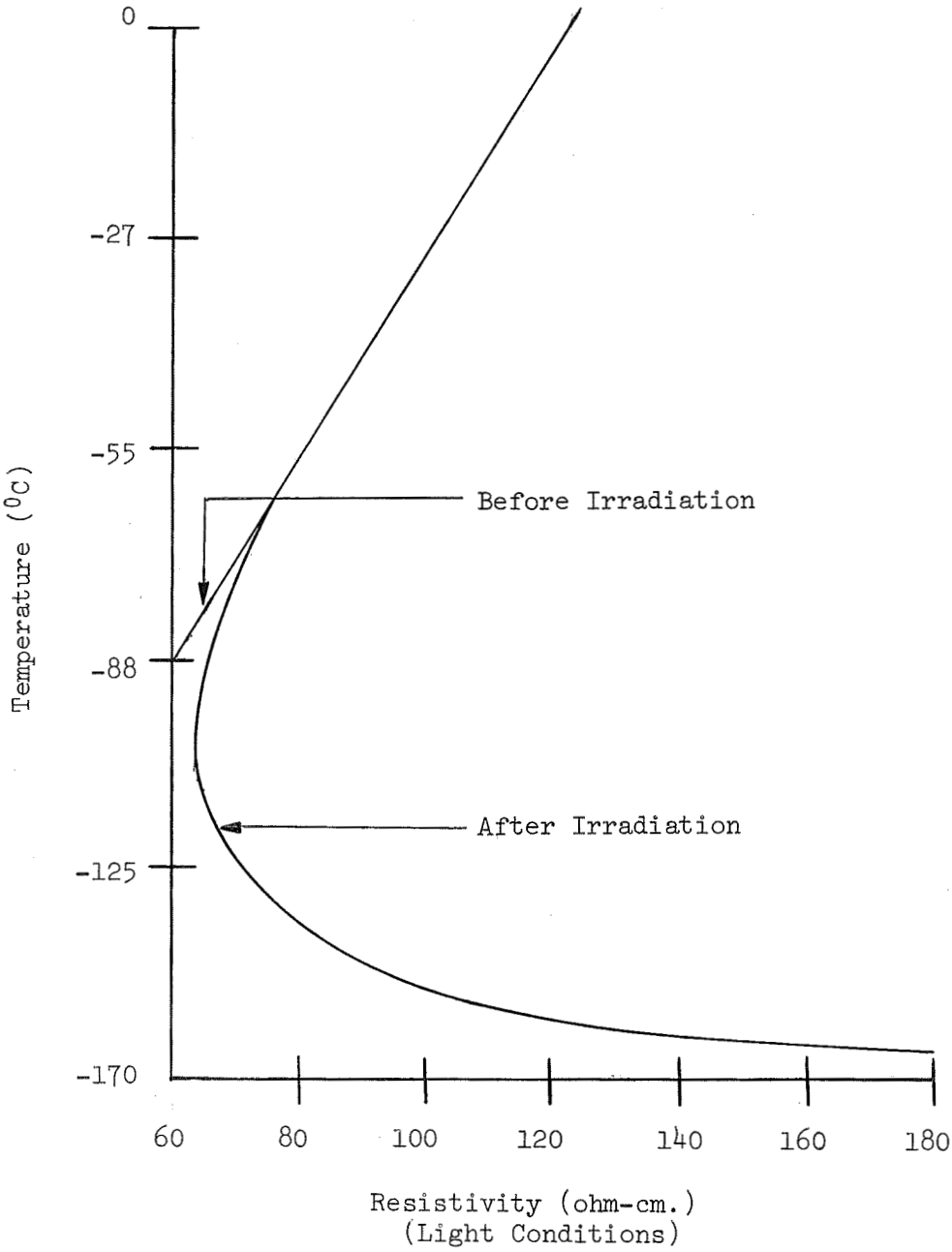

Figure 2.5 Temperature vs. Resistivity Characteristics for a 100 ohm-cm. n-Type Device

$$n_0 = 2\,(2\pi\ kT/h^2)^{3/2}\ (m_e\ m_h)^{3/4}\ e^{-E_g/2kT}. \tag{2.24}$$

In the extrinsic case, if we let $N_a = KN_d$,

$$n_0 = N_c\ \text{exp.}\ \{-(E_c - E_f)/kT\}, \tag{2.25}$$

leading to $n_0 = 2\,(2\pi\ m_e\ kT/h^2)^{3/2}\ e^{-E_f/kT}$ (2.26)

where E_c is taken in reference.

Now,

$$n_0 = N_d - f\ N_a \tag{2.27}$$

since the electrons in the conduction band must come mainly from the impurity level (minus those trapped by the trapping level at E_a);

$$f = \frac{1}{1 + \beta e^{(E_a - E_f)/kT}}$$

is the probability of an electron occupying a particular level.

Equations (2.26) and (2.27) lead to

$$n_0 = \frac{-[1 + B(N_a - N_d)] + \sqrt{[1 + B(N_a - N_d]^2 + 4BN_d}}{2B} \tag{2.28}$$

where

$$B = \frac{e^{-E_a/kT}}{\beta\ N_c} = \frac{e^{-E_a/kT}}{\beta 2\ (2\pi\ m\ kT/h^2)^{3/2}}. \tag{2.29}$$

Since $N_a >> N_d$, $[1 + B\ (N_a - N_d)] >> 4B\ N_d$, and

$$n_0 = \frac{[1 + B\ (N_a - N_d)]}{2B} \left\{ -1 + \sqrt{1 + \frac{4B\ N_d}{[1 + B\ (N_a - N_d)^2]^2}}. \right\} \tag{2.30}$$

Let

$$x = \frac{4B\ N_d}{[1 + B\ (N_a - N_d)]^2}$$

where $x \ll 1$, now

$$(1 + x)^{1/2} \simeq 1 + x/2 \text{ for } x \ll 1$$

so that

$$n_0 = \frac{[1 + B\ (N_a - N_d)]}{2B} \left\{ -1 + 1 + \frac{4B\ N_d}{2\ [1 + B\ (N_a - N_d)^2]^2} \right\} \quad (2.31)$$

or

$$n_0 = \frac{N_d}{1 + B\ (N_a - N_d)}. \quad (2.32)$$

But $N_a \gg N_d$, so $B(N_a - N_d) \gg 1$ and

$$n_0 \simeq \frac{N_d}{B\ N_a} \quad (2.33)$$

and

$$n_0 \simeq \frac{N_d}{N_a \frac{e^{-E_a/kT}}{\beta\ N_c}} = \frac{N_d}{N_a}\ \beta\ N_c\ e^{E_a/kT}$$

$$= \frac{N_d}{N_a}\ 2\beta\left(\frac{2\pi\ m_e\ kT}{h^2}\right)^{3/2}\ e^{+E_a/kT}. \quad (2.34)$$

We defined $E_g = -E_a$, hence

$$n_0 = \frac{2N_d}{N_a}\ \beta\left(\frac{2\pi\ m_e\ kT}{h^2}\right)^{3/2}\ e^{-E_g/kT}. \quad (2.35)$$

Now comparing the two by taking the ratio of the intrinsic case to

that of the extrinsic case.

$$\frac{(n_0)_i}{(n_0)_e} = \frac{N_a\ (m_e\ m_h)^{3/4}\ e^{-E_g/2kT}}{N_d\beta\ (m_e)^{3/2}\ e^{-E_g/kT}}, \tag{2.36}$$

for $m_e \simeq m_h$

$$\frac{(n_0)_i}{(n_0)_e} = \frac{N_a}{N_d\beta}\ e^{E_g/2kT} = \frac{K}{\beta}\ e^{E_g/2kT}. \tag{2.37}$$

At 77°K, $2kT \simeq .012ev$ the ratio becomes

$$\frac{(n_0)_i}{(n_0)_e} = \frac{K}{\beta}\ e^{0.47/.012} = \frac{K}{\beta}\ e^{39.1}. \tag{2.38}$$

From equation (2.38) one sees that the density of electrons at 77°K for the intrinsic case is extremely higher than that of the extrinsic case, especially since K will usually be approximately 10 or more. Thus for the same intensity of radiation incident upon the two materials, the change in conductivity of the extrinsic material will be much greater.

This section has shown that there was good reason to suspect that extrinsic photoconductivity was exhibited in irradiated silicon, and that the degree to which it was exhibited was greater than in one alternate case. The researcher, therefore, endeavored to determine the presence of this photoconductivity, and if it were present, to determine the degree to which it was present. His primary concern was to determine whether or not the magnitude of the

change in conductivity was great enough to be detected, and whether or not the lifetime of the excited carriers was long enough for the photoconductivity to be observed.

CHAPTER III

INSTRUMENTATION

3.1. THE DETECTION SYSTEM

The detection of the photoconductive process depends upon the detection of the change in conductivity of the device. Assuming a perfectly resistive device, one could obtain this result by detection of a change of voltage across the device when the device is placed in series with a resistor of comparable size and a d.c. bias source. Changing the conductance of a device in such a circuit by periodically irradiating the device would result in a voltage containing a periodic component to appear across the resistor. This circuit would thus provide an elementary detection system as shown in Fig. 3.1.

One basic problem with this circuit is the lack of ability to detect very small changes in the resistance. Typically one might expect signal outputs across R_c on the order of microvolts. This problem will necessitate the addition of some type of amplifier. This amplifier should be selected to fit the requirements of the particular case at hand. The requirements will be dictated by the resistance of the device, as mentioned previously, and the size of the signal output. The resistance will determine the necessary input impedance of the amplifier to insure proper coupling between R_L and the measurement instrument. The size of the output signal

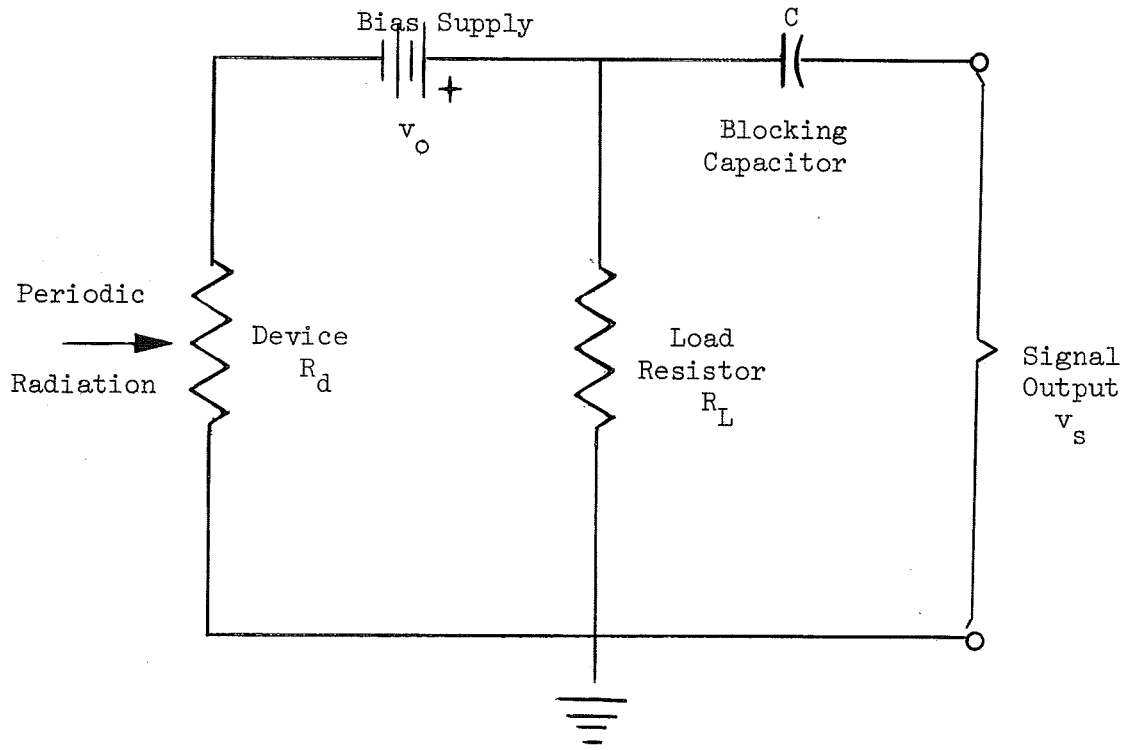

Figure 3.1 An Elementary Detection System

will determine the necessary gain. With this modification the problem of calibration appears. W. L. Eisenman [13] suggests the addition of a resistor whose resistance is negligible in comparison to that of the load and device resistors into a ground leg of the circuit. An external signal voltage injected into the system through this resistor can be used to determine the system gain over the desired frequency range.

A means of realizing the periodic irradiation is also necessary. A widely used method is to place a motor driven notched disk, called a "chopper," in the optical path between source and device. Additional discussion of this device is deferred to a later section of this chapter. In addition, a source of radiation of known spectral distribution is also a necessary part of the system.

The mentioned items thus comprise a somewhat more sophisticated detection system than that of the circuit shown in Fig. 3.1. This more complete system, shown in Fig. 3.2, forms a basis for evaluating the performance of a photoconductor. Additional modifications may be necessary due to unusual detector characteristics, but this basic system, through the use of procedures outlined by Eisenman [13] and R. Clark Jones [14], can be used to determine the figures of merit necessary to characterize the performance of the given photoconductor.

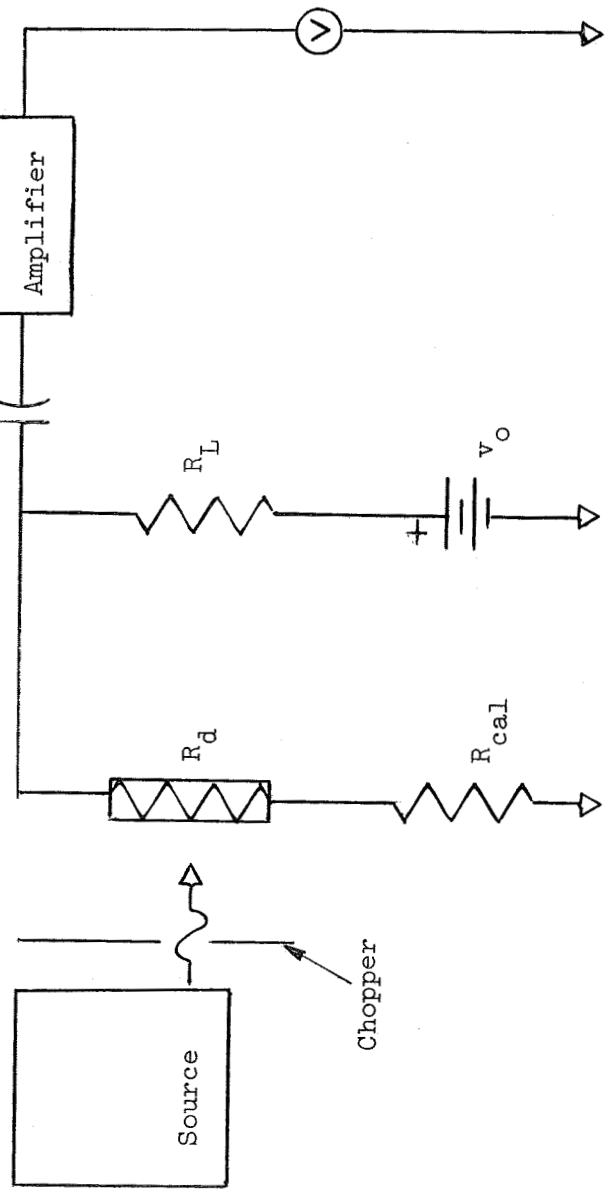

Figure 3.2 A Basic Detection System

3.2. PROBLEMS ENCOUNTERED

Three basic problems arose when the given detector system was constructed for use with the irradiated silicon samples. These problems were:

(1) the detection and measurement of small signal voltages, on the order of microvolts, across device resistances ranging from $10^6\Omega$ to $10^{11}\Omega$;

(2) the reduction of noise in such a circuit to a level where device noise is detectable from circuit noise;

(3) the calibration of the output signal voltage against the gain of the amplifier in order to obtain the true device signal output.

The extremely high device resistance ($\sim 10^{10}$ ohms) caused the greatest problems. A Tektronix type 122 preamplifier modified for low noise and having an input impedance of $10^7\Omega$ was first used as the detection system amplifier. No success was obtained from this arrangement, and attempts were made to couple the circuit and the 122 by means of a cathode follower suggested by Eisenman [16, 17]. These attempts were also not successful, again due to high device resistance. Another facet of the high resistance problem was the RC time constant problem posed by the high device resistance and low capacitance of the leads; this time constant was low enough to cause a cutoff frequency below 100 Hz. Both of these problems were solved with the development of a low-noise, transistorized

preamplifier having the necessary input impedance (>>5 x 10^8 ohms) and employing a capacitive feedback loop to provide "negative" capacitance to "tune out" capacitance in the device leads. The complete preamplifier and biasing circuit were small enough to be mounted directly to the cryogenic container housing the device, thereby reducing lead length and hence capacitance. A more complete description of the preamplifier will be given in the following section.

Noise did not present as big a problem as anticipated. Batteries were first used as the bias supply, but as higher bias voltages were needed the switch to the Fluke model 407 power supplies described in the next section was necessitated. These power supplies with an additional RC filter combined with the use of shielded leads and "mini boxes" and with the final mounting of the detection circuit and amplifier as close to the device as possible lowered the noise to a level low enough to be negligible in comparison to device noise in most instances.

The calibration was accomplished by the addition of a 50 ohm resistor to the bias circuit. First attempts placed R_{cal} between the bias source and load resistor. The external signal voltage was injected through an isolation transformer. A better arrangement was found to be that as shown in Fig. 3.2. In this configuration R_{cal} was placed in a ground leg with the "common" side of R_d, the cryogenic container, "floating" 50 ohms above ground.

3.3. BLACK BODY RESPONSIVITY EQUIPMENT AND SYSTEM

Having described the general detection system and the problems arising in its modification for this investigation, a description of the two developed systems,the original and a subsequent improved one, is presented. The first system, incorporating a black body source, was used for the measurement of responsivity, chopping frequency response, and noise voltage. The improved system provided not only the black body capabilities of the first system, but also spectral capabilities through the use of a monochromatic source of radiation contained in the system. This section will be concerned with the development of the original system, while the following section will discuss the improved system.

Devices which were prepared and mounted on brass pads as outlined in the Appendix were mounted on the end of the cold finger of a dewar specially fabricated for photoconductive studies at the N.A.S.A. Langley Research Center. The dewar consisted of two concentric flanged cylinders, the inner of which contained a reservoir for liquid nitrogen and had attached to it the cold finger. The two cylinders when bolted together through the flanges formed an empty space which was evacuated by means of a vent through the wall of the outer cylinder. A pressure of 10^{-5} to 10^{-4} mm. of mercury was maintained in the dewar providing insulation for liquid nitrogen in the reservoir and allowing the device to reach liquid nitrogen temperature. A germanium window, which transmits ~50%

of the incident radiation in the range of approximately 1.6μ to 20μ as verified by spectrophotometric tests was mounted in the outer cylinder wall in the optical path between the source collimator and the detector. A radiation shield enclosing the device except for an aperture in the optical path was used to limit background radiation from the outer cylinder walls. Electrical contact was made with the device by means of a vacuum BNC connector installed in the dewar with the common side being that of the brass pad. A thermocouple fastened to the cold finger acted as a monitor of the device temperature. The vacuum system used consisted of a converted bell jar evaporation system employing both mechanical and diffusion pumps. Fig. 3.3 shows a cut-away view of a sample mounted in the dewar.

The black body source was constructed from a cylindrical block of copper as outlined in Kruse et al [2]. A conical cavity of half angle 15° was cut from one end of the cylinder which was then placed in a cylindrical bore furnace. A water cooled brass collimator was placed at the end of the furnace bore and was maintained a known distance from the copper cylinder. Three bolts through the collimator not only maintained the distance, but also insured that the apex of the conical cavity was colinear with the center of the collimator aperture. The cylinder was heated to 500°C and allowed to oxidize, after which it was maintained at 500°K by a control system employing an API Instrument Company

"Temptender" temperature controller. A thermocouple installed in the back face of the copper cylinder controlled the power flow into the furnace through the controller. Fig. 3.4 shows a cut-away view of the black body source.

The dewar and black body source were mounted such that the optical path between the source and detector was maintained at a distance of 0.1 m. The total black body output at 500°K was determined to be 0.449 watts [18] according to the Steffan-Boltzmann relation. The detector had an area of 10^{-5} m^2, giving a rate of energy flow of 2.24×10^{-5} watts onto the device surface with the consideration of the germanium window transmissivity.

A chopper was mounted in the optical path between source and detector for the purpose of modulating the source radiation. The chopper was fabricated from 1/8 inch aluminum stock as a notched disk having a 3 1/4 inch radius. Twelve notches were cut in the disk, leaving twelve "teeth" to pass in front of the circular black body collimator aperture. The chopper was mounted on the shaft of a Lamb Electric Company motor and was capable of reaching chopping frequencies of up to 1350 Hz. The work of McQuistan [19] enabled the author to determine the amplitude of any harmonic of the chopping frequency by consideration of the aperture-radius-to-tooth-width ratio. For the case of a tooth width greater than the collimator aperture diameter, McQuistan derived the following expression for the number of photons per unit time striking the

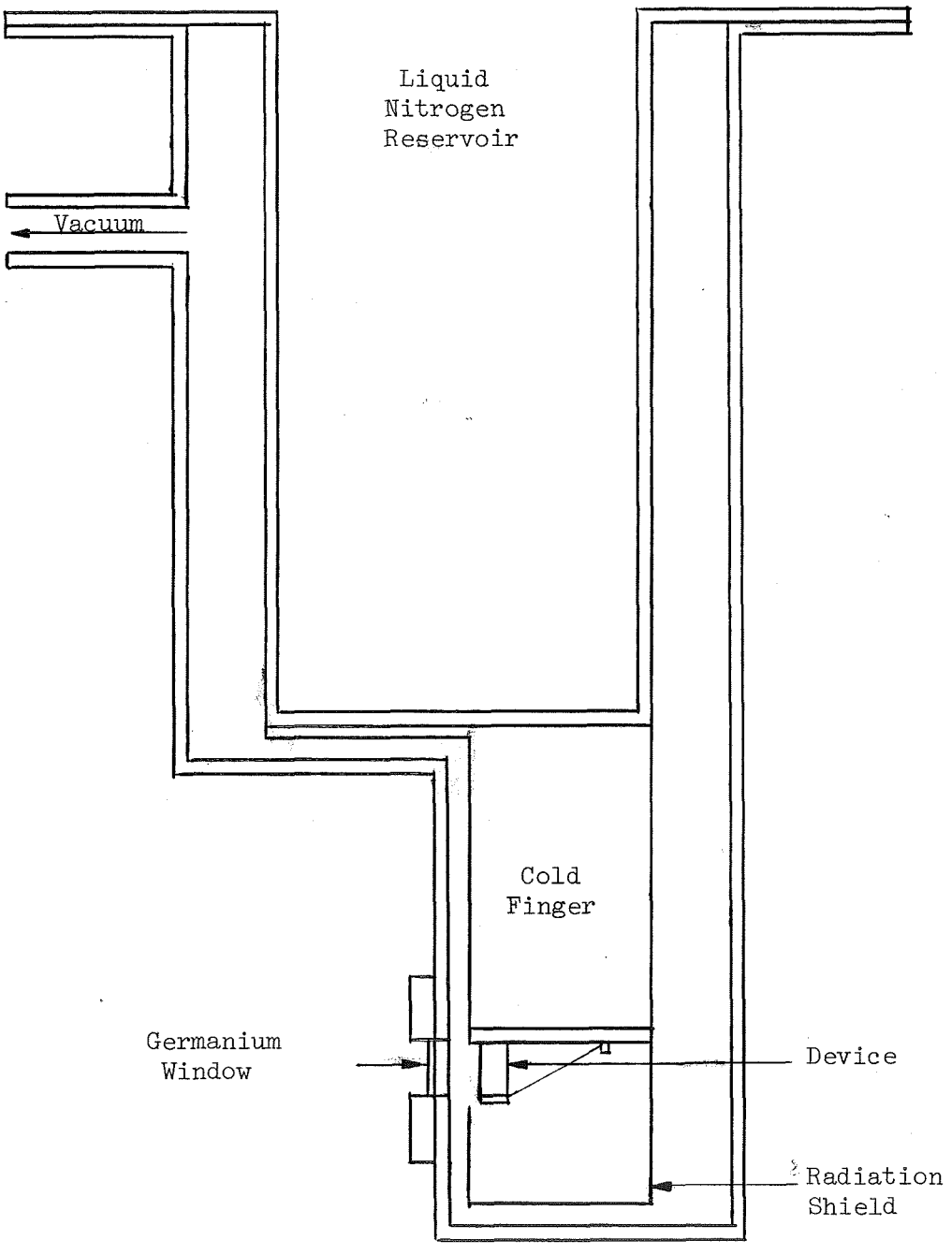

Figure 3.3 A Cut-Away View of a Sample Mounted in the Dewar of the Original System

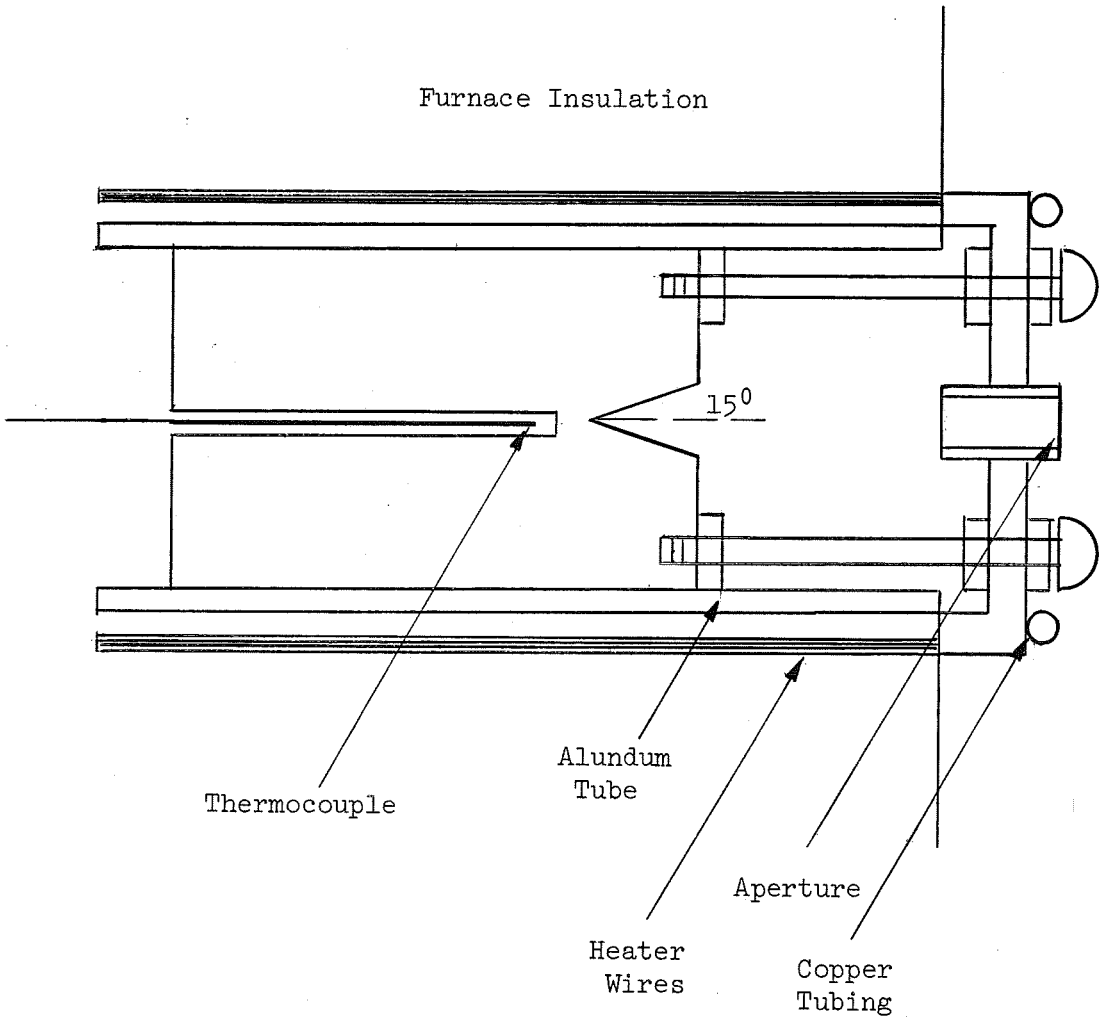

Figure 3.4 A Cut-Away View of the Black Body Source

detector, N(t),

$$N(t) = \frac{\pi R^2}{2} I_0 \left[1 - 8 \sum_{k=1}^{\infty} \frac{2r}{K^2 \pi^2 R} J_1\left(\frac{K\pi R_a}{2r}\right) \sin \frac{K\pi}{2} \times \cos K\omega t\right] \qquad (3.1)$$

where R_a = radius of collimator aperture

r = half the chopping tooth width where the tooth-notch ratio is unity

J_1 = first-order Bessel function

I_0 = radiation incident on the chopper

ω = chopping frequency.

As mentioned previously, the development of an amplifier capable of meeting the needs of this investigation proved to be a difficult problem. Besides the schemes mentioned in a previous section, a preamplifier utilizing a K&M Electronics Corporation FET Operational Amplifier with an input impedance of $10^{12}\Omega$ was being considered. The final design, however, was that of a low noise, transistorized preamplifier featuring a capacitive feedback loop, permitting "negative" capacitance feedback to cancel the effects of capacitance in the dewar and in the device leads. The input impedance of this preamplifier was greater than $5 \times 10^8\Omega$ and an output impedance was of $10^4\Omega$. With a fixed 5×10^7 load resistor, this preamplifier was found to be suitable for the majority of samples investigated. The biasing circuit and preamplifier were mounted in an aluminum box and were connected directly to the dewar by means of a vacuum BNC connector in the dewar. Fig. 3.5 shows a schematic diagram of

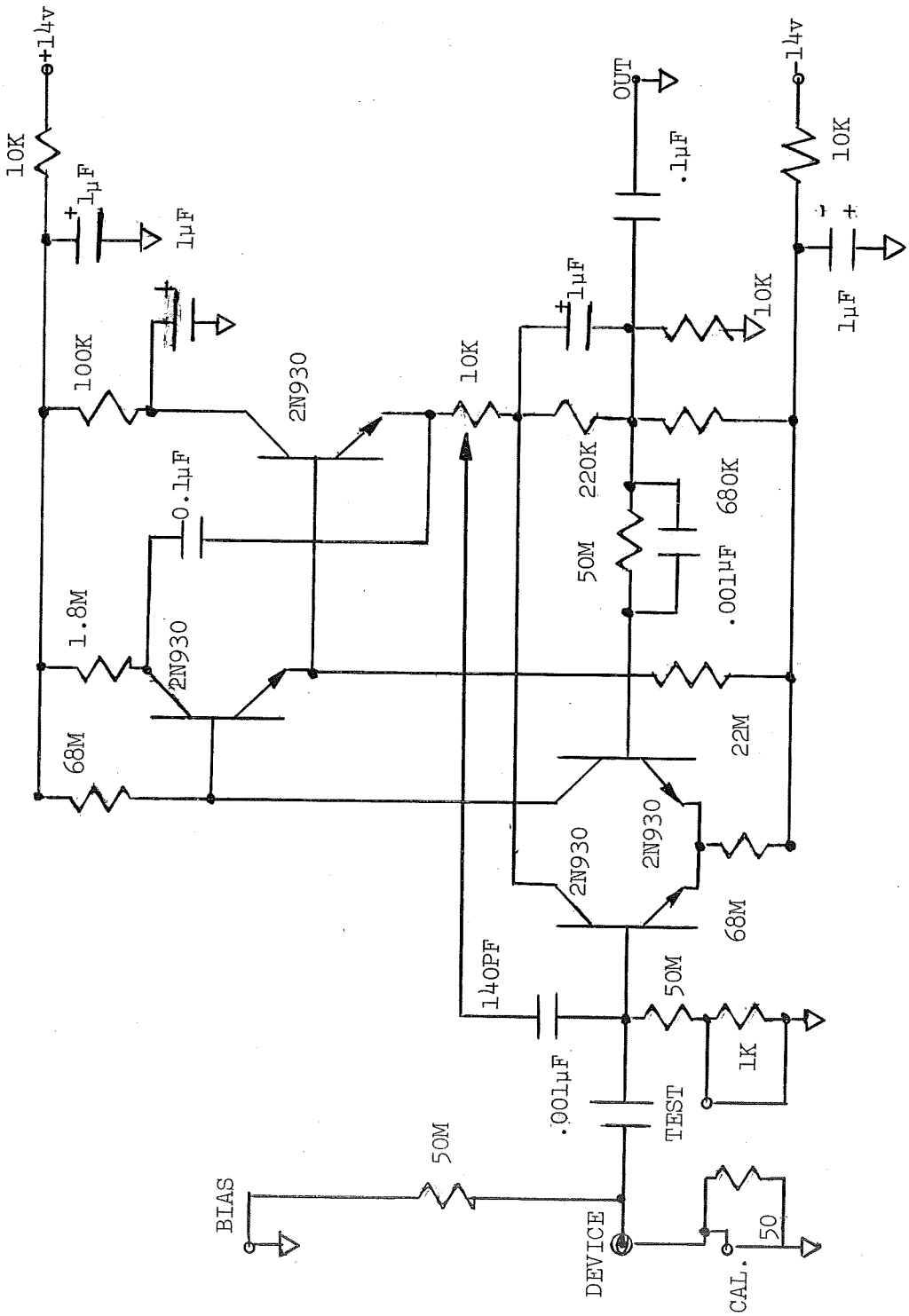

Figure 3.5 Schematic Diagram of Biasing Circuit and Preamplifier

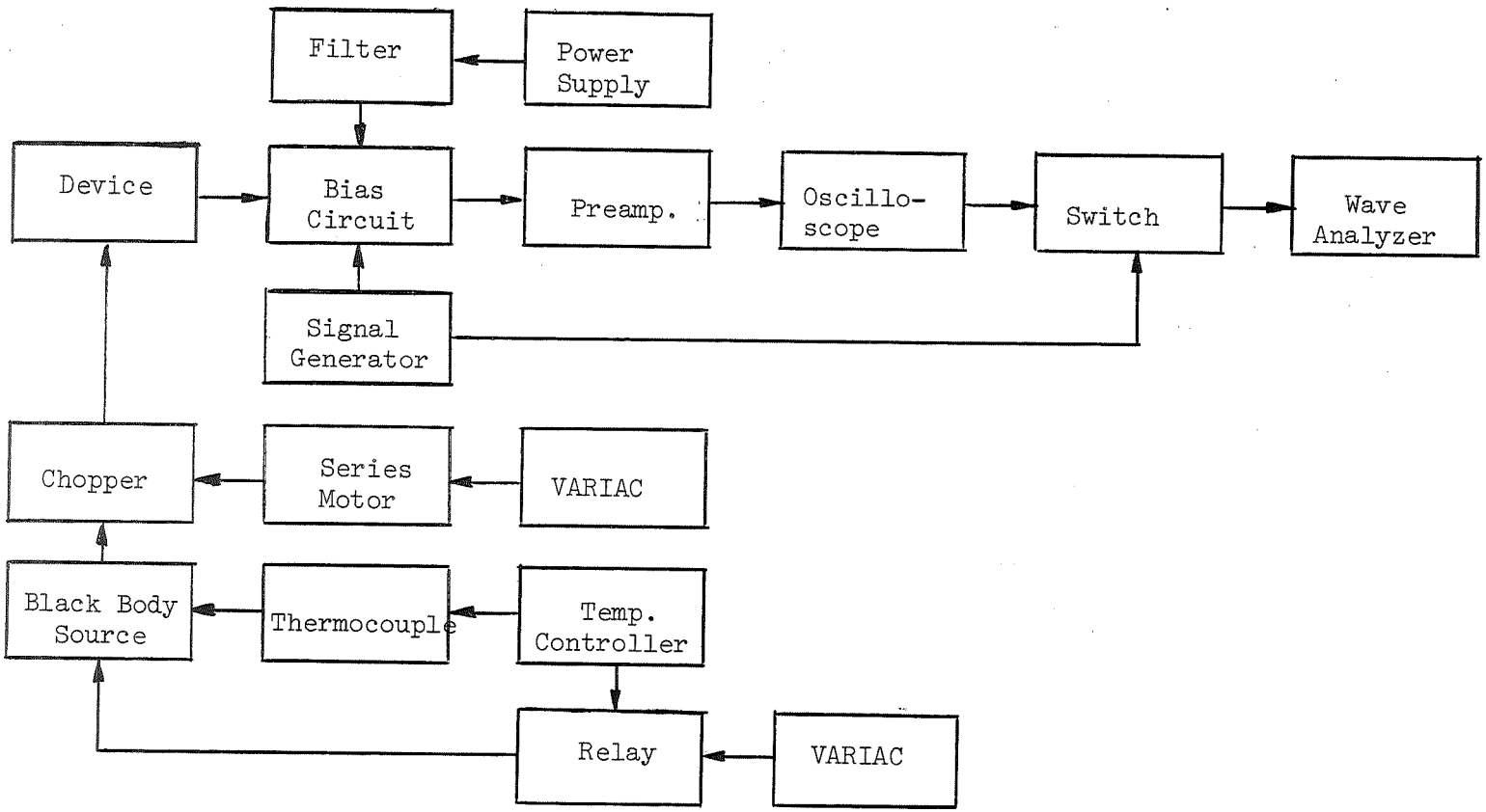

Figure 3.6 Block Diagram of Responsivity and Frequency Response Equipment

the biasing circuit and preamplifier. Note that the "negative" capacitance feedback is calibrated by means of a square wave fed into "test".

The bias supply used for the bias circuit was a low-noise Fluke model 407 power supply. A four-stage RC filter was added to reduce 60 cycle ripple and harmonics thereof.

With the mentioned components assembled, the system appeared as shown in Fig. 3.6. Additional components shown in this figure include:

(1) a Hewlett-Packard H21-521C counter which was used to monitor chopping frequency;

(2) a Tektronix type 317 oscilloscope which monitored the output of the preamplifier;

(3) a Hewlett-Packard model 302A wave analyzer which was used as the frequency sensitive voltmeter;

(4) a BNC switch connecting the wave analyzer to one of two inputs, the preamplfier output or the signal generator output, was installed to facilitate rapid calibration measurements.

The black body responsivity system thus developed provided a means of obtaining the noise root power spectrum as well as the black body responsivity as a function of chopping frequency and bias voltage across the device. The following procedures were used to obtain the above mentioned information and to calculate various figures of merit from this data:

1. The device output signal voltage was taken without regard to system gain. Bias voltage across the device was set, and the output signal voltage, v_s, was taken as a function of chopping frequency.
2. The chopper was stopped and positioned so that no incident source radiation fell on the device. Device and circuit noise, E_T, was taken as a function of frequency with the wave analyzer.
3. The signal generator was used to supply an external signal voltage to the bias circuit which caused an output signal voltage equal in magnitude and frequency to that obtained in step (1). The BNC switch was then used to quickly find the output of the signal generator, V_{cal}. V_{cal} not only gave the true device signal output voltage, but also enabled one to find the system gain, g, as a function of frequency.
4. Circuit noise was obtained by following step (2) with the device leads short-circuited.
5. The bias voltage was changed and steps (1) - (4) were repeated for each succeeding change in bias voltage.

These procedures yielded the device output signal voltage, V_{cal}, the gain of the system, g, the device noise, N(f), and the circuit noise, N_c. These values were found as functions of chopping frequency and device bias voltage, and the voltage values

were given in r.m.s. values.

The noise root power spectrum was then found by means of the relation due to Eisenman [13]

$$N(f) = \frac{E_T^2(f) - E_{cir}(f)^2}{g^2}^{1/2} \Delta f \qquad (3.2)$$

where Δf is the noise bandwidth of the wave analyzer.

Black body responsivity was obtained by means of the relation [13]

$$R_{bb} = \frac{V(rms)}{J(rms)A_0} \qquad (3.3)$$

where V(rms) = V_{cal} or the corrected device output.

J(rms) = rms value of the fundamental component of the incident energy flux

A_0 = adopted area of the detector.

The relative frequency response, R(f), was then found by

$$R(f) = \frac{K\, V_{cal}}{g(f)} \qquad (3.4)$$

where K = constant of proportionality.

3.4. IMPROVED AND CONSOLIDATED SYSTEM

The original plans for determining spectral response called for the use of a converted Baird Associates, Inc., Infrared Recording Spectrophotometer. However, the procurement of a Jarrell-Ash model 82-410 monochrometer led to the design of an improved and consolidated system which was used in this investigation. A new

research dewar was purchased from Sulfrian Cryogenics, Inc., and a smaller black body source was fabricated for use with this system. The sources were situated so that one could gather spectral or black body data by choosing the rotational position of the dewar.

The new dewar offered three distinct advantages over the original dewar:

(1) liquid helium temperature capability;

(2) a heated device holder allowing device operation at a temperature ranging from near 4°K to approximately 400°K;

(3) a spring loaded device holder and electrical contact.

The last advantage eliminated the need for mounting the devices on separate brass pads with conducting epoxy. Quite a deal of trouble was encountered in using this epoxy since it had to be changed after the device was annealed at an elevated temperature. The dewar itself consisted of two liquid gas reservoirs; the innermost was intended for liquid helium use while the outer was used for liquid nitrogen use as insulation for the helium. The dewar cold finger was thermally connected to the liquid helium reservoir, and attached to the device cold finger containing the heated device holder mentioned previously. This cold finger was made at the N.A.S.A. Langley Research Center and was identical to one used in a similar dewar at that location. The sample holder consisted of a base in the cold finger and a spring-loaded contact, the shaft of which was embedded in teflon insulation. One radiation shield fit over the

sample holder cold finger and was thermally connected to the liquid helium reservoir. A larger second radiation shield fit over the dewar cold finger and first radiation shield and was thermally connected to the liquid nitrogen reservoir. Both radiation shields had four apertures which were aligned with the four windows on the removable external bottom of the dewar thus providing four optical paths from the outside of the dewar to the sample holder. Presently three of the external windows are steel, and the fourth is the germanium window. Leads for the device holder, heater, and a temperature monitoring thermocouple mounted on the cold finger were brought through external lead-ins in the dewar.

The biasing circuit and preamplifier were mounted directly on the side of the dewar by means of a nylon screw. This arrangement "separated" the dewar exterior and ground by the 50 ohm calibration resistor.

The Jarrel-Ash model 82-410 monochrometer when used with four different diffraction gratings provided a usable output, the wavelength of which varied from 1.0 to 20 microns. 1.0 mil entrance and exit slits were used with the monochrometer.

The source used for spectral measurements was an electrically heated silicon carbide rod available under the trade name Globar. It was maintained at 1100°C and was enclosed in a water cooled jacket. At this temperature it emitted maximum energy at a wavelength of about 2 microns, and its energy distribution with respect

to wavelength was approximately that of a black body heated to the same temperature. A curve of the emission from a black body source at 1100°C versus wavelength is shown in Fig. 3.7 [16]. The Globar was mounted directly in front of the monochrometer entrance slit, and a water cooled copper plate containing an aperture aligned with the Globar cooling jacket aperture and the monochrometer entrance slit was inserted between the two to prevent heat damage to the monochrometer. This plate and the cooling jacket were supplied by the same water source.

Radiation from the source was incident upon the monochrometer entrance slit. The radiation left the exit slit as monochromatic radiation after which it was modulated by a 10 Hz. chopper. This chopper consisted of a circular disk, one half of which was silvered, the other half empty. Hence the monochrometer output was split into two 10 Hz. chopped beams. The beam passing through the empty half of the chopper was focused on the germanium window of the dewar by the use of two mirrors, one a concave front mirror, the other a flat front surface mirror fabricated by aluminum deposition on glass. The second beam (reflected by the silvered half of the chopper) was focused on a bolometer element by means of a concave front surface mirror.

The bolometer provided an approximately uniform response to all wavelengths of infrared radiation. The sensitive element of the bolometer was a thin strip of platinum which was coated on

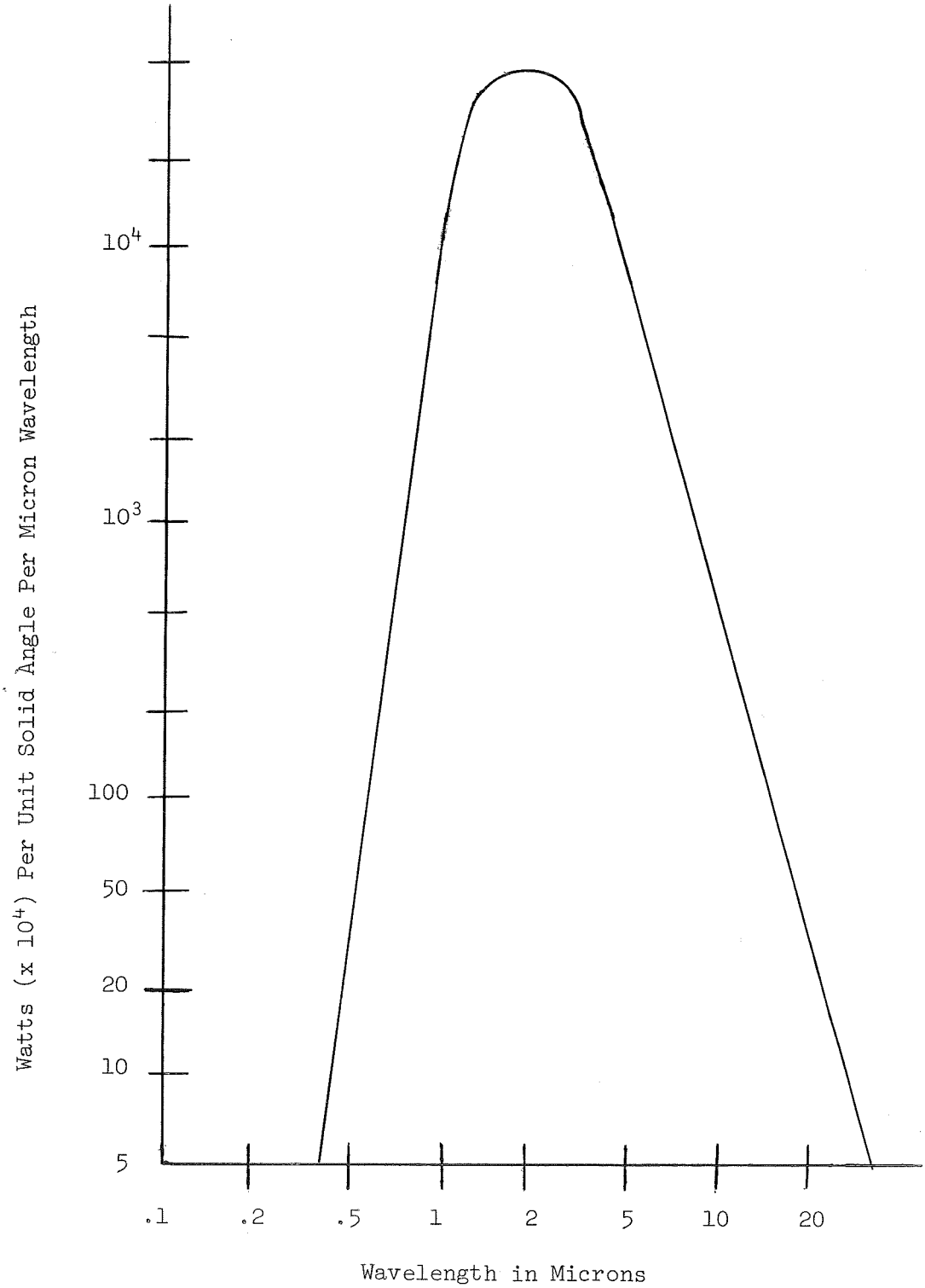

Figure 3.7 Distribution of Radiation from a One Cm. Square Black Body Source at 1100°C

its receiving side with a thin layer of gold black which served as a highly efficient radiation absorber uniformly effective at all wavelengths. The bolometer element was mounted in a vacuum tight housing maintained at low pressure to prevent "swish" noise [20]. The housing was provided with a potassium bromide window which was transparent to infrared radiation out to a wavelength of 28 microns. The bolometer operated by virtue of a change in the resistance of the platinum strip due to a change in temperature. The strip was connected as one arm of a balanced Wheatstone bridge excited by current from a 6 volt battery. A change in the temperature of the strip as little as 10^{-5}°C was measurable [20].

The 10 Hz. signal developed by the bolometer bridge was fed into a high gain, low noise W. S. McDonald Company type 37A voltage amplifier having a bandwidth of approximately one cycle centered at 10 cycles. The bolometer bridge was located within the amplifier chassis and was connected to the bolometer by shielded leads. The power supply used was a Fluke model 407 converted to take the place of the noisier original supply. The amplifier gain was adjusted from about 10^3 to 10^6. The manufacturer stated that the bolometer was flat at infrared wavelengths and had a sensitivity of 4 volts/watt. Hence by knowing the gain of the system, the power incident on the bolometer element could be found.

The smaller black body incorporated the use of the same copper cylinder and water cooled collimator, but used a smaller

housing than the original black body source. The copper cylinder was placed in a small alundum tube which was then wound with Kanthal wire insulated and held by alumina cement. The tube was then mounted in a housing having a radius of approximately 3 1/2 inches and a length of 4 1/2 inches. Fiberglass insulation was placed between the tube and the housing. The electrical leads were brought to an external terminal strip. The original thermocouple cavity in the back face of the cylinder was enlarged so that the alundum tube encased thermocouple was approximately 1/8 inch from the apex of the conical cavity. The thermocouple was secured in this position with sauterizing cement. The control system for maintaining a constant temperature was the same as that described for the original black body source.

An additional Fluke 407 power supply was procured to permit higher bias voltages across the device. The second supply was connected in series with the original giving the capability of bias voltages up to 1100 volts. The filter was also changed so that it consisted of four configurations of three, 125μf, 400v capacitors in series; each parallel configuration separated by a series 1.8KΩ resistor. Shielded 58/u cable was used for leads to the bias circuit.

A block diagram of the improved system is shown in Fig. 3.8. For spectral data the dewar was rotated so that it received 10 Hz. radiation from the monochromatic source. Bias voltage across

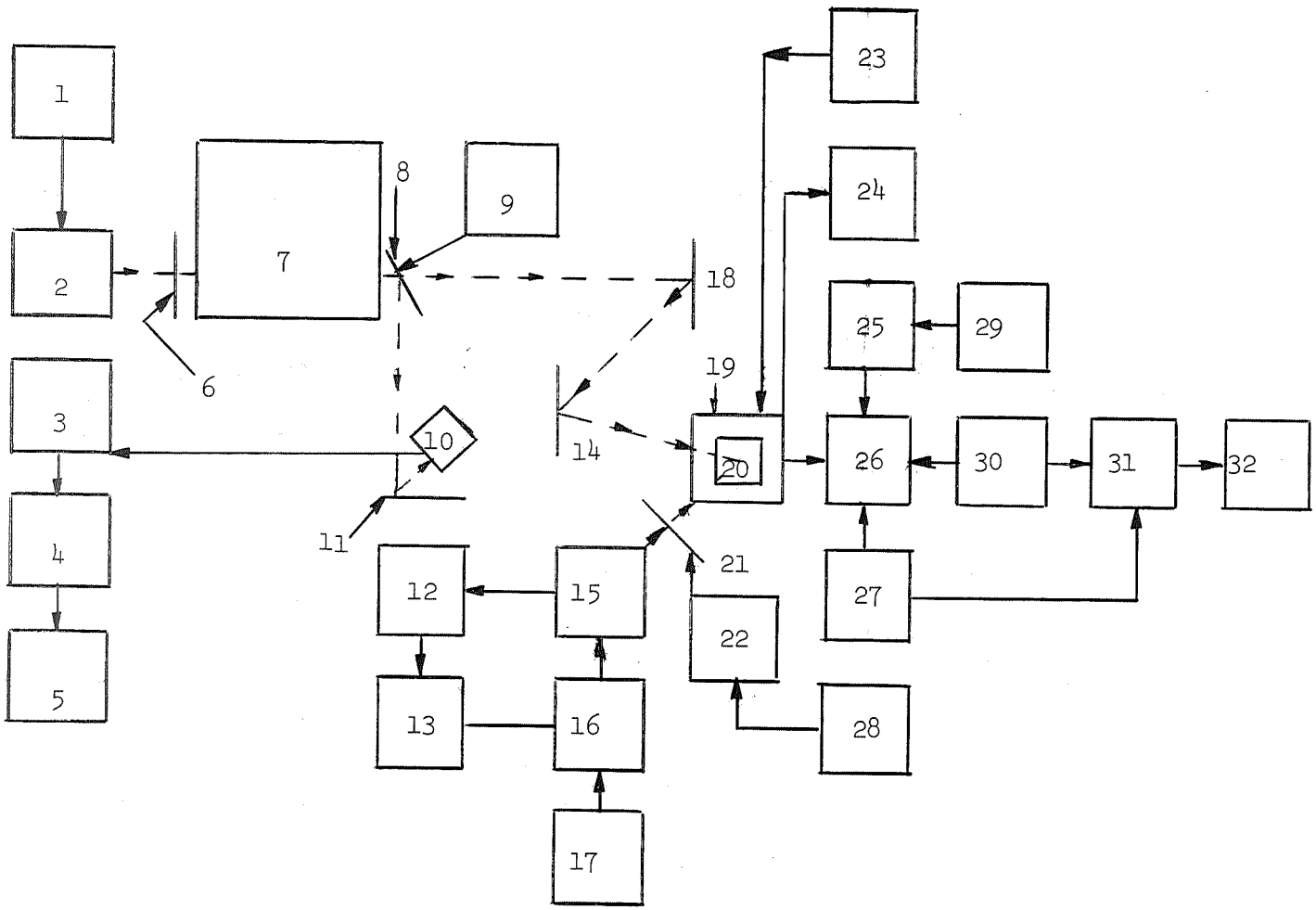

(See "Legend for Figure 3.8" for Identification)

Figure 3.8 Block Diagram of Consolidated Responsivity, Frequency Response, and Spectral Response Equipment

Legend for Figure 3.8

1. Globar Source Transformer
2. Globar Source
3. Bolometer 10 Hz. Amplifier
4. Bolometer Monitor Oscilloscope
5. Phase-Lock Microvoltmeter
6. Water-Cooled Shielding Plate
7. Monochrometer
8. 10 Hz. Chopper
9. 10 Hz. Chopper Motor
10. Bolometer
11. Concave Front Surface Mirror
12. Thermocouple
13. Temperature Controller
14. Front Surface Mirror
15. Black Body Source
16. Relay
17. Variac
18. Concave Front Surface Mirror
19. Dewar
20. Device
21. Black Body Source Chopper
22. Series Motor
23. Cold Finger Heater Power Supply
24. Cold Finger Thermocouple Millivoltmeter
25. Bias Supply Filter
26. Bias Circuit and Preamplifier
27. Signal Generator
28. Variac
29. Bias Supply
30. Device Monitor Oscilloscope
31. BNC Switch
32. Wave Analyzer, or Phase-Lock Microvoltmeter

the device was set, and the output signal voltage was taken as a function of wavelength. A Hewlett Packard 3410A phase lock voltmeter was used instead of the wave analyzer for measurement since it appeared to give better performance at this low frequency. Likewise, the bolometer output signal voltage was taken as a function of wavelength. The wavelength was then adjusted to the peak response wavelength, and output signal voltage was taken as a function of bias voltage.

The dewar was then rotated to receive radiation from the black body source, and the procedures for gathering black body data outlined in the last section were followed. Since the distance from source to detector had changed slightly, this fact had to be taken into account in determining black body figures of merit.

The improved system then gave the information obtained by use of the original system, namely, $N(f)$, $R_{bb}(f, V_0)$, and $R(f)$. In addition, the relative spectral response, absolute spectral responsivity, and detectivity could be found from data given by the spectral response.

The relative spectral response was calculated by

$$L(\lambda) = \frac{E_1(\lambda)}{E_2(\lambda)} \tag{3.5}$$

where E_1 = device output due to a spectral source

E_2 = bolometer output due to a spectral source.*

*The supplier of the bolometer guaranteed it to have invariant spectral response from 1 to 20 microns.

The absolute spectral responsivity was then given by

$$R(\lambda) = R_{bb} \frac{L(\lambda)\ P_{rms}}{\int L(\lambda)\ P(\lambda)_{rms} d\lambda} \tag{3.6}$$

where $P(\lambda)_{rms}$ is the spectral power of P_{rms}, the black body power.

Spectral detectivity, D^*_λ, was found by means of

$$D^*_\lambda = (A_0 \Delta f)^{1/2}\ R(\lambda)/N_{rms} \tag{3.7}$$

where A_0 = the adopted device area

Δf = the noise bandwidth

and N_{rms} = the noise voltage at the maximum bias, maximum chopping frequency values.

CHAPTER IV

RESULTS AND CONCLUSIONS

4.1. RESOLVING THE EXPERIMENTAL QUESTION

Through the use of the two systems mentioned in the last chapter the fact that irradiated silicon does exhibit photoconductivity has been established. The degree of photoconductivity has been established in a widely accepted manner by means of the procedures outlined for determining the various figures of merit. By interpretation of spectral data the wavelength giving peak response has been found, and the fact that the photoconductivity does result from defect centers has been ascertained.

4.2. BLACK BODY RESPONSIVITY AS A FUNCTION OF BIAS VOLTAGE ACROSS THE DEVICE AND MODULATION FREQUENCY OF INCIDENT RADIATION

The test procedures outlined in the previous chapter were used, and R_{bb} as a function of bias voltage across the device and of radiation modulation frequency was taken. A device output was found from all seven of the resistivities and types of silicon tested. These were 10, 1, and 0.1 ohm-cm. p-type and 1.0, 0.4, 0.1, and 0.03 ohm-cm. n-type. Shown in Figs. 4.1 through 7 are sample curves of responsivity versus black body radiation modulation frequency for each of the resistivities used. The modulation frequency was taken over the range 30 - 1100 Hz., while the total

bias across device and load resistor was set at values of 100, 300, and 500 volts for those samples tested with the original system and at values of 200, 400, 600, 800, and 1000 volts for those tested with the improved system. Fig. 4.1 shows a curve of black body responsivity versus changing frequency for a 1.0 ohm-cm. n-type device and is typical of all curves of the devices tested in that the responsivity increased with decreasing radiation modulation frequency. As an example of the black body responsivity calculations, the case of device number 329N1.0 shown in Fig. 4.1 is considered. At 100 Hz. chopping frequency and with 500 volt total bias the calibrated output was 9.52×10^{-2} volts, and the r.m.s. value of power incident on the device was 2.24×10^{-5} watts yielding a black body responsivity of 4.7×10^{3} volts watt^{-1}. The liquid nitrogen resistance of 329N1.0 was found to be 7.7×10^{8} ohms. Figs. 4.2, 4.3, 4.4, 4.5, 4.6, 4.7 show curves of R_{bb} versus f for a 0.1 ohm-cm. n-type device with a 77°K resistance of 3.3×10^{8} ohms, 10 ohm-cm. p-type device with a 77°K resistance of 8×10^{11} ohms, 1.0 ohm-cm. p-type device whose 77°K resistance was nonlinear, 0.1 ohm-cm. p-type device with a 77°K resistance of 7.0×10^{4} ohms, 0.03 ohm-cm, n-type device with a 77°K resistance of 2.2×10^{11} ohms, and a 0.4 ohm-cm. n-type device whose 77°K resistance was 3.5×10^{9} ohms.

R_{bb} as a function of bias voltage across the device was linear in the majority of samples tested. Fig. 4.8 shows R_{bb}

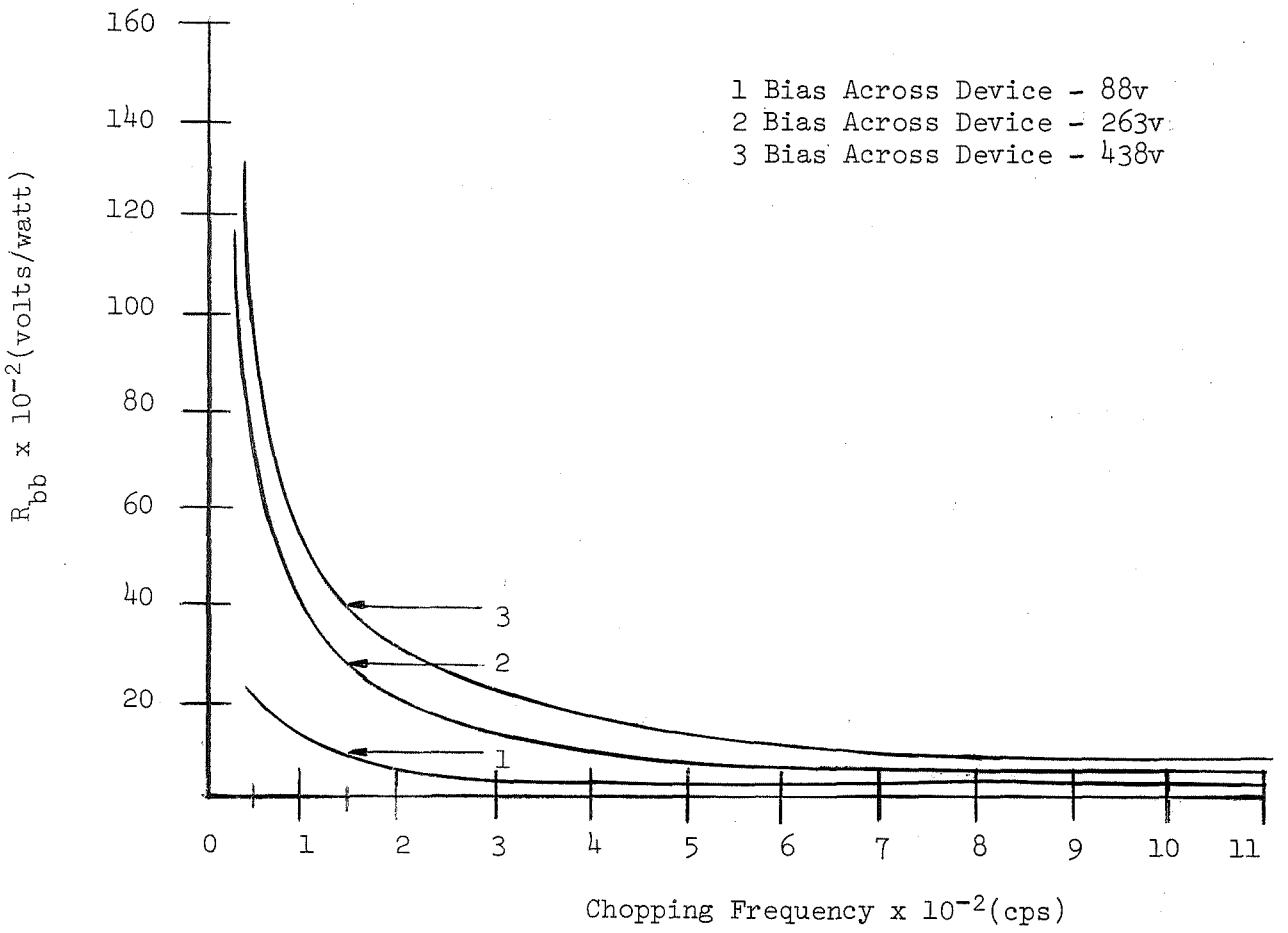

Figure 4.1 Black Body Responsivity vs. Chopping Frequency for a Typical n-Type Device Whose Initial Resistivity was 1Ω cm. (Device 329N1.0)

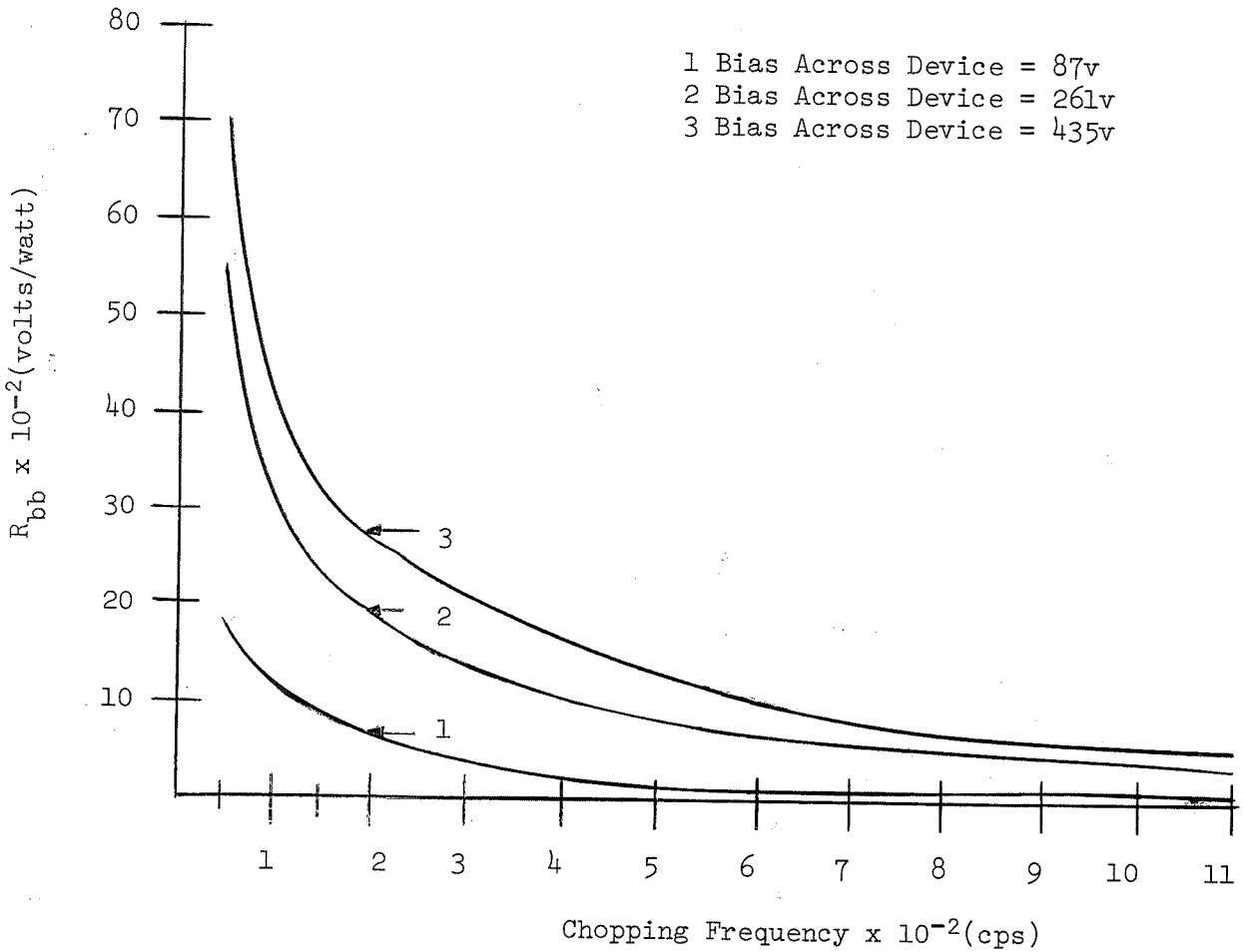

Figure 4.2 Black Body Responsivity vs. Chopping Frequency for a Typical n-Type Device Whose Initial Resistivity was .1Ω cm. (Device 823N0.1)

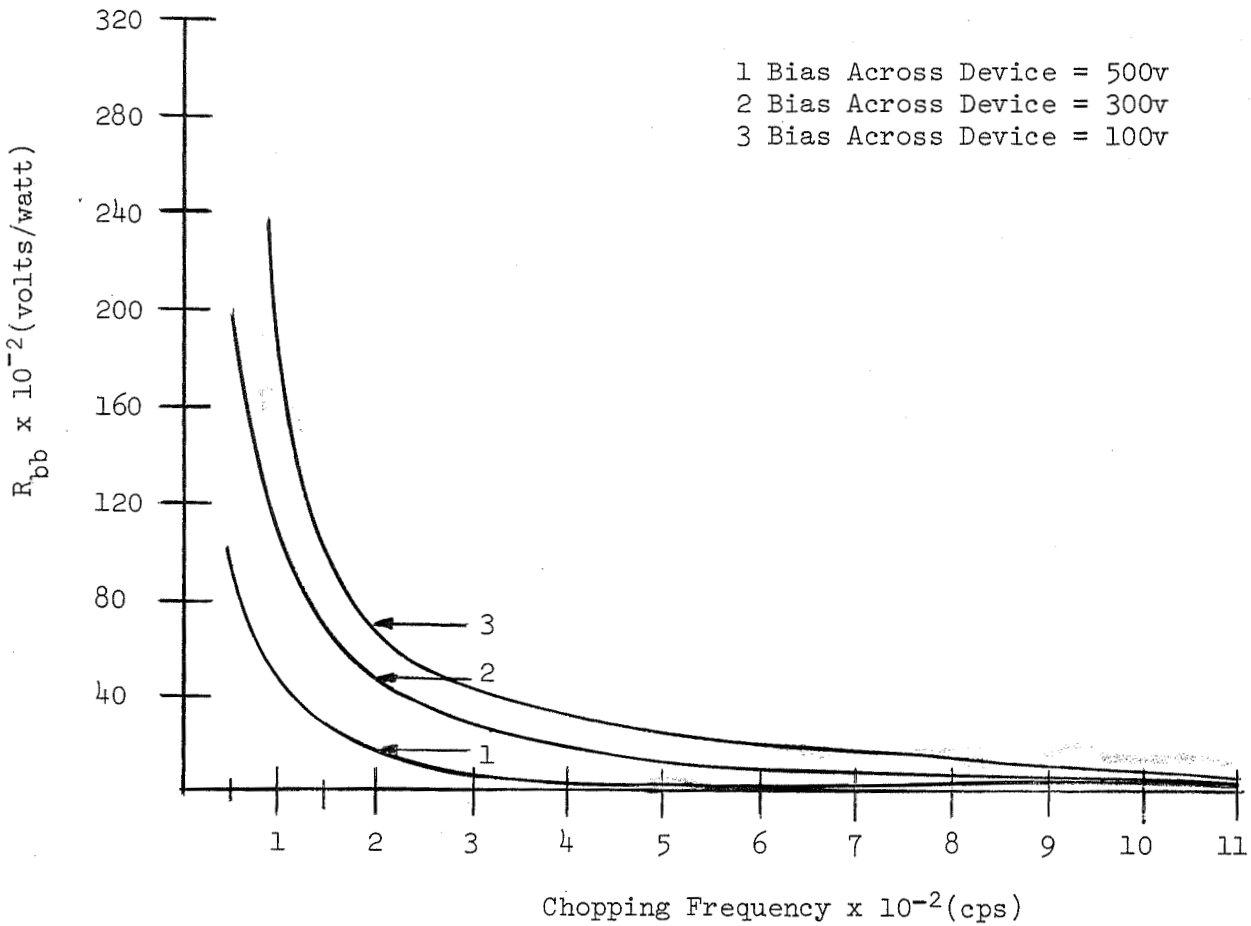

Figure 4.3 Black Body Responsivity vs. Chopping Frequency for a Typical p-Type Device Whose Initial Resistivity was 10Ω cm. (Device 704P10)

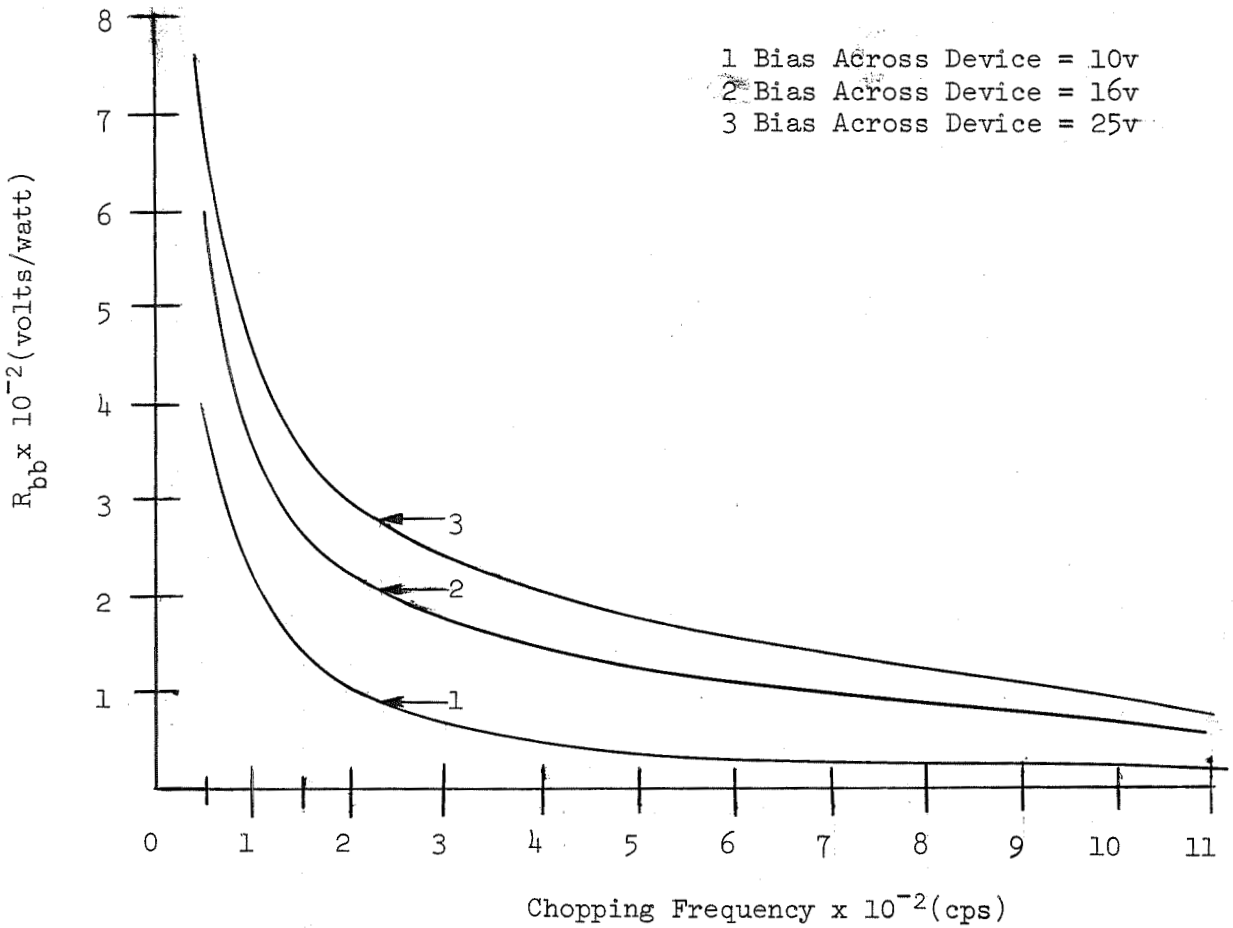

Figure 4.4 Black Body Responsivity vs. Chopping Frequency for a Typical p-Type Device Whose Initial Resistivity was 1Ω cm. (Device 504P1.0)

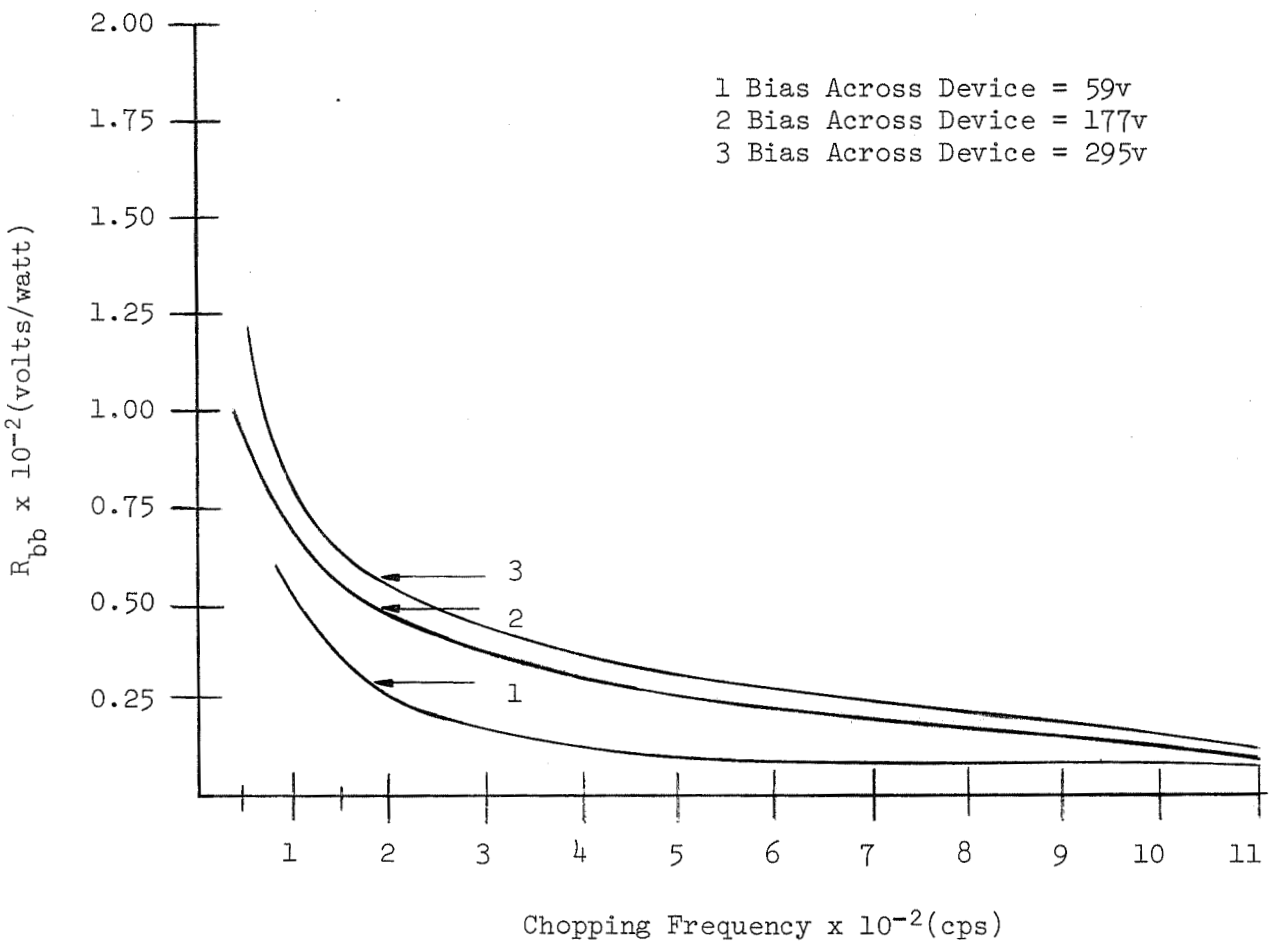

Figure 4.5 Black Body Responsivity vs. Chopping Frequency for a Typical p-Type Device Whose Initial Resistivity was .1Ω cm. (Device 431P0.1)

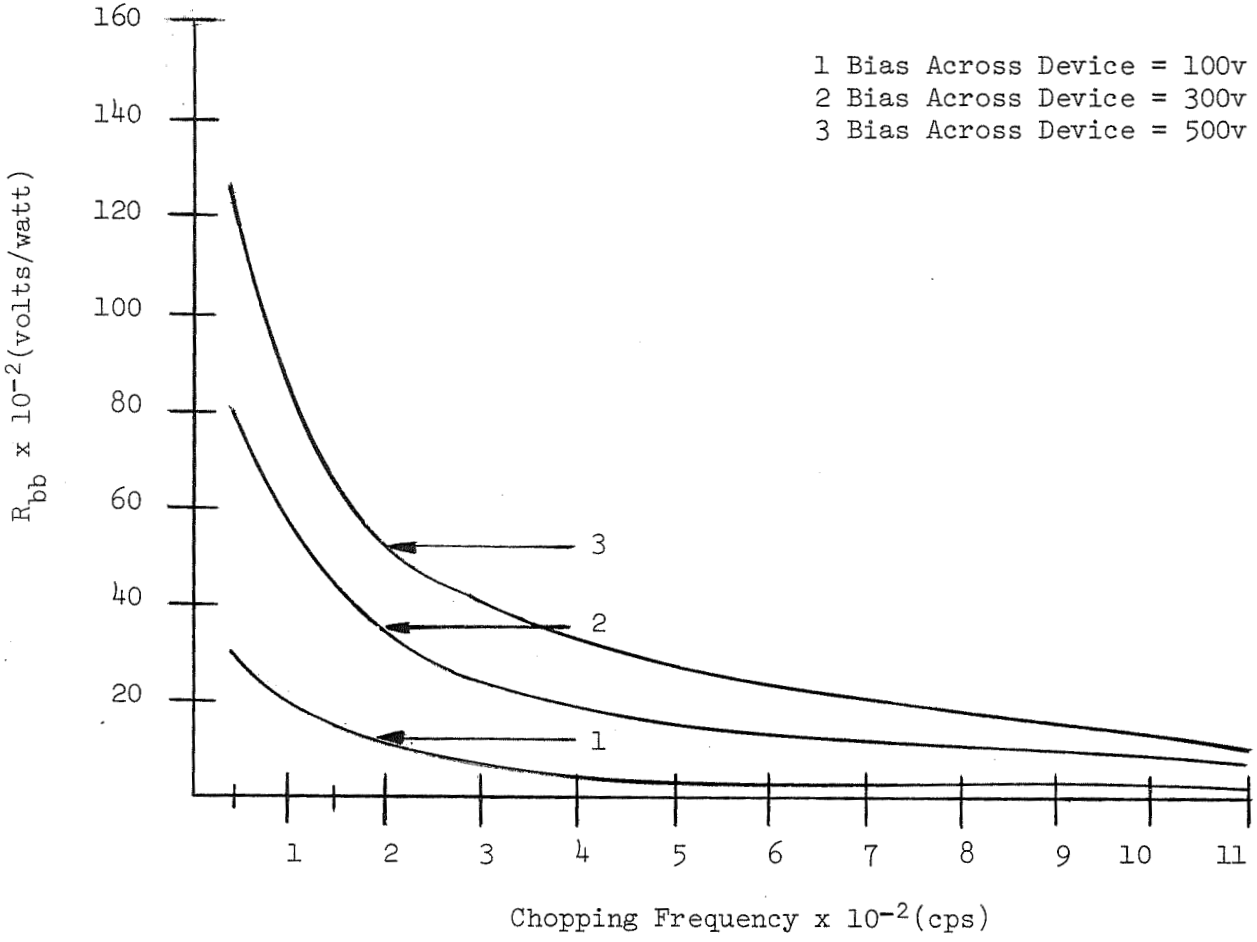

Figure 4.6 Black Body Responsivity vs. Chopping Frequency for a Typical n-Type Device Whose Initial Resistivity was .03Ω cm. (Device 626N0.03)

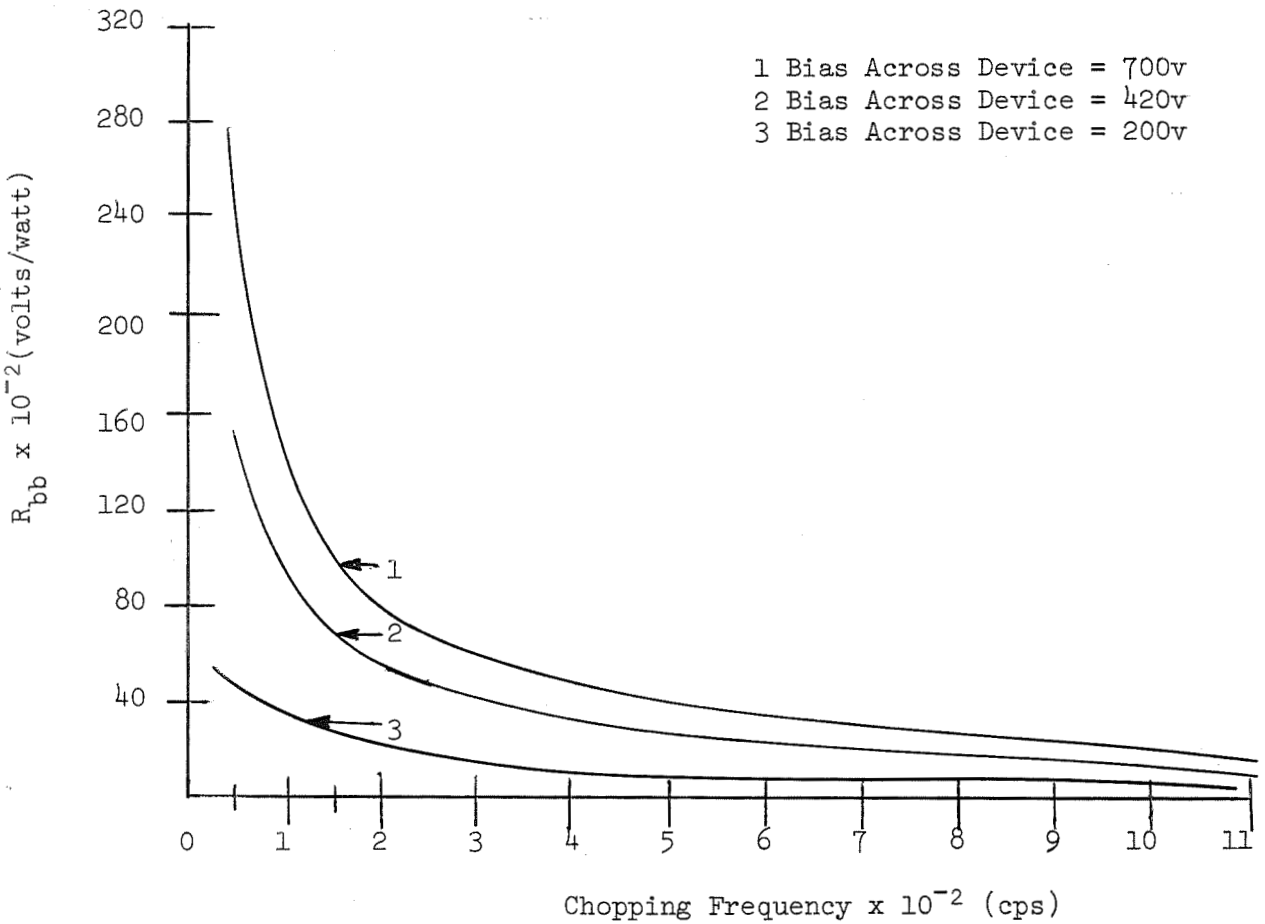

Figure 4.7 Black Body Responsivity vs. Chopping Frequency for a Typical n-Type Device Whose Initial Resistivity was .4Ω cm. (Device S-13-N.4)

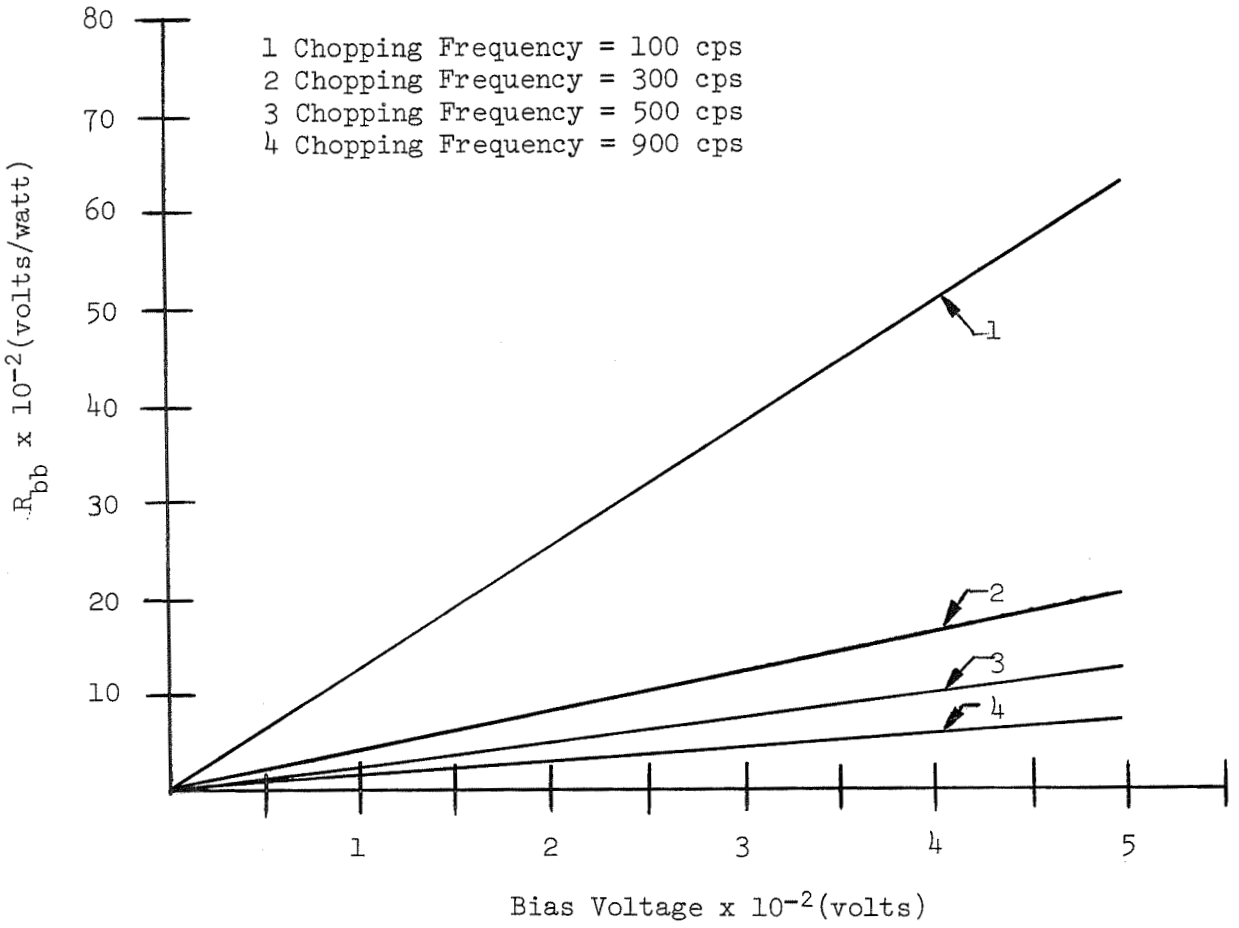

Figure 4.8 Black Body Responsivity vs. Bias Voltage (Device 333N1.0)

versus bias voltage across the device for a typical 1 ohm-cm. n-type device having a 77°K resistance of 3.2×10^8 ohms. This particular device (333N1.0) was used in annealing studies and the curves shown in Fig. 4.8 were taken after 24 hours of annealing at 175°C. The curves, however, are typical for the vast majority of samples tested whether they were annealed or not. The curves for samples tested with the improved system showed linearity through the 1100 volt bias capability of the system.

4.3. BLACK BODY RESPONSIVITY AS A FUNCTION OF ANNEALING

Devices fabricated from 1.0 ohm-cm. n-type material were used almost exclusively in annealing studies due to the fact that the current-voltage characteristics at 77°K made for at least one p-type device were slightly nonlinear. Annealing was first employed as a means of reducing the 77°K device resistance to the 10^8 ohm range in some devices whose initial 77°K resistance was some two or three orders of magnitude higher. Annealing at 175°C was used to remove Si-E centers while a higher 275°C was needed for annealing the Si-A centers [7]. The 100 Hz. black body responsivity of devices made from 1 ohm-cm. n-type material generally ranged from 10^2 to 10^4 watts/volt with the highest responsivities usually coming from devices with 77°K resistance in the 10^8 range. The black body responsivity trends for three different devices at 100 Hz. chopping frequency and 500 volts total bias are summarized

in Table 4.1.

Device Number	R_{bb} Before Annealing	R_{bb} After Annealing	Temperature and Duration of Annealing
304N1.0	3.55×10^2	9.1×10^2	175°C - 25 hours
303N1.0	0.88×10^2	1.02×10^2	175°C - 23 hours
		1.23×10^2	175°C - 47 hours 275°C - 10 minutes
301N1.0	9.8×10^2	17.8×10^2	175°C - 41.5 hours 275°C - 10 minutes

Table 4.1
Summary of Annealing Effects on the Black Body Responsivity of 1 ohm-cm., n-type Devices

Two 1 ohm-cm. n-type devices, 332N1.0 and 333N1.0, were carefully examined after successive anneal periods. Fig. 4.9 and 4.10 show the effects of annealing these two devices at 175°C. A definite peak is observed in the black body responsivity of each of the devices after a total annealing time of from 18 to 24 hours; this peak is more pronounced for lower chopping frequencies. Thus the R_{bb} of these devices seems to increase for increased annealing time up to a certain limit beyond which it begins to decrease. Unfortunately device noise also increases in most cases with greater periods of annealing, but this effect is believed to be one that can be reduced or eliminated with further work. The peak is believed indicative of the existence of an optimum defect density.

4.4. NOISE AS A FUNCTION OF BIAS VOLTAGE ACROSS THE DEVICE AND FREQUENCY OF MODULATED INCIDENT RADIATION

Noise has been mentioned as playing an important role in any

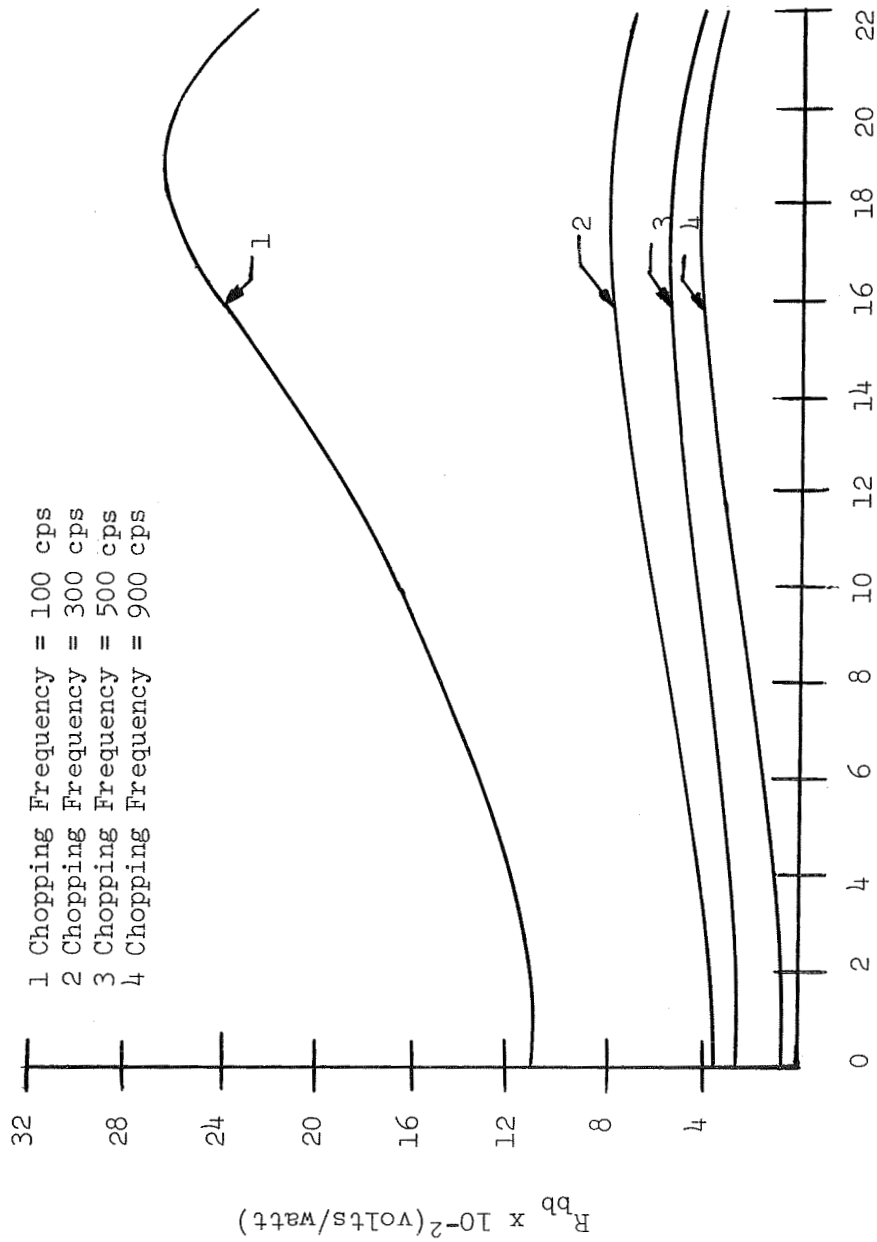

Figure 4.9 Black Body Responsivity vs. Hours of Annealing at 175°C
(Device 332N1.0)

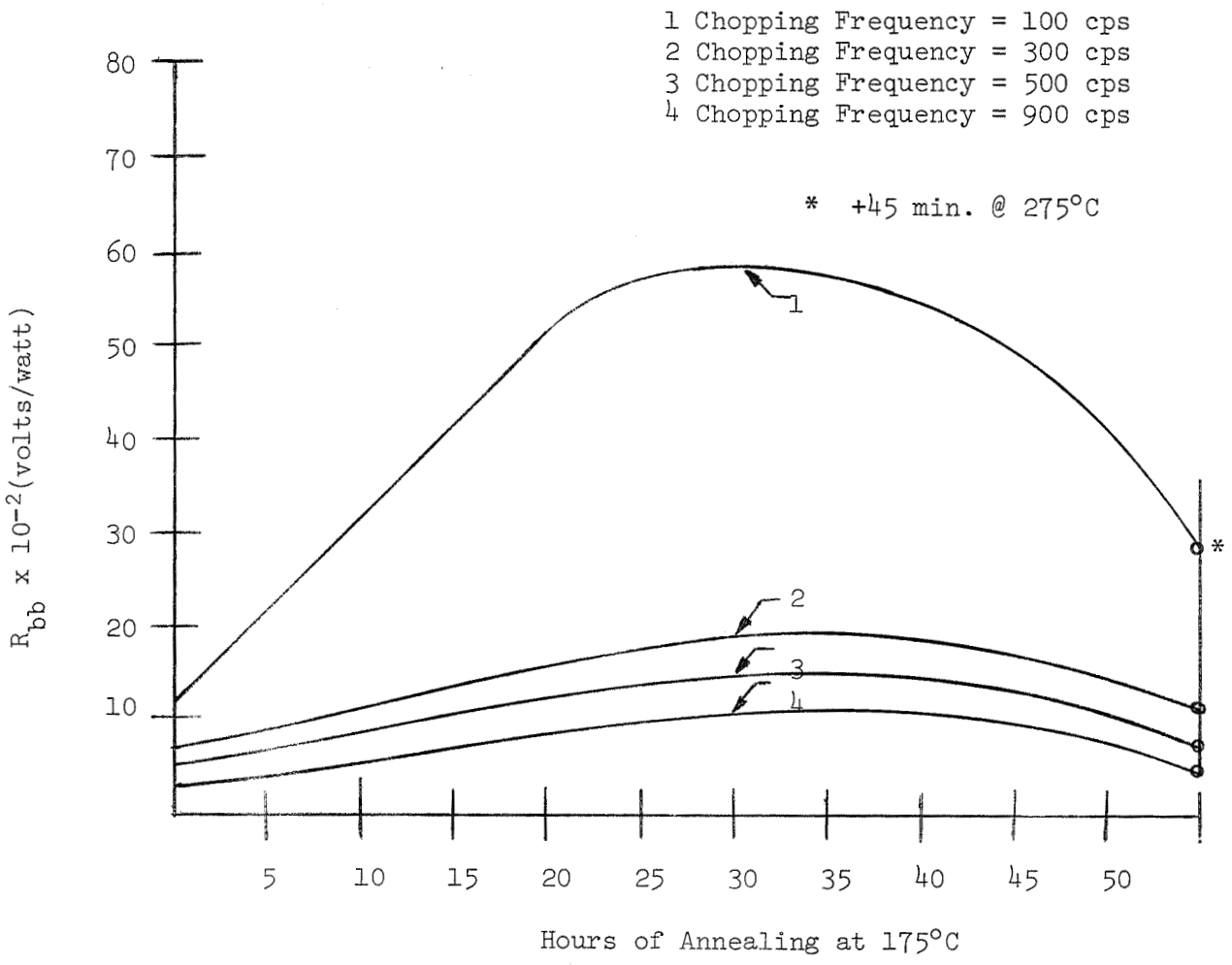

Figure 4.10 Black Body Responsivity vs. Hours of Annealing at 175°C (Device 333N1.0)

photodetective studies due to the fact that it is the ultimate limiting factor of any detector's performance. In the chopping frequency range being used in this investigation the devices are current noise limited. The majority of devices have noise over the chopping frequency and bias voltage ranges mentioned on the order of 1×10^{-6} to 1×10^{-3} volts r.m.s.; this noise being found by use of equation 3.2 given in the previous chapter. Initial noise levels rise with annealing, increased bias voltages, and decreased chopping frequency. Fig. 4.11 shows a typical noise root power spectrum for an 0.4 ohm-cm. n-type device.

4.5. SPECTRAL RELATIVE RESPONSE

The relative spectral response was defined in the last chapter as given by the relation (3.5)

$$L(\lambda) = \frac{E_1(\lambda)}{E_2(\lambda)}$$

where $E_1(\lambda)$ = the detector signal

$E_2(\lambda)$ = the bolometer signal.

This equation will be necessary for finding D^*_λ, the most important figure of merit. $L(\lambda)$ appears in both the numerator and denominator of the relation for D^*_λ so that any constants such as amplifier gains will be superficial in calculating this figure of merit. Thus in these calculations $L(\lambda)$ was taken simply as the ratio of the output of the detector to the output of the bolometer of spectrally flat characteristics.

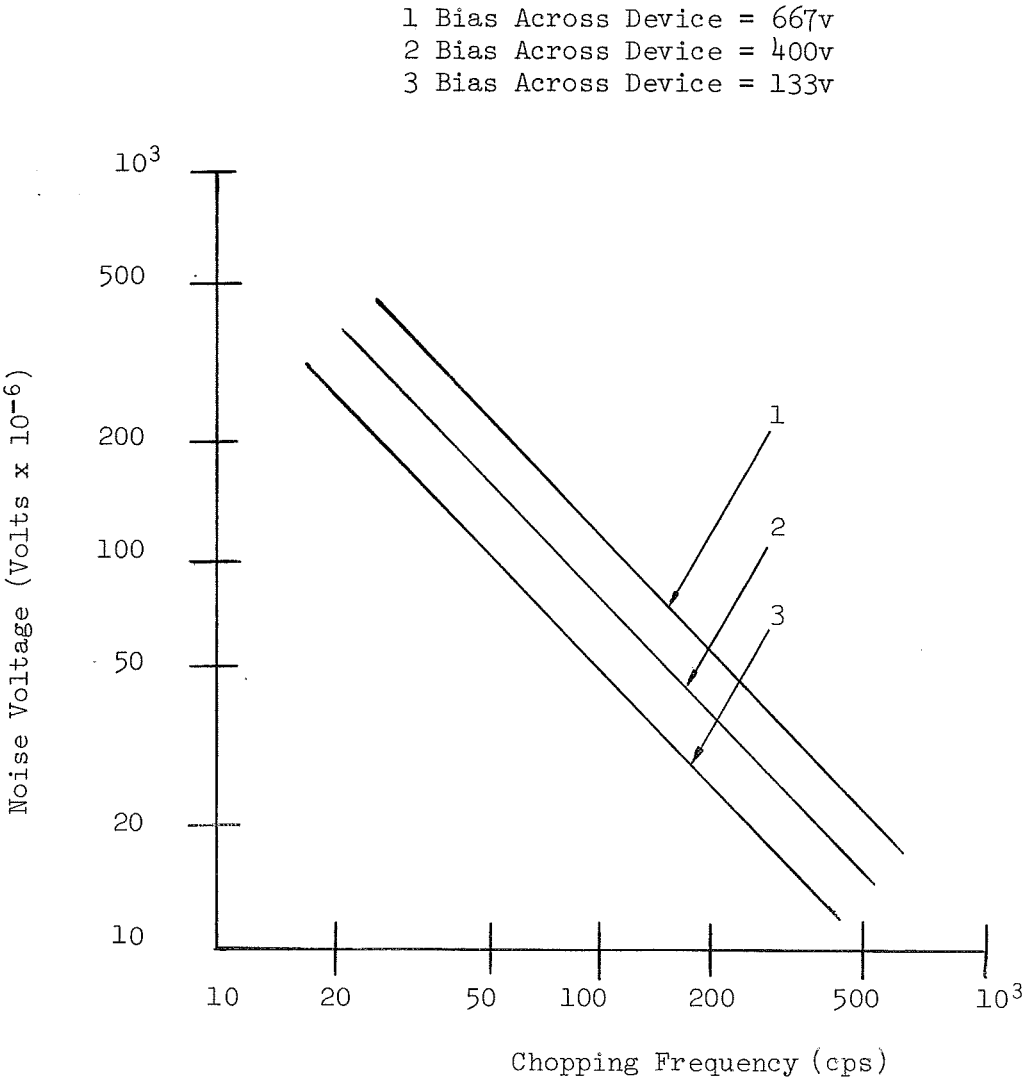

Figure 4.11 A Typical Noise Root Power Spectrum (Device S-12-N.4)

To date spectral data has been taken only on n-type devices which show their peak response to incident radiation of wavelength of approximately 2 microns. This response is indicative of extrinsic photoconduction in that for the case of intrinsic photoconduction one would expect a peak response in the neighborhood of 1 micron. This aspect of the investigation, however, will be discussed in greater detail in a later section. Fig. 4.12 shows the relative spectral response for a 1.0 ohm-cm. n-type device.

4.6. SPECTRAL DETECTIVITY

As was mentioned in Chapter 3, the spectral detectivity can be found from the relative spectral response, the black body responsivity, and the spectral and integrated black body power output. In terms of these parameters the relation for spectral detectivity becomes

$$D^*_\lambda = \frac{(A\ \Delta f)^{1/2}}{N} \frac{L(\lambda)\ P_{rms}}{\int L(\lambda)\ P(\lambda)_{rms}\ d\lambda}\ R_{bb}$$

where now N is the r.m.s. noise voltage at the bias voltage and chopping frequency at which D^*_λ is being evaluated.

This system of calculation has the advantage that the accuracy of the system is solely dependent on the determination of black body responsivity. If the detector signal output and bolometer output are taken almost simultaneously the calculation scheme is independent of time variations in the spectral output of the monochrometer.

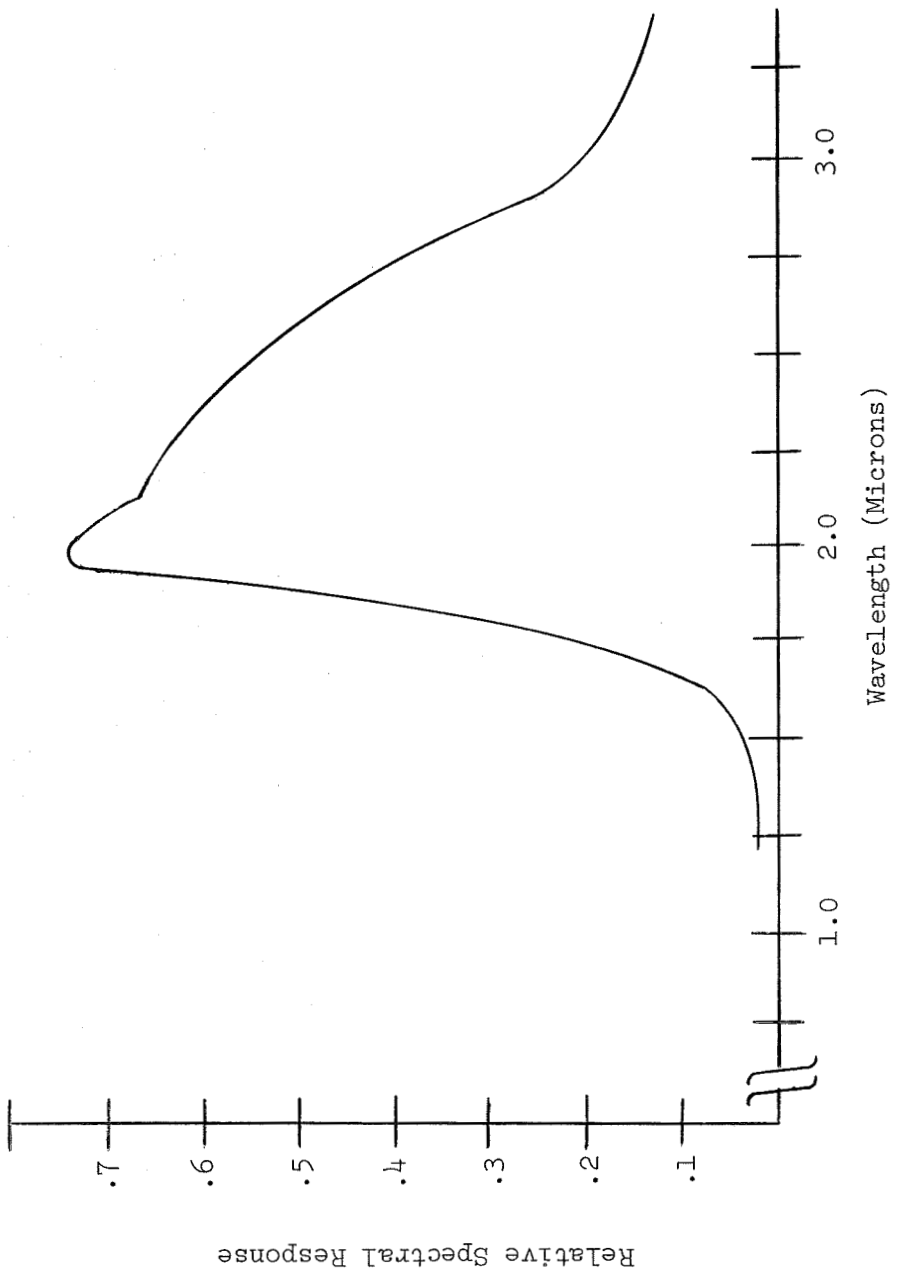

Figure 4.12 A Typical Spectral Relative Response (Device 323NL.0)

A computer program has been perfected which will make the calculations for D^*_λ as a function of chopping frequency, total bias voltage, and wavelength. Ordinarily, D^*_λ is calculated at optimum chopping frequency and bias voltage conditions, but a more complete analysis was sought for use in future optimization work. The program was perfected to compute D^*_λ in steps of 0.2 micron from 1.0 to 4.0 microns for each of the chopping frequencies 1000, 900, 800, 700, 600, 500, 400, 300, 200, 150, 100, 50, and 30 Hz. and for bias voltages of 1000, 800, 600, 400, and 200 volts. $R(\lambda)$ was also computed for the same parameter values.

Thus far the detectivities of only n-type samples have been computed. Detectivities have usually been on the order of 10^9 to $10^{10} \frac{\text{cm. Hz.}^{1/2}}{\text{watt}}$ although one 0.4 ohm-cm. type device was found to have a $D^*_{\lambda max}$ of $1.047 \times 10^{11} \frac{\text{cm. Hz.}^{1/2}}{\text{watt}}$ at a chopping frequency of 800 Hz. and total bias of 1000 volts. A typical curve of D^*_λ at the peak wavelength ($D^*_{\lambda,m}$) versus chopping frequency at optimum bias voltage is shown in Fig. 4.13.

The better detectivities for all devices are shown by the computer read-out to generally be at higher chopping frequencies and/or lower bias voltages. The increased responsivity at low chopping frequencies and high bias voltages does not offset the noise level increase. This fact once again points out the importance of noise reduction.

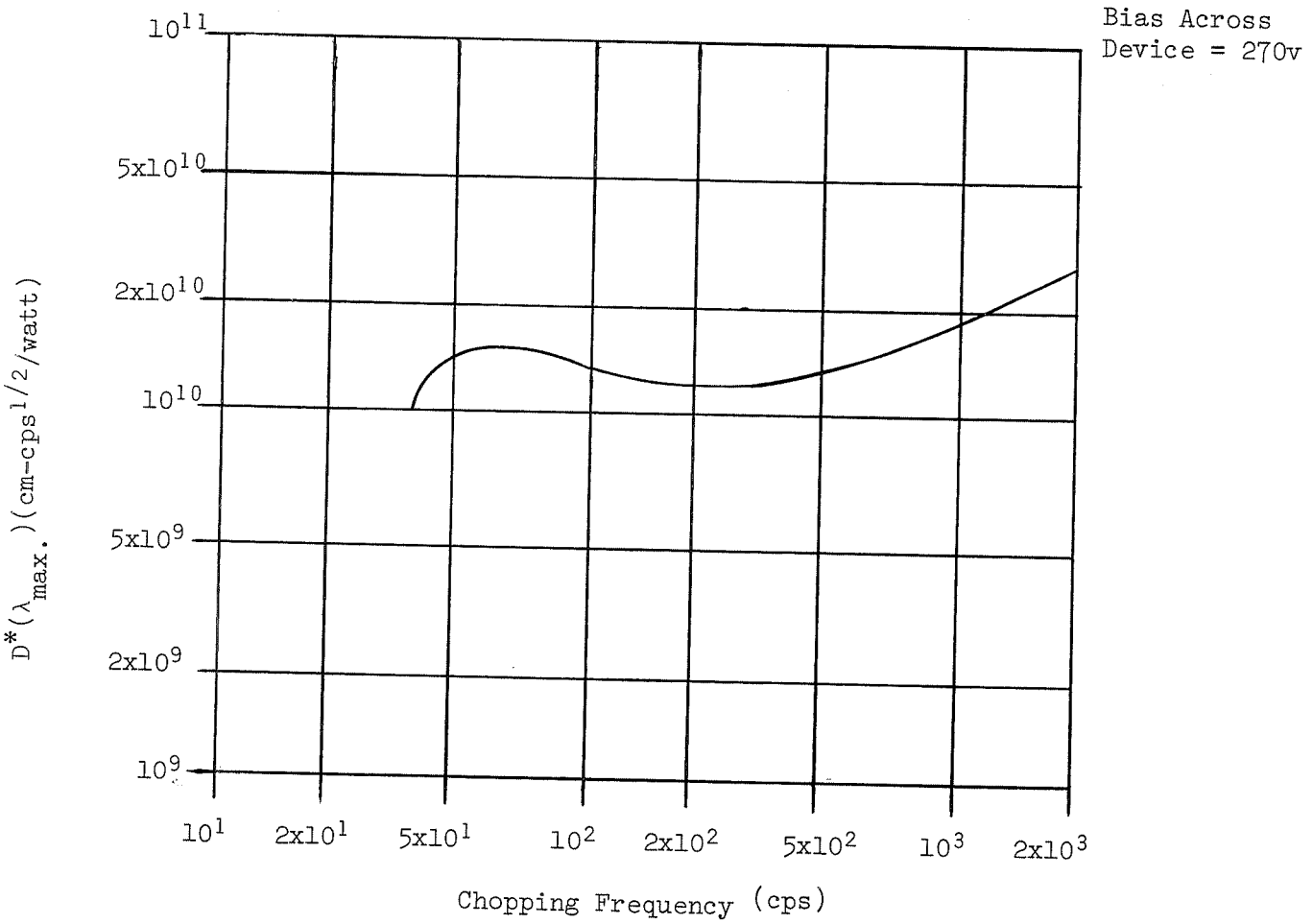

Figure 4.13 Spectral Detectivity at the Peak Wavelength ($D^*_{\lambda,m}$) vs. Chopping Frequency (Device 323N1.0)

4.7. REMARKS

4.7a. General Trends Noted

Irradiated silicon samples have thus been shown to exhibit extrinsic photoconductivity, the degree of which is comparable to currently used detectors. Presently these samples show detectivities generally an order of magnitude less then the widely used lead sulfide cells, although extensive optimization work will probably narrow or close this difference gap. The detectors have been shown to have responsivities which increase with decreasing chopping frequencies and which are linear as a function of bias voltage across the device. Noise has also been found to increase with decreasing chopping frequency and higher bias voltages. The high resistivity n-type samples having liquid nitrogen resistances in the 10^8 ohm range have been found to exhibit the best responses on the average. The peak response has been found to be at approximately 2 microns, and at that wavelength the detectivities have been found to generally be in the order of 10^9 to 10^{10} $\frac{\text{cm. Hz.}^{1/2}}{\text{watt}}$. Annealing at elevated temperatures to remove defect centers has been shown to have a marked effect on black body responsivity, leading to the expectation that an optimum irradiation dosage exists.

4.7b. Areas to be Further Investigated

It was the purpose of this work to show whether or not

irradiated silicon exhibits photoconductivity and if so, to what degree. The fact that photoconductivity does exist to a fairly considerable degree has been shown. Optimization studies should improve the performance of these devices greatly. The most important work it appears would be that of noise reduction. By reducing the noise level by an order of magnitude devices of performance comparable to lead sulfide cells should be produced. The main areas of interest for this work seem to be the electrical contacts and the device size. It also appears that the black body responsivity could be optimized. The optimization of resistivity type and of radiation dosage appear to be the most probable areas. The black body responsivity is also linear as a function of bias voltage up to 1000 volts so higher bias voltages in combination with improvements in the previously mentioned areas could result in significantly improved performance.

4.8. CONCLUSIONS

Naturally, the basic conclusion arrived at during this investigation was the fact that irradiated silicon exhibits extrinsic photoconductivity, and to such a degree that it is comparable in performance to some detectors in use today. The fact that this photoconductivity results from radiation induced defect centers can be realized by consideration of the energy levels in the irradiated silicon and the wavelength of the radiation causing

response.

Certain explanations and discussions are necessary before attempting to identify the dominant mechanism causing photoconductivity in these devices. It should be noted that even though the material used in this experiment is pulled crucible type silicon, one should expect to find E-centers produced. Recent research at the N.A.S.A. Langley Research Center [21] has shown that the A and E center densities are highly dependent upon the doping of the silicon as well as the method used to produce the silicon. For example, one would expect to find in a 1 ohm-cm. n-type device made of pulled crucible silicon and of 77°K resistance of 10^8 ohms densities on the order of 3×10^{15} cm.$^{-3}$ for the Si-E center and 3×10^{15} cm.$^{-3}$ for the Si-A center [22]. A new value has also been found for the E-center level due to recent research. This level is now placed at E_c - 0.40ev [23] instead of the E_c - 0.47ev location given by Sonders and Templeton [7].

An energy level diagram of n-type irradiated silicon would appear as it was shown in Fig. 2.4.

Fig. 4.12 shows the relative spectral response of a typical 1 ohm-cm. n-type device for incident radiation wavelengths from 1μ to 4μ. This information was obtained through the use of a 2.1μ diffraction grating in the monochrometer. Relative peaks were observed at 4μ and 8μ with the use of the 5μ and 10μ gratings. However, the validity of this data was questioned for two reasons:

(1) While the 5μ grating showed a relative peak near 4μ, the 2.1 grating showed no indications of this peak.

(2) Optical filters such as quartz, aluminum oxide, and various glasses with optical cut off wavelengths in the 4μ to 6μ range (as verified by spectrophotometric tests) placed in the optical path between the monochromatic source and the device attenuated the higher wavelength response (8μ) but did not eliminate the response as it should have done.

The responses found with the 2.1 grating were taken to be correct due to the fact that the monochrometer was calibrated with the 2.1 grating by means of a helium-neon laser.

The use of the germanium window also limited the useable portion of the monochrometer output. The window was chosen to stop all visible radiation and has a low cut off wavelength of approximately 1.6μ to 1.7μ.

The shape of the curve shown in Fig. 4.12 is typical of the relative spectral responses found. A "threshold" energy seems to exist at approximately 3.1μ. A "leveling off" of the rapid increase of $L(\lambda)$ appears at about 2.2μ after which another increase is seen to take place at approximately 1.8μ to 2.0μ. Data taken below this value is thought to be incorrect due to the low cut off wavelength of the germanium window.

Based on the relative spectral response curves obtained thus

far and on other considerations the mechanism causing photoconductivity in irradiated silicon is thought to be electron transitions from the Si-E center level to the conduction band. Furthermore, the increase in $L(\lambda)$ noted slightly below 2μ is believed to be associated with the 1.8μ absorption band noted by numerous researchers, many of whom disagree on the mechanism causing this band.

Fig. 4.14 which shows the energy of incident radiation as a function of the wavelength of the radiation shows that radiation of wavelength less than 3.1μ would be required to cause transitions from the E_c-0.4ev level to the conduction band.

Calculation of the Fermi level and of the density of electrons at the donor, Si-A and Si-E levels seem to rule out transitions from the valence band to defect levels or between defect levels.

For example, consider a device with a 77°K resistance of 10^8 ohms.

$$R = \rho \ell \tag{3.6}$$

and

$$\sigma = q \mu_n n \tag{3.7}$$

giving

$$n = \frac{\ell}{q \mu_n RA}$$

For a typical device with a 77°K resistance of 10^8 ohms, ℓ = 5×10^{-1} cm., A = 4×10^{-2} cm.^{2} giving

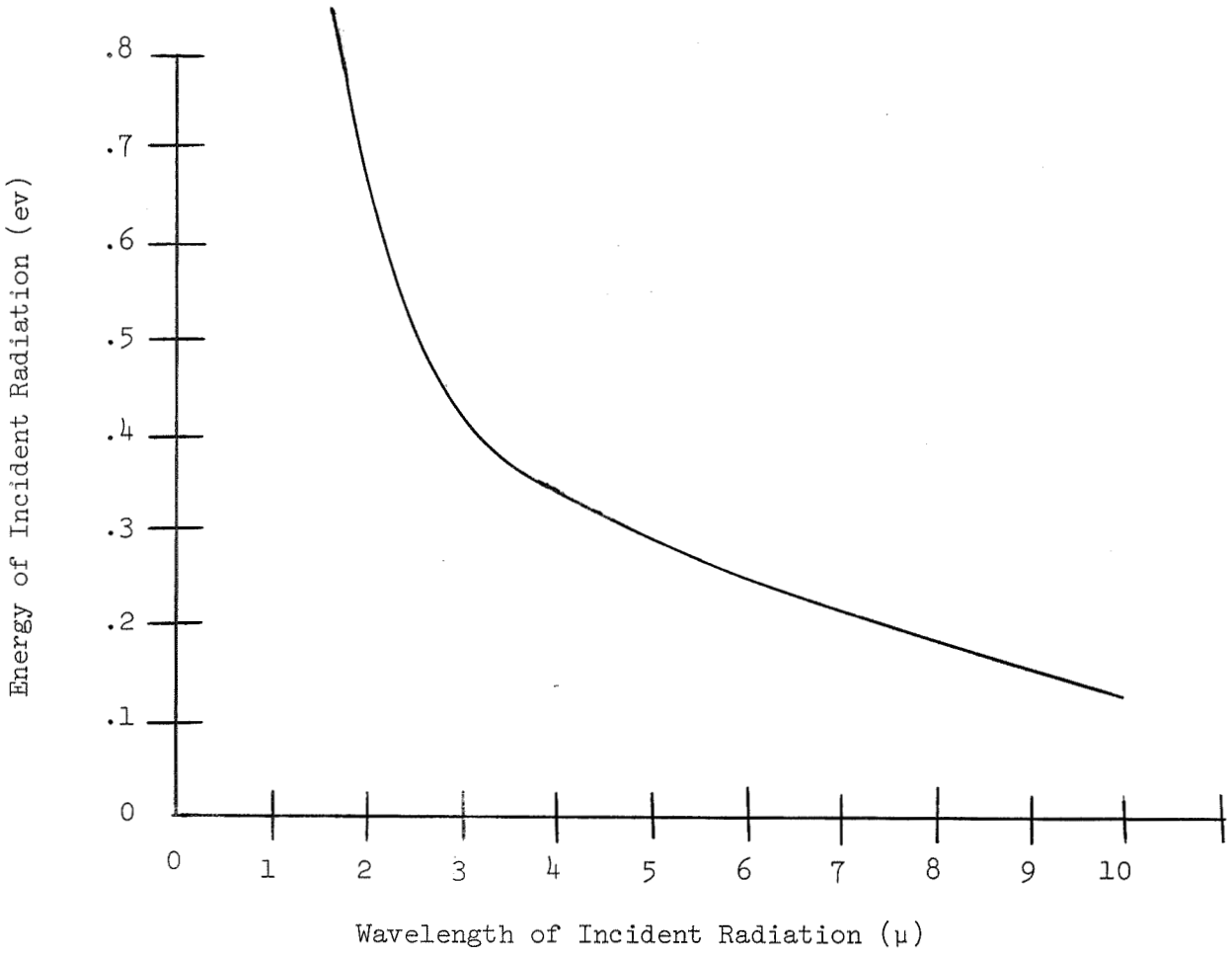

Figure 4.14 Energy of Incident Radiation vs. Wavelength of Incident Radiation

$$n = \frac{5 \times 10^{-1}}{6.4 \times 10^{-13} \mu_n}$$

μ_n has been found by means of Hall measurements to be approximately 8000 cm.^{2} v^{-1} sec.$^{-1}$ [24]. Thus $n = 9.76 \times 10^7$ cm.$^{-3}$.

Now,

$$n = N_c \, e^{-(E_c - E_f)/kT} \tag{3.8}$$

$$\ln \frac{n}{N_c} = (E_c - E_f)/kT \tag{3.9}$$

$$-kT \log_{10} \frac{N_c}{n} = .434 \, (E_c - E_f) \tag{3.10}$$

$$N_c = 2(2\pi \, m_c \, kT)/h^2)^{3/2}. \tag{3.11}$$

At 77°K

$$N_c \simeq 3.56 \times 10^{18} \text{ cm.}^{-3}. \tag{3.12}$$

Now, $-.0064 \, [\log_{10} 3.647 \times 10^{10}] = .434(E_c - E_f)$

$$E_f = E_c - 0.157\text{ev.} \tag{3.13}$$

At the donor level, the number of electrons per unit volume occupying the donor level is

$$n_d = \frac{N_d}{1 + 1/2 \, e^{(E_d - E_f)/kT}} = \frac{N_d}{1 + 1/2 \, e^{16.4}} \simeq 10^{-6} \, N_d. \tag{3.14}$$

The Fermi level calculated lies near the Si-A center level, and work conducted at the N.A.S.A. Langley Research Center has placed the Fermi level at the Si-A center level for an n-type device

with a 77°K resistance of 10^8 ohms. One would therefore expect that the Si-A center acceptor level would not be filled, but that the Si-E center level would. This fact tends to support the idea that the transitions take place from the Si-E level to the conduction band since the Si-E level is filled preventing transitions from the valence band to the Si-E level. Transitions from the Si-E center level to the Si-A center level should not give the response noted.

The increase in $L(\lambda)$ at approximately 1.8μ is believed to be associated with a 1.8μ absorption band observed by various researchers [23, 25]. The cause of the band has been the subject of many theories. Fan and Ramdas [25] were of the opinion that this band is associated with energy levels in the neighborhood of E_c-0.21ev. Plotnikov [26] attributed the 1.8μ band to electron transitions from the valence band to the E_c-0.4ev level. This explanation appears suspect because neutron irradiated silicon was used for this particular work, and as of 1966 no one had observed the E_c-0.4ev level in neutron irradiated silicon [26]. However, Lotkova [26] and Kurskii [27] agree that the 1.8μ band is associated with the excitation of the Si-A centers and is observed whenever the E_c-0.17ev level is free of electrons.

The 1.8μ absorption band has not been investigated fully due to the cutoff wavelength imposed by the germanium window. Research involving this band is foreseen in the immediate future.

In addition to these conclusions, the general trends noted in a preceeding section of this chapter would suffice for conclusions arrived at in regard to device performance and characteristics.

BIBLIOGRAPHY

1. S. Larach, editor, Photoelectronic Materials and Devices. Princeton, New Jersey: D. Van Nostrand Company, Inc., 1965.

2. P. W. Kruse, L. D. McGlauchlin, and R. B. McQuistan, Elements of Infrared Technology. New York: John Wiley and Sons, Inc., 1962.

3. W. L. Eisenman and A. B. Naugle, "Properties of Photodetectors Series, 45th Report," NAVWEPS Report 7181, Naval Ordinance Laboratory Corona, California, June, 1961.

4. W. L. Eisenman, A. B. Naugle, and J. D. Merriam, "Properties of Photodetectors, Photodetector Series, 75th Report," NOLC Report 734, Naval Ordinance Laboratory Corona, California, August, 1967.

5. R. A. Soreff, "Extrinsic Infrared Photoconductivity of Silicon Doped with B, Al, Ga, P, As, or Sb," Journal of Applied Physics, Vol. 38, No. 13, December, 1967.

6. E. Sonder and L. C. Templeton, "Gamma Irradiation of Silicon I. Levels in n-type Material Containing Oxygen," Journal of Applied Physics, Vol. 31, No. 7, July, 1960.

7. E.Sonder and L. C. Templeton, "Gamma Irradiation of Silicon II. Levels in n-type Float-Zone Material," Journal of Applied Physics, Vol. 34, No. 11, November, 1963.

8. E. Sonder and L. C. Templeton, "Gamma Irradiation of Silicon III. Levels in p-type Material," Journal of Applied Physics, Vol. 36, No. 6, June, 1965.

9. G. D. Watkins and J. W. Corbett, "Defects in Irradiated Silicon I. Electron Spin Resonance of the Si-A Center," Physical Review, Vol. 121, No. 4, February, 1961.

10. J. W. Corbett et al., "Defects in Irradiated Silicon II. Infrared Absorption of the Si-A Center," Physical Review, Vol. 121, No. 4, February, 1961.

11. G. A. Watkins and J. W. Corbett, "Defects in Irradiated Silicon: Electron Paramagnetic Resonance and Electron Nuclear Double Resonance of the Si-E Center," Physical Review, Vol. 134, No. 5A, June, 1964.

12. R. J. Mattauch, University of Virginia - R.L.E.S. Proposal EE-NASA-308-670, 1968.

13. W. L. Eisenman, "Procedures Used in the Study of the Properties of Photodetectors," NOLC Report 541, Naval Ordinance Laboratory Corona, California, July, 1961.

14. R. Clark Jones, "Methods of Rating the Performance of Photoconductor Cells," Proc. IRIS, Vol. 2, No. 1, June, 1957.

15. J. J. Brophy, "Low Noise Modification of the Tektronix Type 122 Preamplifier," Review of Scientific Instruments, Vol. 26, No. 11, November, 1955.

16. W. L. Eisenman, Personal Correspondence, July, 1968.

17. P. C. Caringella and W. L. Eisenman, "System for Low-Frequency Noise Measurements," Review of Scientific Instruments, Vol. 33, No. 6, June, 1962.

18. R. J. Mattauch, "Investigation of the Detectivity of Radiation Produced Defect Levels in n- and p-type Silicon and Germanium," First Semiannual Progress Report, August, 1968.

19. R. B. McQuistan, "On an Approximation to Sinusoidal Modulation," Journal of the Optical Society of America, Vol. 48, No. 1, January, 1958.

20. _____, "Instruction Manual for Infrared Recording Spectrophotometer," Baird Associates, Inc., Cambridge, Massachusetts.

21. C. Gross, Private Communication, April, 1969.

22. C. Gross, Private Communication, May, 1969.

23. V. S. Vavilov, Effects of Radiation on Semiconductors (translated from the Russian); New York: Consultants Bureau, 1965.

24. C. Gross, Private Communication, May, 1969.

25. H. Y. Fan and A. K. Ramdas, "Infrared Absorption and Photoconductivity in Irradiated Silicon," Journal of Applied Physics, Vol. 30, No. 8, August, 1959.

26. E. N. Lotkova, "Investigation of the Infrared Absorption Spectrum of Neutron - Irradiated Silicon," Proceedings of the P. N. Lebedev Physics Institute (translated from the Russian), Vol. 37, 1968.

27. Y. A. Kurskii, "Absorption and Recombination Radiation Connected with an A-Center in Silicon," Soviet Physics-Solid State (translated from Fizika Tverdogo Tela, Vol. 6, No. 8), Vol. 6, No. 8, February, 1965.

APPENDIX

PREPARATION OF SAMPLES

Silicon wafers one inch in diameter and 2mm thick of six different resistivities were purchased from the General Diode Corporation. These wafers were procured under the stipulation that they would be produced by the pulled quartz crucible method. The wafers had one surface highly polished to insure that each device would have one face with a relatively low recombination velocity.

The wafers were mounted on the chuck of a thin sectioning machine manufactured by the South Bay Technological Group, and 2mm x 2mm x 5mm bars were cut from them. The sectioning machine used a slow moving 5 mil or 10 mil wire with an abrasive slurry (no. 600 grit) which effectively lapped the unwanted areas between devices without producing deep work damage microcracks in the crystal. The devices were then washed first in distilled water, then boiling acetone, and finally distilled water again to remove all traces of the glycerine-based slurry. The samples were then stored in methyl alcohol before being sent to the N.A.S.A. Langley Research Center where their ends were covered with vapor deposited indium or arsenic doped gold, depending upon the bar type. The gold was then alloyed into the bars at 650°C for 5 minutes, after which a layer of the same type gold was vapor deposited on the bar ends. The devices were returned and were nickel plated by chemical

solution. Their ends were masked in piceal wax, after which the devices were etched in a 95% HNO_3, 5% HF solution for 3 minutes. The devices were then rinsed with distilled water, methyl alcohol, and finally trichloroethylene to remove the wax end masks.

The devices were then ready for irradiation at the N.A.S.A. Space Radiation Effects Laboratory (SREL) at Newport News, Virginia. A linear accelerator capable of producing a beam of 10 Mev electrons was used for the majority of the irradiations (a 2 Mev Dynamitron was used shortly while the lineac was out of operation). A target set-up such as that shown in Fig. A.1. was used. The beam of electrons was focused by the bending magnetic on a circular aluminum plate held in the beam path. The plate had an aperture and acted as a collimator focusing the beam only on samples held by a teflon insulated spring loaded sample holder. A Faraday cup completed the beam circuit, and a current integrator integrated the beam current incident on the Faraday cup.

The approximate number of particles incident on the samples could be determined from geometrical considerations involving the collimator, the device exposed area and from the number of particles indicated by the current integrator. The device resistance was monitored by means of finding the voltage across the device with a constant current of 1 ma driven through it by the constant current source. The beam was turned off periodically, and the resistance and resistivity of the device checked. This information

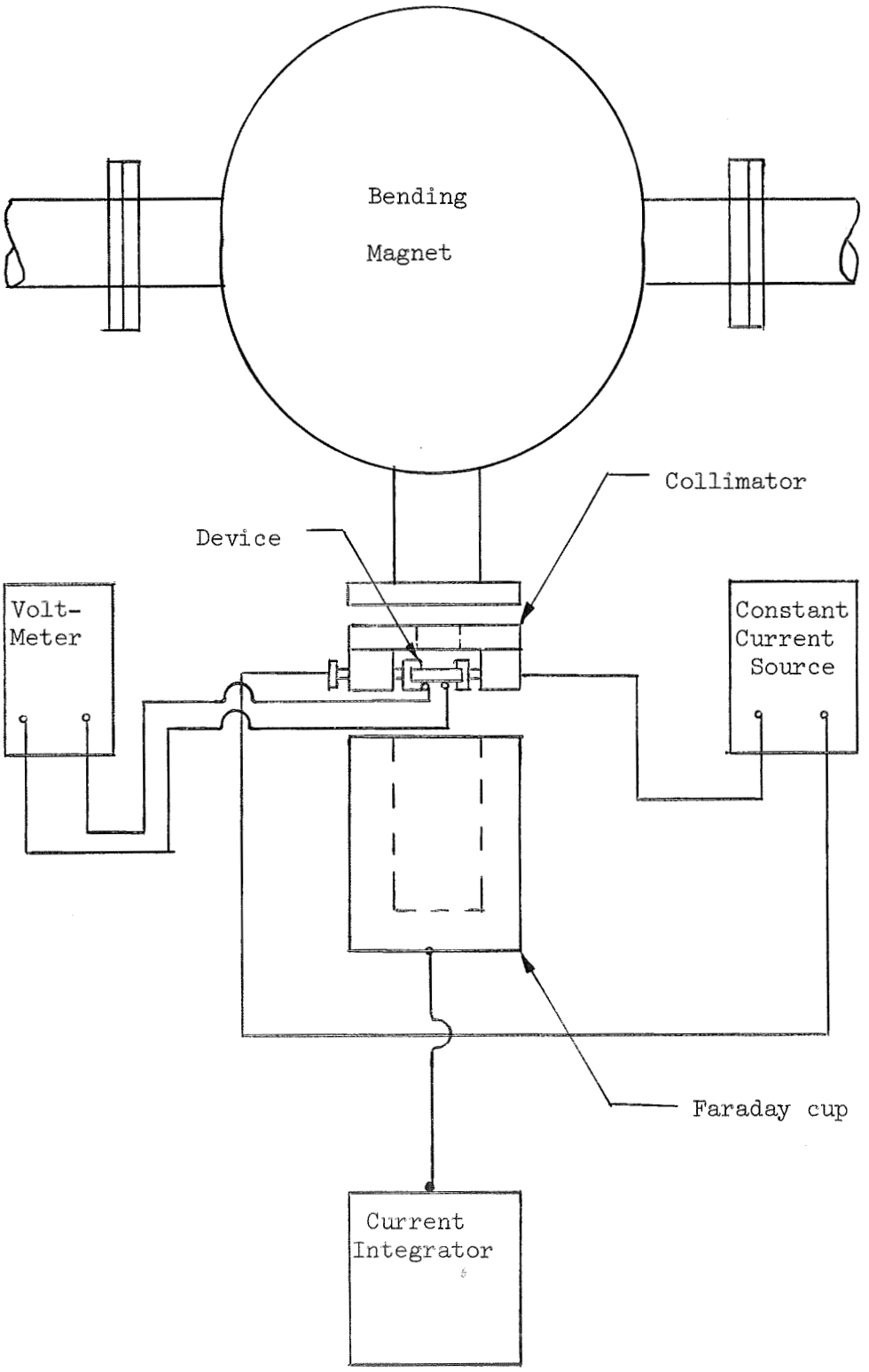

Figure A.1 Diagram of Target Area for Sample Irradiation

allowed the author to make an order-of-magnitude calculation as to the number of defects introduced into the device crystalline structure per unit volume.

The beam current was maintained at a current on the order of 10^{-7} to 10^{-6} ampere with the electrons having energy of approximately 8 Mev. During the first irradiation the beam current had to be kept at low values to prevent annealing the defects introduced. The collimator was air cooled for these irradiations, but recently N.A.S.A. personnel have developed a water cooled collimator enabling more samples to be irradiated at once using higher beam currents.

The devices were separated before irradiation and numbered according to a system whereby each device was identified by three numerals, its type (a letter), and its resistivity.

For use with the original system one end of each sample was mounted on a separate one-half inch brass pad cut to fit the end of the dewar cold finger. A 5 mil tinned copper wire was attached to the other end. The mounting and wire attachments were accomplished by means of Dynaloy 320 conductive silver epoxy. Several types of conductive epoxies were tried, and while the above mentioned is far from satisfactory in the extreme temperature range used it is the best of the products tried. For the improved system no mounting had to be done for the spring loaded holder. Additional samples of 0.4 ohm-cm. n-type silicon and 1 ohm-cm. n-type germanium were supplied by N.A.S.A.

DISTRIBUTION LIST

Copy No.	
1-10	National Aeronautics and Space Administration Scientific and Technical Information Division Code US, Attn: Winnie M. Morgan Washington, D.C. 20546
11-12	National Aeronautics and Space Administration Langley Research Center Langley Station Hampton, Virginia 23365 Attn: Instrument Research Division
13	A. R. Kuhlthau
14	G. A. McAlpine
15	C. M. Siegel
16-17	R. H. Austin Science/Technology Information Center Alderman Library
18-19	R. J. Mattauch
20-30	RLES Files